

**NASA  
Technical  
Paper  
1965**

**AVRADCOM  
Technical  
Report  
81-B-6**

December 1981

# Two-Dimensional Aerodynamic Characteristics of an Airfoil Designed for Rotorcraft Application

Gene J. Bingham,  
Kevin W. Noonan,  
and William G. Sewall

**NASA**

National Aeronautics  
and Space Administration

Scientific and Technical  
Information Branch

**NASA  
Technical  
Paper  
1965**

**AVRADCOM  
Technical  
Report  
81-B-6**

1981

# Two-Dimensional Aerodynamic Characteristics of an Airfoil Designed for Rotorcraft Application

Gene J. Bingham and Kevin W. Noonan  
*Structures Laboratory  
AVRADCOM Research and Technology Laboratories  
Langley Research Center  
Hampton, Virginia*

William G. Sewall  
*Langley Research Center  
Hampton, Virginia*



National Aeronautics  
and Space Administration

Scientific and Technical  
Information Branch

## SUMMARY

An airfoil designed for helicopter rotor application has been investigated at Mach numbers from about 0.35 to 0.90 at Reynolds numbers from  $5.1 \times 10^6$  to  $9.6 \times 10^6$ . The airfoil, designated as the NASA RC(1)-10, was designed to increase the maximum normal-force coefficient while maintaining the favorable drag-divergence and pitching-moment characteristics observed earlier for the 10-64C airfoil. The RC(1)-10 airfoil has a thickness-to-chord ratio of 0.10 with maximum thickness located at 40 percent chord and maximum camber located at 27 percent chord. The tests of the RC(1)-10 airfoil displayed an unexpected drag increase (or creep) at Mach numbers below those for drag divergence and at zero and negative normal-force coefficients. An analysis indicated that the drag might be decreased by reducing the ordinates in the lower-surface leading-edge region. Therefore, two modifications were made in the lower-surface region and were also tested at Mach numbers from about 0.35 to 0.90 at Reynolds numbers from about  $5.0 \times 10^6$  to  $13.9 \times 10^6$ .

With natural transition, the maximum normal-force coefficient of the RC(1)-10 airfoil varies from 1.14 to 0.90 at Mach numbers from about 0.35 to 0.65, an increase of 0.06 to 0.16 over that of the 10-64C airfoil. The drag-divergence Mach number of the RC(1)-10 airfoil is about equal to that of the 10-64C airfoil at normal-force coefficients from 0 to 0.4. At normal-force coefficients from 0.4 to 0.8, the drag-divergence Mach number of the RC(1)-10 is less than that of the 10-64C airfoil. The greatest difference in drag-divergence Mach number measured for the two airfoils is indicated at a normal-force coefficient of -0.2. This difference results from shock-wave/boundary-layer interaction influences near the lower-surface leading edge for the RC(1)-10 airfoil. The two modifications made to the RC(1)-10 airfoil contour decreased the drag coefficient at zero normal-force coefficient for Mach numbers near drag divergence, but were less beneficial at a normal-force coefficient of -0.2.

## INTRODUCTION

The design of airfoil sections for helicopter rotor blades requires simultaneous consideration of (1) the maximum lift coefficient at Mach numbers up to about 0.50, (2) the drag-divergence Mach number at lift coefficients from near -0.2 to the maximum lift coefficient, and (3) the pitching-moment coefficient at corresponding lift coefficients and Mach numbers. The drag-divergence and pitching-moment characteristics of airfoils are presently more accurately predicted analytically than is the maximum lift coefficient. For example, the drag-divergence Mach number and pitching-moment characteristics for several NACA airfoils were analytically evaluated in reference 1 and the analysis was determined to be qualitatively correct by reference 2.

The 10-64C airfoil of reference 2 had favorable drag-divergence and pitching-moment characteristics compared with a number of current helicopter rotor airfoils, but the maximum lift (normal-force coefficient) was lower than desired. Therefore, the design approach discussed in reference 1 was again applied to define a new 10-percent-thick airfoil which might provide increased maximum normal-force coefficient at Mach numbers to about 0.50 while maintaining the favorable drag and pitching-moment characteristics. The airfoil, designated the NASA RC(1)-10, has a new thickness distribution and camber line defined to decrease the magnitude of the negative pressure coefficients in the leading-edge region at angles of attack that generally

correspond to the maximum lift coefficient. The maximum thickness of the airfoil is located at 40 percent chord. The leading-edge radius of the RC(1)-10 configuration is increased 25 percent compared with that of the 10-64C airfoil of reference 2 (0.01378c compared with 0.01102c) and the camber is increased forward of 35 percent chord.

The RC(1)-10 airfoil was tested in the Langley 6- by 28-Inch Transonic Tunnel at Mach numbers from 0.35 to 0.90. The Reynolds number was varied from  $5.1 \times 10^6$  to  $9.6 \times 10^6$  from the lowest to the highest Mach number. Normal-force and pitching-moment coefficients were determined from measurements of airfoil-surface static pressures, and drag coefficients were determined from measurements of wake total and static pressures.

Analysis of the results indicated an unexpected drag increase (or creep) at Mach numbers below that for drag divergence and at zero and negative normal-force coefficients. An analysis made by applying the method of reference 3 indicated that the drag might be decreased by reducing the ordinates in the lower-surface leading-edge region. As a result, two modifications of the RC(1)-10 airfoil were made and tested. The modified sections are identified as the RC(1)-10 Mod 1 and RC(1)-10 Mod 2.

#### SYMBOLS

The units used for the physical quantities in this paper are given in both the International System of Units (SI) and U.S. Customary Units. The measurements and calculations were made in U.S. Customary Units.

$C_p$  static-pressure coefficient,  $\frac{p_l - p_\infty}{q_\infty}$

$c$  airfoil chord, cm (in.)

$c_d$  section profile-drag coefficient,  $\sum_{\text{Wake}} c_d' (\Delta h/c)$

$c_d'$  point-drag coefficient,

$$2 \left( \frac{p}{p_\infty} \right)^{6/7} \left[ \frac{(p_t/p)^{2/7} - 1}{(p_{t,\infty}/p_\infty)^{2/7} - 1} \right]^{1/2} \left\{ \left( \frac{p_t}{p_{t,\infty}} \right)^{1/7} - \left[ \frac{(p_t/p_\infty)^{2/7} - 1}{(p_{t,\infty}/p_\infty)^{2/7} - 1} \right]^{1/2} \right\}$$

$c_{d,w}$  section wave-drag coefficient

$c_m$  section pitching-moment coefficient about quarter-chord,

$$\sum_{\text{U.S.}} \left[ c_p \left( 0.25 - \frac{x}{c} \right) \left( \frac{\Delta x}{c} \right) + c_p \left( \frac{z}{c} \right) \left( \frac{\Delta z}{c} \right) \right] + \sum_{\text{L.S.}} \left[ c_p \left( 0.25 - \frac{x}{c} \right) \left( \frac{\Delta x}{c} \right) + c_p \left( \frac{z}{c} \right) \left( \frac{\Delta z}{c} \right) \right]$$

$c_{m,o}$  section pitching-moment coefficient about aerodynamic center

$c_n$  section normal-force coefficient,  $\sum_{\text{U.S.}} c_p (\Delta x/c) + \sum_{\text{L.S.}} c_p (\Delta x/c)$

$h$	distance traveled by the wake-survey probe, cm (in.)
$M$	Mach number
$M_{dd}$	Mach number for drag divergence, $\frac{dc_d}{dM} = 0.1$
$p$	static pressure, Pa (psi)
$q$	dynamic pressure, $\frac{1}{2} \rho V^2$ , Pa (psi)
$R$	Reynolds number based on airfoil chord and free-stream conditions
$t$	airfoil thickness, cm (in.)
$V$	velocity, m/sec (ft/sec)
$x$	airfoil abscissa, cm (in.)
$z$	airfoil ordinate, cm (in.)
$z_c$	ordinate of airfoil mean line, cm (in.)
$\alpha$	angle of attack, angle between airfoil chord line and airstream direction, deg
$\alpha_c$	angle of attack corrected for lift-interference effects, deg
$\rho$	density, kg/m <sup>3</sup> (slugs/ft <sup>3</sup> )

Subscripts:

$l$	local
max	maximum
sonic	Mach number equal to 1
$t$	total
$\infty$	free stream

Abbreviations:

L.S.	lower surface
U.S.	upper surface

## APPARATUS AND METHODS

### Airfoils

The profile, thickness distribution, and mean line of the RC(1)-10 airfoil (the initial configuration investigated) are presented in figures 1 and 2, and the design coordinates are presented in table I. The airfoil has a maximum thickness of

10 percent chord located at 40 percent chord. The maximum camber is located at 27 percent chord and the leading-edge radius is 1.378 percent chord.

After an analysis of wind-tunnel data obtained with the RC(1)-10 airfoil, the lower-surface leading-edge region was modified twice by reducing the ordinates of the lower surface forward of 25 percent chord. As mentioned in the Introduction, this was done to reduce the drag coefficient at Mach numbers significantly less than that for drag divergence and at zero and negative normal-force coefficients. The initial and modified coordinates are compared in figure 1(b) and table II, and a complete set of coordinates for the modified sections are presented in tables III and IV.

The model was machined from a stainless-steel block and had a surface finish of  $0.813 \mu\text{m}$  ( $0.000032 \text{ in.}$ ) (root-mean-square). The model had a chord and a span of  $15.24 \text{ cm}$  ( $6.00 \text{ in.}$ ) with a leading-edge orifice and with 22 orifices (table V) located on each surface in chordwise rows; the rows were positioned 12.5 percent span on either side of the midspan. Slots were milled in the airfoil surface, and tubes were placed in the slots and covered with epoxy to restore the airfoil profile. The orifices were then drilled from the metal side of the model to the embedded tubes so there were no surface irregularities near the orifice row. The orifices had diameters of  $0.0508 \text{ cm}$  ( $0.020 \text{ in.}$ ) and were drilled perpendicular to the local surface. The models were mounted to circular end plates which were flush with the tunnel walls.

#### Wind Tunnel

Tunnel description.— The Langley 6- by 28-Inch Transonic Tunnel (ref. 4) is a blowdown wind tunnel with a slotted floor and ceiling having an open-area ratio of 0.125 and is generally operated at stagnation pressures from about 207 to 620 Pa (30 to 90 psia) and at Mach numbers from 0.35 to 0.90. At a stagnation pressure of 620 Pa, the maximum Reynolds number, based on a  $15.24\text{-cm}$  ( $6.00\text{-in.}$ ) chord, varies from  $7.2 \times 10^6$  at a Mach number of 0.35 to  $14.2 \times 10^6$  at a Mach number of 0.90. Mach number is controlled by hydraulically actuated choker doors located downstream of the test section. The airfoil model spans the  $15.24\text{-cm}$  ( $6.00\text{-in.}$ ) width of the tunnel (fig. 3) and is rigidly attached by mounting tangs to two circular end plates which are driven by a hydraulic actuator to position the airfoil at the desired angle of attack. A test run usually consists of an angle-of-attack sweep at a constant Mach number and Reynolds number.

Two-dimensionality of flow.— The results of an earlier investigation of rotorcraft airfoils in the Langley 6- by 28-Inch Transonic Tunnel (ref. 5) have shown that the indicated maximum normal-force coefficient is reduced by tunnel sidewall boundary-layer influences. This is characteristic of two-dimensional wind tunnels without proper sidewall boundary-layer control.

A comparison of the NACA 0012 data measured in this facility (ref. 5) with unpublished data from two other facilities has been useful in indicating the magnitude of the maximum normal-force coefficient losses. The facilities are the Langley Low-Turbulence Pressure Tunnel and the United Technologies Research Center 8-foot tunnel. At similar Reynolds numbers and at a Mach number of 0.36, the maximum normal-force coefficients measured are about 0.15 higher than those from the Langley 6- by 28-Inch Transonic Tunnel. The difference between the data from the Langley 6- by 28-Inch Transonic Tunnel and the United Technologies data decreases to 0.10 at a Mach number of about 0.55. The same trends could reasonably be expected for other airfoil sections, although the numerical increments may be different.

An investigation conducted in the Office National d'Études et de Recherches Aéronautiques (ONERA) R1 Ch wind tunnel (ref. 6) has shown that the tunnel sidewall boundary layer can affect the normal-force coefficients at all angles of attack (that is, with either attached or separated boundary layers). In the investigation of reference 6, the sidewall boundary-layer thickness was varied by applying sidewall suction upstream of the model while the Mach number and Reynolds number were held constant. Generally, an increase in sidewall boundary-layer thickness resulted in a decrease in the normal-force coefficient at a given angle of attack.

Although some progress has been made toward an understanding of the influences of the tunnel sidewall boundary layer on airfoil test results (refs. 7 and 8), the state of the art does not permit a general correction of two-dimensional wind-tunnel data to account for these influences. Because of this, test results in this report are compared (as appropriate) to those for the NACA 0012 airfoil tested in the same wind tunnel (ref. 5) at comparable Reynolds numbers.

### Apparatus

Wake-survey probe.- A traversing wake-survey probe is cantilevered from one tunnel sidewall to measure the profile drag of the airfoils. The probe vertical sweep rate, which was selected after experimental determination of acceptable lag time in the pressure measurements, was about 2.54 cm/sec (1.00 in/sec).

The probe (fig. 3) was located 1.67c (based on the 15.24-cm (6.00-in.) chord model) downstream of the airfoil trailing edge. Data are acquired with four total-pressure tubes, which are made of stainless-steel tubing with a 1.53-mm (0.060-in.) outside diameter, a 1.02-mm (0.040-in.) inside diameter, and are spaced 0.953 cm (0.375 in.) apart laterally as shown in figure 4.

Instrumentation.- All measurements were obtained with a high-speed, computer-controlled digital data acquisition system and were recorded by a high-speed tape recording unit (ref. 4). All free-stream conditions were determined from stagnation and static pressures. All airfoil surface pressures and all wake pressures were measured with precision capacitive potentiometer pressure transducers. The electrical outputs from each of these transducers were connected to individual autoranging signal conditioners which have seven available ranges. The output signals from the four signal conditioners measuring the wake pressures were filtered with 20-Hz low-pass filters before input to the data acquisition system; the range of frequencies to be passed was experimentally determined during a previous investigation. The geometric angle of attack was determined from the output of a digital shaft encoder attached to a pinion engaging a rack on one model support end plate.

### Tests and Methods

The tests of the RC(1)-10 and RC(1)-10 Mod 1 configurations were made at a constant stagnation pressure at Mach numbers from 0.35 to 0.90. These conditions resulted in Reynolds numbers of  $5.1 \times 10^6$  and  $9.6 \times 10^6$  at the lowest and highest test Mach numbers. The RC(1)-10 Mod 1 and Mod 2 were tested at Reynolds numbers from about  $5.0 \times 10^6$  to  $13.9 \times 10^6$  for the same Mach number range. The higher Reynolds numbers are near the maximum of the 6- by 28-Inch Wind Tunnel with a 15.24-cm-chord model and represent possible flight values for some helicopter rotor configurations. Geometric angles of attack ranged from  $-4.0^\circ$  to  $14.0^\circ$  in  $2.0^\circ$  increments at the lower

test Mach numbers; this range was decreased at the higher test Mach numbers. The RC(1)-10 airfoil was tested with both a smooth surface and with a narrow strip of No. 220 carborundum grit applied to the upper and lower surfaces to assure boundary-layer transition. The grit size was determined by the method of reference 9. The 1.2-mm (0.047-in.) wide grit strip was centered at 8.8 percent chord. The density of the grit coverage was about 5 to 10 percent.

Section normal-force and pitching-moment coefficients were calculated from the airfoil surface pressures by a trapezoidal integration of the pressure coefficients. Each of the pressure coefficients represents the average of five measurements obtained in a 1.0-sec interval. A form of the equation described in reference 10 was used to calculate the point-drag coefficients from the measured wake pressures, and a trapezoidal integration of the point-drag coefficients was used to calculate the drag coefficient. The static pressures used in the wake-drag calculation were measured with tunnel sidewall orifices located at the same longitudinal tunnel station as the tips of the tubes on the wake-survey probes. All of the drag coefficients represent the mean of the measurements made with four total-pressure tubes on the wake-survey probe in one sweep through a wake.

The corrections for lift interference (ref. 11), which have been applied to the angles of attack, are given by the equations that follow:

$$\alpha_c = \alpha + \Delta\alpha$$

where

$$\Delta\alpha = -c_n c (0.1876)$$

where  $c$  is the airfoil chord in centimeters,  $\alpha$  is the angle of attack in degrees,  $c_n$  is the section normal-force coefficient, and the constant (0.1876) is in degrees per centimeter.

The analysis of reference 7 indicates that  $\Delta\alpha$  should be about  $-c_n c (0.1624)$ . However, the earlier value of reference 11 has been used herein to be consistent with previous data published from this facility. Reference 8 also indicates that there may be a small Mach number correction to which all two-dimensional wind-tunnel data are subject. This Mach number correction has not been applied.

## PRESENTATION OF RESULTS

The results of this investigation have been reduced to coefficient form and are presented as follows:

### Force- and moment-coefficient data

Figure

Aerodynamic characteristics of RC(1)-10 airfoil . . . . .	5
Aerodynamic characteristics of RC(1)-10 Mod 1 airfoil . . . . .	6
Aerodynamic characteristics of RC(1)-10 Mod 2 airfoil . . . . .	7



Variation of maximum section normal-force coefficient with Mach number for RC(1)-10, RC(1)-10 Mod 1, RC(1)-10 Mod 2, NACA 0012, and 10-64C airfoils . . . . .	8
Variation in section pitching-moment coefficient at zero normal-force coefficient with Mach number . . . . .	9
Variation in section profile-drag coefficient with Mach number for RC(1)-10 and 10-64C airfoils . . . . .	10
Comparison of RC(1)-10 and 10-64C airfoil section normal-force coefficient at drag-divergence Mach number . . . . .	11
Variation of experimental and theoretical section wave-drag coefficient with Mach number for RC(1)-10 airfoil . . . . .	12
Variation in theoretical section wave-drag coefficient with Mach number for RC(1)-10 and RC(1)-10 Mod 1 airfoils . . . . .	13
Variation in section profile-drag coefficient with Mach number for RC(1)-10 and RC(1)-10 Mod 1 airfoils . . . . .	14
Variation in section wave-drag coefficient with Mach number for RC(1)-10 Mod 1 and RC(1)-10 Mod 2 airfoils . . . . .	15
Variation in section profile-drag coefficient with Mach number for RC(1)-10 Mod 1 and RC(1)-10 Mod 2 airfoils . . . . .	16

#### Pressure distributions

Pressure distribution over RC(1)-10 airfoil . . . . .	17
Pressure distribution over RC(1)-10 Mod 1 airfoil . . . . .	18
Pressure distribution over RC(1)-10 Mod 2 airfoil . . . . .	19

### DISCUSSION OF RESULTS

#### Normal Force

The maximum normal-force coefficients  $c_{n,max}$  of the RC(1)-10 airfoil were obtained from the data of figure 5 and are summarized in figure 8. In this figure, results are presented as a function of Mach number (with free transition) along with data for the NACA 0012 airfoil (ref. 5) and the 10-64C airfoil (ref. 2) measured in the same facility. With free transition, the indicated  $c_{n,max}$  varies from 1.14 to 0.90 at Mach numbers from 0.35 to 0.65 for the RC(1)-10 airfoil. Within this Mach number range the maximum normal-force coefficient for the RC(1)-10 airfoil is from 0.02 to 0.16 greater than that of the NACA 0012 airfoil and from 0.06 to 0.16 greater than that for the 10-64C airfoil. As anticipated, the combined increase in camber and leading-edge radius has a favorable influence on  $c_{n,max}$  for the Mach number range of figure 8.

The addition of roughness at 8.8 percent chord had little influence on the maximum normal force of the RC(1)-10 airfoil (fig. 5). This result was not expected, based on results for the 10-64C and NACA 0012 airfoils. For those airfoils, the addition of roughness decreased  $c_{n,max}$  about 0.01 to 0.04 (refs. 2 and 5). In reference 2, the influence of roughness on the 10-64C airfoil was attributed to thickening of the upper-surface boundary layer, which was believed to be turbulent at a point forward of the roughness. For the present case, it is possible that the natural boundary-layer transition (laminar bubble which reattaches as a turbulent boundary layer) is at the roughness location and has little influence on the subsequent boundary-layer thickness. With or without roughness, the normal-force curves

indicate a gradual stall, and the static-pressure plateau in the trailing-edge region (fig. 17) suggests a stall of the trailing-edge type.

An analysis of the static-pressure distributions at  $M = 0.35$  (fig. 17(a)) also indicates subcritical flow at all orifice locations at  $c_{n,max}$ . Therefore, at  $M = 0.35$  and below, the  $c_{n,max}$  is determined only by the viscous influences. At a stream Mach number of 0.41 (fig. 17(b)), a local Mach number as great as 1.25 was calculated at  $c_{n,max}$  ( $\alpha_c = 9.2^\circ$ ). Therefore, the observed decrease in  $c_{n,max}$  is a result of the combined effects of compression or shock waves, which terminate the supercritical-flow region and thicken the boundary layer. At stream Mach numbers of about 0.50 to 0.65, an analysis of the static-pressure distributions (fig. 17) indicates maximum local Mach numbers between 1.5 and 1.6 at  $c_{n,max}$ .

The lower-surface leading-edge region modifications described earlier have little influence on  $c_{n,max}$  (figs. 6(a), 7(a), and 8) and also have little influence on the surface static pressures at angles of attack near  $c_{n,max}$  (figs. 17, 18, and 19). Also, the variations in Reynolds number in figure 6 have only a small influence on  $c_{n,max}$  for the RC(1)-10 Mod 1 configuration (fig. 8).

#### Pitching Moment

The pitching-moment coefficient about the aerodynamic center  $c_{m,o}$  (coefficient at zero normal force) of the basic RC(1)-10 airfoil is about -0.020 to -0.025 at Mach numbers from 0.35 to 0.55 (figs. 5(b) and 9). At Mach numbers of 0.50 and below, an analysis of the static-pressure distributions (fig. 17) indicates that the flow about the RC(1)-10 airfoil is subcritical at all orifice locations at zero normal force; the onset of supercritical flow with increasing stream Mach number (at zero normal force) occurs in the lower-surface leading-edge region at a Mach number near 0.55. The supercritical flow results in a change in the pitching-moment coefficient about the aerodynamic center from about -0.025 at  $M = 0.55$  to about -0.045 at  $M = 0.89$  with natural transition. The slopes of the pitching-moment curves of figure 5(b) are positive, indicating a forward movement of the center of pressure with positive increasing normal-force coefficient and an aerodynamic center forward of the quarter-chord. The development of supercritical flow results in an increase in slope of the curves (compared with  $M = 0.35$  to  $M = 0.50$ ), indicating a more rapid forward movement of center of pressure with increasing normal-force coefficient. The addition of roughness to the RC(1)-10 airfoil generally had little influence on pitching moment except at near maximum normal-force coefficient (fig. 5(b)).

The pitching-moment coefficient about the aerodynamic center is about 0.01 less negative for the RC(1)-10 Mod 1 configuration than for the RC(1)-10 configuration at Mach numbers from about 0.35 to 0.79 (figs. 5(b), 6(b), and 9). An analysis of the static-pressure distributions (figs. 17 and 18) indicates that the change in pitching-moment coefficient results from less negative pressure coefficients in the lower-surface leading-edge region where the airfoil-section modifications were made. The modification from the RC(1)-10 to the RC(1)-10 Mod 1 has little influence on the pitching-moment coefficient about the aerodynamic center at Mach numbers of about 0.84 and 0.88 (fig. 9).

Generally, neither the increase in Reynolds number (fig. 6(b)) nor the shape change from the RC(1)-10 Mod 1 to the RC(1)-10 Mod 2 configuration has a significant

influence on pitching-moment coefficient (figs. 6(b), 7(b), and 9). Although not shown in figure 9, the pitching-moment coefficients of the RC(1)-10 Mod 2 and the 10-64C (ref. 2) are generally equal.

### Drag Coefficient

Minimum drag coefficient.- The minimum section profile-drag coefficient  $c_d$  of the RC(1)-10 airfoil with natural transition (fig. 5(c)) occurs at a normal-force coefficient of about 0.2, which is included in the plot of  $c_d$  as a function of Mach number in figure 10. The minimum  $c_d$  is about constant at 0.0065 for Mach numbers up to 0.69 and is about equal to that of the NACA 0012 airfoil (not shown) tested in the same facility (ref. 5). An analysis of the static-pressure coefficients (fig. 17) indicates that sonic velocity is reached on the lower surface (at 0.025c) at a stream Mach number of 0.65 ( $\alpha_c = -0.5$ , the angle for minimum measured drag coefficient), and that supercritical flow is indicated at a Mach number of 0.69. As the supercritical-flow region expands, the minimum drag coefficient increases to 0.0075 at a Mach number of 0.75 and then increases more rapidly at Mach numbers from 0.79 to 0.84.

The addition of the fixed transition strip to the airfoil surface increases the minimum drag about 0.0010 to 0.0015 at Mach numbers from 0.35 to 0.79 due to earlier boundary-layer transition and/or thickening of the turbulent boundary layer. At a Mach number of 0.84, the minimum drag is increased about 0.0025 by the transition strip; at  $M = 0.89$ , minimum drag is not identified.

Drag divergence.- The drag coefficients of figure 5(c) have been cross-plotted as a function of Mach number for several constant normal-force coefficients and the results are presented in figure 10. Arrows are located on the curves to indicate the drag-divergence Mach number  $M_{dd}$ , where  $M_{dd}$  is defined as  $dc_d/dM = 0.1$ . A summary of  $c_n$  as a function of  $M_{dd}$  is given in figure 11. Data for the 10-64C airfoil (ref. 2) are also included in figures 10 and 11 because, as noted in the Introduction, one objective of the RC(1)-10 airfoil design was to maintain as much of the favorable drag characteristics of the 10-64C airfoil as possible while increasing the maximum lift coefficient at Mach numbers to about 0.50.

The greatest difference in the drag characteristics of the two airfoils is indicated at a normal-force coefficient of -0.2 (fig. 10). An analysis of the pressure distributions of the RC(1)-10 airfoil at a normal-force coefficient of about -0.2 indicates supercritical flow in the lower-surface leading-edge region at stream Mach numbers equal to or greater than 0.45. Therefore, the indicated increase in section profile-drag coefficient for the RC(1)-10 airfoil at Mach numbers greater than 0.50 (fig. 10) is related, at least in part, to shock-wave/boundary-layer interaction in the supercritical-flow region.

At  $c_n = 0$ , the difference in section profile-drag coefficients between the RC(1)-10 and 10-64C airfoils (fig. 10) is significant but less than that at  $c_n = -0.2$ . Although the drag coefficients are higher for the RC(1)-10 airfoil than the 10-64C at Mach numbers greater than 0.60, the drag-divergence Mach numbers ( $dc_d/dM = 0.1$ ) of the two airfoils are about equal (fig. 11). An analysis of the RC(1)-10 static-pressure coefficients indicates supercritical flow in the lower-surface leading-edge region at stream Mach numbers near 0.55 and greater compared with the previously noted 0.45 at  $c_n = -0.2$ . The resulting influence of shock-wave/boundary-layer interaction on drag coefficient is greater at  $c_n = -0.2$  than that at  $c_n = 0$ .

As the normal-force coefficient is increased to 0.2 and 0.4, the difference in section profile-drag coefficients between the RC(1)-10 and the 10-64C airfoils approaches zero (fig. 10), so the drag-divergence Mach numbers are about equal (fig. 11). At  $c_n = 0.6$ , the RC(1)-10 airfoil again has a higher drag coefficient (fig. 10) and a lower drag-divergence Mach number (fig. 11). An analysis of the pressure distributions of the two airfoils at Mach numbers greater than 0.65 (fig. 17 and ref. 2) indicates higher local Mach numbers followed by shock waves for the RC(1)-10 airfoil, which results in the higher drag. At  $c_n = 0.8$ , the drag increase with Mach number (fig. 10) occurs at a higher Mach number for the RC(1)-10 airfoil, but because of the shape of the curves the drag-divergence Mach number is still lower than that of the 10-64C airfoil (fig. 11). In this case, the lift-curve slope is near constant ( $M \approx 0.63$ ) for the RC(1)-10 airfoil (fig. 5(a)), but not for the 10-64C airfoil (ref. 2). This result indicates the onset of boundary-layer separation for the latter airfoil, which results in an increase in drag coefficient. It is interesting to note that at this normal-force coefficient (0.8), the pressure distributions (fig. 17 and ref. 2) indicate a more severe pressure rise for the 10-64C airfoil at Mach numbers of about 0.55 to 0.68. The more severe pressure rise would contribute to the boundary-layer separation.

Comparison with theory.- Because of the unexpected level of drag observed at normal-force coefficients of -0.2 and 0, an analysis was made using the theoretical method of reference 3. Figure 12 presents both experimental and theoretical section wave-drag coefficients as a function of Mach number for  $c_n = -0.2$  and  $c_n = 0$ . Wave drag is defined herein as the difference between the subcritical-flow ( $M < 0.45$ ) drag coefficient and the drag coefficient at supercritical-flow Mach numbers. At Mach numbers of 0.79 and below, the experimental wave-drag coefficient is at least double the predicted value and the corresponding drag-divergence Mach numbers are 0.56 for the experimental and 0.83 for the predicted data. An analysis of the pressure distributions at normal-force coefficients near -0.2 ( $\alpha_c \approx -3.5$ , fig. 17) indicates lower-surface supercritical flow at Mach numbers greater than 0.45. The supercritical flow is terminated by a supersonic compression-wave system instead of by a discrete shock wave at the maximum local Mach number.

Theory predicts more negative pressure peaks than measured values followed by a more rapid pressure rise. This theoretical method does not account for a laminar boundary-layer displacement thickness or the presence of a laminar separation bubble in the boundary-layer transition region. It seems possible that the boundary layer in the supercritical-flow region of the lower-surface leading edge has a primary influence on the differences between the theoretical and experimental drag coefficients at  $c_n = -0.2$  shown in figure 12.

Section modification.- As previously noted, an analysis of the pressure distributions of the RC(1)-10 airfoil at  $c_n = -0.2$  and  $c_n = 0$  indicates supercritical flow in the lower-surface leading-edge region that contributes to a significant drag increase. Additional analysis made by the techniques of reference 3 indicates that the influence of supercritical flow on drag coefficient could be decreased by modifying the airfoil shape in this region (fig. 13). As previously noted, the modification consisted of decreasing the airfoil thickness in the lower-surface leading-edge region (fig. 1 and table II), and the airfoil is designated as the RC(1)-10 Mod 1 airfoil. This airfoil was investigated at about the same Reynolds numbers (compare figs. 5 and 6) as the RC(1)-10 and at higher Reynolds numbers of possible interest for some helicopter applications. At  $c_n = -0.2$ , figure 6(c) indicates that the increase in Reynolds number generally results in a decrease in section profile-drag coefficient, apparently because of a decrease in boundary-layer thickness. At

$c_n = 0$  to  $c_n = 0.4$ , Reynolds number has little influence on drag coefficient. Then, at normal-force coefficients of 0.6 to near stall, an unexpected increase in drag coefficient is indicated with an increase in Reynolds number at Mach numbers below 0.64. This increase may be because of increases in stream turbulence level with increases in Reynolds number, resulting in increased thickness of the boundary layer. An increase in stream turbulence level with increases in Reynolds number has been indicated by unpublished drag-coefficient data from the Langley 6- by 28-Inch Transonic Tunnel.

The influence of the airfoil modification on section profile-drag coefficient is indicated in figure 14, where data from figures 5(c) and 6(c) for the RC(1)-10 and the RC(1)-10 Mod 1 airfoils are plotted as a function of Mach number. At  $c_n = -0.2$ , the RC(1)-10 Mod 1 airfoil data display an unexpected increase in section profile-drag coefficient compared with the RC(1)-10 airfoil data (fig. 14). An analysis of the pressure distribution data indicates that the drag increase over that for the unmodified airfoil results from increases in subcritical-flow boundary-layer thickness; that is, comparisons of the pressure distributions (figs. 17 and 18) indicate that the anticipated decrease in local Mach number results from the modification. For example, at a Mach number of 0.55, the maximum local Mach number of the modified airfoil was about 1.05 ( $C_p \approx -1.8$ ) compared with 1.35 ( $C_p \approx -2.75$ ) for the unmodified airfoil. The pressure distributions in the mid- and aft-chord regions of the airfoil are not significantly altered. Therefore, a longer separation bubble with boundary-layer reattachment is implied for the RC(1)-10 Mod 1 airfoil.

At  $c_n = 0$ , figure 14 shows that the section profile-drag coefficient has been reduced by the modification; the reduction is about 0.0045 at a Mach number of 0.80. (Note at  $c_n = 0$ , data for the RC(1)-10 Mod 1 airfoil at both Reynolds numbers are colinear.) It is interesting to note that the drag-divergence Mach number is decreased about 0.02 by the airfoil modification. Therefore, it is apparent that an increase in drag-divergence Mach number is not a unique factor in defining airfoil performance improvements if significant drag increases occur with increases in Mach number prior to drag divergence.

After the investigation of the RC(1)-10 Mod 1 airfoil, it was concluded by analysis (fig. 15) that the drag characteristics at zero normal force might be improved by a second modification of the airfoil (see table II), which is designated as RC(1)-10 Mod 2. The second modification also was accomplished by decreasing the airfoil thickness in the lower-surface leading-edge region. Section profile-drag coefficient data (fig. 7(c)) for the RC(1)-10 Mod 2 airfoil (taken at Reynolds numbers similar to the higher set of fig. 6) are cross-plotted in figure 16. As observed with the first modification, the second modification results in additional drag increases at a lower Mach number for  $c_n = -0.2$ . Apparently the increase results from boundary-layer influences similar to those previously discussed. At  $c_n = 0$ , the drag coefficients at Mach numbers above 0.60 are decreased compared with the RC(1)-10 Mod 1, and an increase in drag-divergence Mach number of about 0.01 is indicated (fig. 16). At higher normal-force coefficients, the modification has less influence on the drag coefficient.

## CONCLUSIONS

The RC(1)-10 airfoil, which was designed for helicopter rotor application, has been investigated in the Langley 6- by 28-Inch Transonic Tunnel at Mach numbers from about 0.35 to 0.90 and at Reynolds numbers from about  $5.0 \times 10^6$  to  $13.9 \times 10^6$ . The

airfoil has a thickness-to-chord ratio of 0.10 with maximum thickness located at 40 percent chord and maximum camber located at 27 percent chord. The airfoil was designed to increase the maximum normal-force coefficient while maintaining favorable drag-divergence characteristics and pitching-moment coefficients compared to the 10-64C airfoil investigated earlier in the same facility. Two modifications were also made to the RC(1)-10 airfoil contour in the lower-surface leading-edge region. An analysis of the data for the RC(1)-10 airfoil and a comparison of data for the two modified configurations have resulted in the following conclusions:

1. With free transition and at similar Reynolds numbers, the maximum normal-force coefficient of the RC(1)-10 airfoil varies from 1.14 to 0.90 at Mach numbers from 0.35 to 0.65; within this Mach number range, the maximum normal-force coefficient for the RC(1)-10 airfoil is from 0.06 to 0.16 greater than that of the 10-64C airfoil. Both the addition of fixed transition strips at 8.8 percent chord and the two modifications made to the lower-surface leading-edge region of the RC(1)-10 airfoil (RC(1)-10 Mod 1 and RC(1)-10 Mod 2) have little influence on the maximum normal-force coefficient.

2. The pitching-moment coefficient about the aerodynamic center of the RC(1)-10 airfoil is about -0.020 to -0.025 at Mach numbers from 0.35 to 0.55. The value increases to about -0.045 at a Mach number of 0.89. The coefficient of the RC(1)-10 Mod 1 is about 0.01 less negative at Mach numbers from 0.35 to 0.79. The shape change to the RC(1)-10 Mod 2 has little influence, and the coefficients are generally equal to those for the 10-64C airfoil.

3. The drag-divergence Mach number of the RC(1)-10 airfoil is about equal to that of the 10-64C airfoil at normal-force coefficients from 0 to 0.4. At normal-force coefficients from 0.4 to 0.8, the drag-divergence Mach number of the RC(1)-10 is less than that of the 10-64C airfoil.

4. The greatest difference in drag-divergence Mach number for the RC(1)-10 and 10-64C airfoils is at a normal-force coefficient of -0.2. This difference results from shock-wave/boundary-layer interaction influences near the lower-surface leading edge for the RC(1)-10 airfoil. The modifications made to the RC(1)-10 decrease the drag coefficient at zero normal-force coefficient at Mach numbers near drag divergence, but are less beneficial at a normal-force coefficient of -0.2.

Langley Research Center  
National Aeronautics and Space Administration  
Hampton, VA 23665  
November 24, 1981

#### REFERENCES

1. Bingham, Gene J.: An Analytical Evaluation of Airfoil Sections for Helicopter Rotor Applications. NASA TN D-7796, 1975.
2. Bingham, Gene J.; and Noonan, Kevin W.: Experimental Investigation of Three Helicopter Rotor Airfoils Designed Analytically. NASA TP-1396, AVRADCOM TR 79-11, 1979.
3. Bauer, F.; Garabedian, P.; and Korn, D.: A Theory of Supercritical Wing Sections, With Computer Programs and Examples. Volume 66 of Lecture Notes in Economics and Mathematical Systems, Springer-Verlag, 1972.
4. Ladson, Charles L.: Description and Calibration of the Langley 6- by 28-Inch Transonic Tunnel. NASA TN D-8070, 1975.
5. Noonan, Kevin W.; and Bingham, Gene J.: Two-Dimensional Aerodynamic Characteristics of Several Rotorcraft Airfoils at Mach Numbers From 0.35 to 0.90. NASA TM X-73990, 1977.
6. Bernard-Guelle, René: Influence of Wind Tunnel Wall Boundary Layers on Two-Dimensional Transonic Tests. NASA TT F-17,255, 1976.
7. Barnwell, Richard W.: Design and Performance Evaluation of Slotted Walls for Two-Dimensional Wind Tunnels. NASA TM-78648, 1978.
8. Sewall, W. G.: The Effects of Sidewall Boundary Layers in Two-Dimensional Subsonic and Transonic Wind Tunnels. AIAA-81-1297, June 1981.
9. Braslow, Albert L.; and Knox, Eugene C.: Simplified Method for Determination of Critical Height of Distributed Roughness Particles for Boundary-Layer Transition at Mach Numbers From 0 to 5. NACA TN 4363, 1958.
10. Baals, Donald D.; and Mourhess, Mary J.: Numerical Evaluation of the Wake-Survey Equations for Subsonic Flow Including the Effect of Energy Addition. NACA WR L-5, 1945. (Formerly NACA ARR L5H27.)
11. Davis, Don D., Jr.; and Moore, Dewey: Analytical Study of Blockage- and Lift-Interference Corrections for Slotted Tunnels Obtained by the Substitution of an Equivalent Homogeneous Boundary for the Discrete Slots. NACA RM L53E07b, 1953.

TABLE I.- DESIGN COORDINATES FOR RC(1)-10 AIRFOIL

[Stations and ordinates given in percent airfoil chord]

Upper surface		Lower surface	
Station	Ordinate	Station	Ordinate
0.00	0.00	0.00	0.00
.23	1.17	.77	-.94
.43	1.45	1.07	-1.09
.87	1.90	1.63	-1.29
1.54	2.42	2.46	-1.48
2.01	2.74	2.99	-1.55
2.48	3.01	3.52	-1.60
2.94	3.27	4.06	-1.63
3.43	3.51	4.57	-1.65
4.40	3.97	5.60	-1.66
5.42	4.38	6.58	-1.66
7.04	4.91	7.96	-1.67
9.68	5.52	10.32	-1.75
14.82	6.32	15.18	-1.92
19.91	6.80	20.09	-2.11
24.98	7.09	25.01	-2.30
30.05	7.24	29.95	-2.43
35.10	7.26	34.90	-2.66
40.12	7.18	39.88	-2.81
45.15	7.01	44.85	-2.91
50.16	6.74	49.84	-2.96
55.17	6.39	54.83	-2.95
60.16	5.96	59.84	-2.89
65.16	5.46	64.85	-2.76
70.14	4.89	69.86	-2.57
75.13	4.25	74.87	-2.31
80.11	3.54	79.89	-1.99
85.09	2.77	84.91	-1.61
90.06	1.94	89.94	-1.17
95.03	1.05	94.97	-.66
100.00	.10	100.00	-.10



TABLE II.- COMPARISON OF COORDINATES OF AIRFOILS  
IN REGION OF MODIFICATION

[Stations and ordinates given in percent airfoil chord]

Station	RC(1)-10	RC(1)-10 Mod 1	RC(1)-10 Mod 2
0.00	0.00	0.00	0.00
.77	-.94	-.66	-.57
1.07	-1.09	-.77	-.67
1.63	-1.29	-.93	-.82
2.46	-1.48	-1.07	-.99
2.99	-1.55	-1.14	-1.08
3.52	-1.60	-1.19	-1.14
4.06	-1.63	-1.24	-1.22
4.57	-1.65	-1.28	-1.27
5.60	-1.66	-1.36	-1.36
6.58	-1.66	-1.42	-1.42
7.96	-1.67	-1.50	-1.50
10.32	-1.75	-1.64	-1.64
15.18	-1.92	-1.88	-1.88
20.09	-2.11	-2.09	-2.09
25.01	-2.30	-2.30	-2.30

TABLE III.- DESIGN COORDINATES FOR RC(1)-10 MOD 1 AIRFOIL

[Stations and ordinates given in percent airfoil chord]

Upper surface		Lower surface	
Station	Ordinate	Station	Ordinate
0.00	0.00	0.00	0.00
.23	1.17	.77	-.66
.43	1.45	1.07	-.77
.87	1.90	1.63	-.93
1.54	2.42	2.46	-1.07
2.01	2.74	2.99	-1.14
2.48	3.01	3.52	-1.19
2.94	3.27	4.06	-1.24
3.43	3.51	4.57	-1.28
4.40	3.97	5.60	-1.36
5.42	4.38	6.58	-1.42
7.04	4.91	7.96	-1.50
9.68	5.52	10.32	-1.64
14.82	6.32	15.18	-1.88
19.91	6.80	20.09	-2.09
24.98	7.09	25.01	-2.30
30.05	7.24	29.95	-2.43
35.10	7.26	34.90	-2.66
40.12	7.18	39.88	-2.81
45.15	7.01	44.85	-2.91
50.16	6.74	49.84	-2.96
55.17	6.39	54.83	-2.95
60.16	5.96	59.84	-2.89
65.16	5.46	64.85	-2.76
70.14	4.89	69.86	-2.57
75.13	4.25	74.87	-2.31
80.11	3.54	79.89	-1.99
85.09	2.77	84.91	-1.61
90.06	1.94	89.94	-1.17
95.03	1.05	94.97	-.66
100.00	.10	100.00	-.10

TABLE IV.- DESIGN COORDINATES FOR RC(1)-10 MOD 2 AIRFOIL

[Stations and ordinates given in percent airfoil chord]

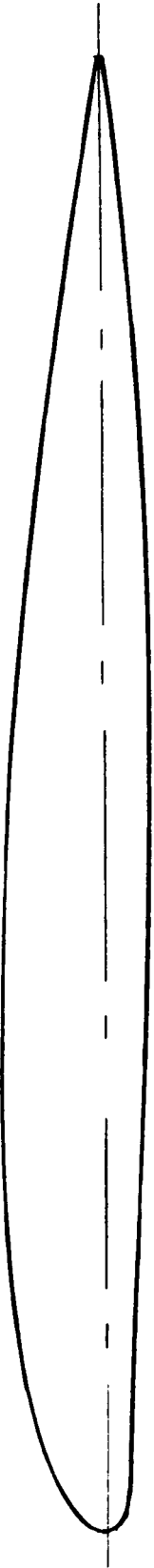
Upper surface		Lower surface	
Station	Ordinate	Station	Ordinate
0.00	0.00	0.00	0.00
.23	1.17	.77	-.57
.43	1.45	1.07	-.67
.87	1.90	1.63	-.82
1.54	2.42	2.46	-.99
2.01	2.74	2.99	-1.08
2.48	3.01	3.52	-1.14
2.94	3.27	4.06	-1.22
3.43	3.51	4.57	-1.27
4.40	3.97	5.60	-1.36
5.42	4.38	6.58	-1.42
7.04	4.91	7.96	-1.50
9.68	5.52	10.32	-1.64
14.82	6.32	15.18	-1.88
19.91	6.80	20.09	-2.09
24.98	7.09	25.01	-2.30
30.05	7.24	29.95	-2.43
35.10	7.26	34.90	-2.66
40.12	7.18	39.88	-2.81
45.15	7.01	44.85	-2.91
50.16	6.74	49.84	-2.96
55.17	6.39	54.83	-2.95
60.16	5.96	59.84	-2.89
65.16	5.46	64.85	-2.76
70.14	4.89	69.86	-2.57
75.13	4.25	74.87	-2.31
80.11	3.54	79.89	-1.99
85.09	2.77	84.91	-1.61
90.06	1.94	89.94	-1.17
95.03	1.05	94.97	-.66
100.00	.10	100.00	-.10

TABLE V.- STATIC-PRESSURE ORIFICE LOCATIONS

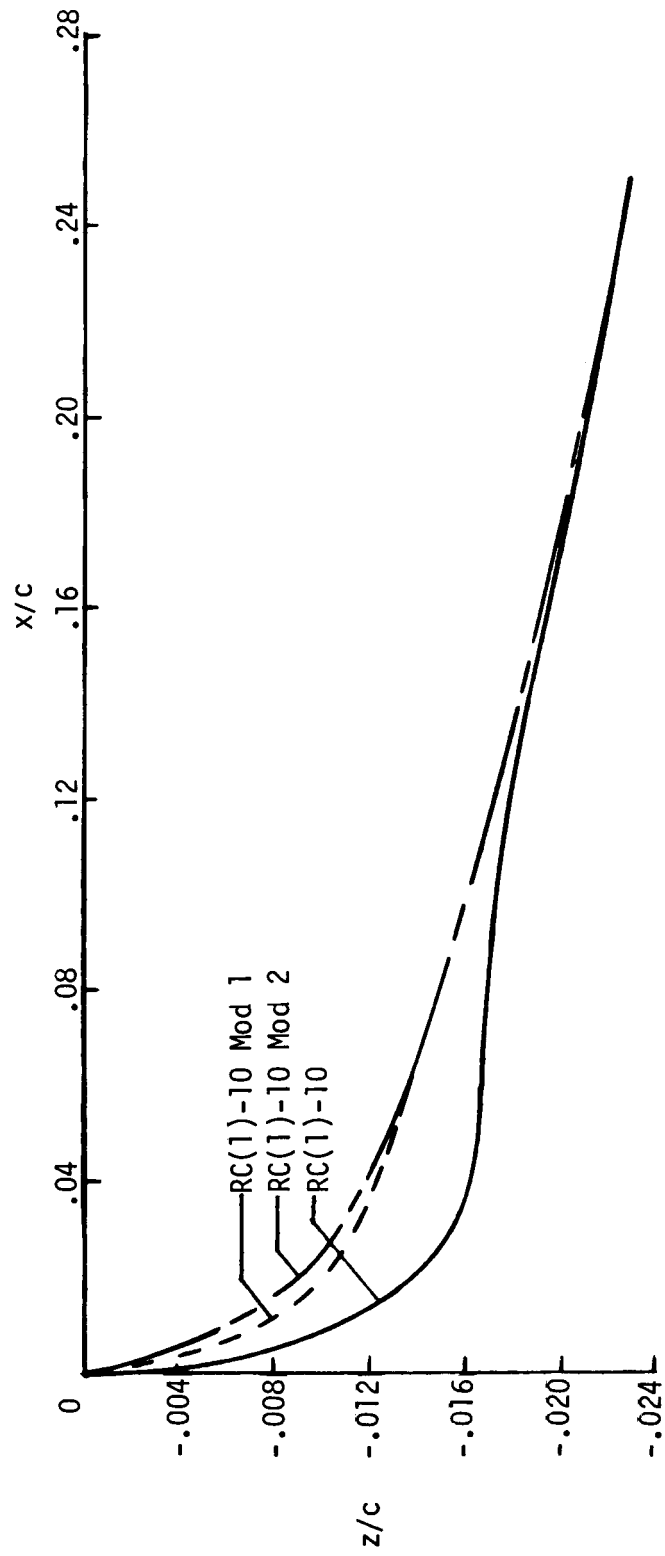
FOR RC(1)-10

[Locations given in percent airfoil chord]

Upper-surface station	Lower-surface station
0.03	
1.20	1.13
2.41	2.38
4.86	4.93
7.37	7.43
9.99	9.94
14.99	14.93
20.00	19.96
24.96	24.94
29.96	29.92
34.98	34.89
39.97	39.91
44.98	44.91
49.98	49.93
54.99	54.93
60.03	59.93
64.97	64.92
69.97	69.94
74.97	74.95
80.00	79.94
85.01	84.93
90.01	89.94
95.02	94.93



(a) RC(1)-10 airfoil profile.



(b) Lower-surface leading-edge profile.

Figure 1.- RC(1)-10 airfoil and lower-surface leading-edge profiles.

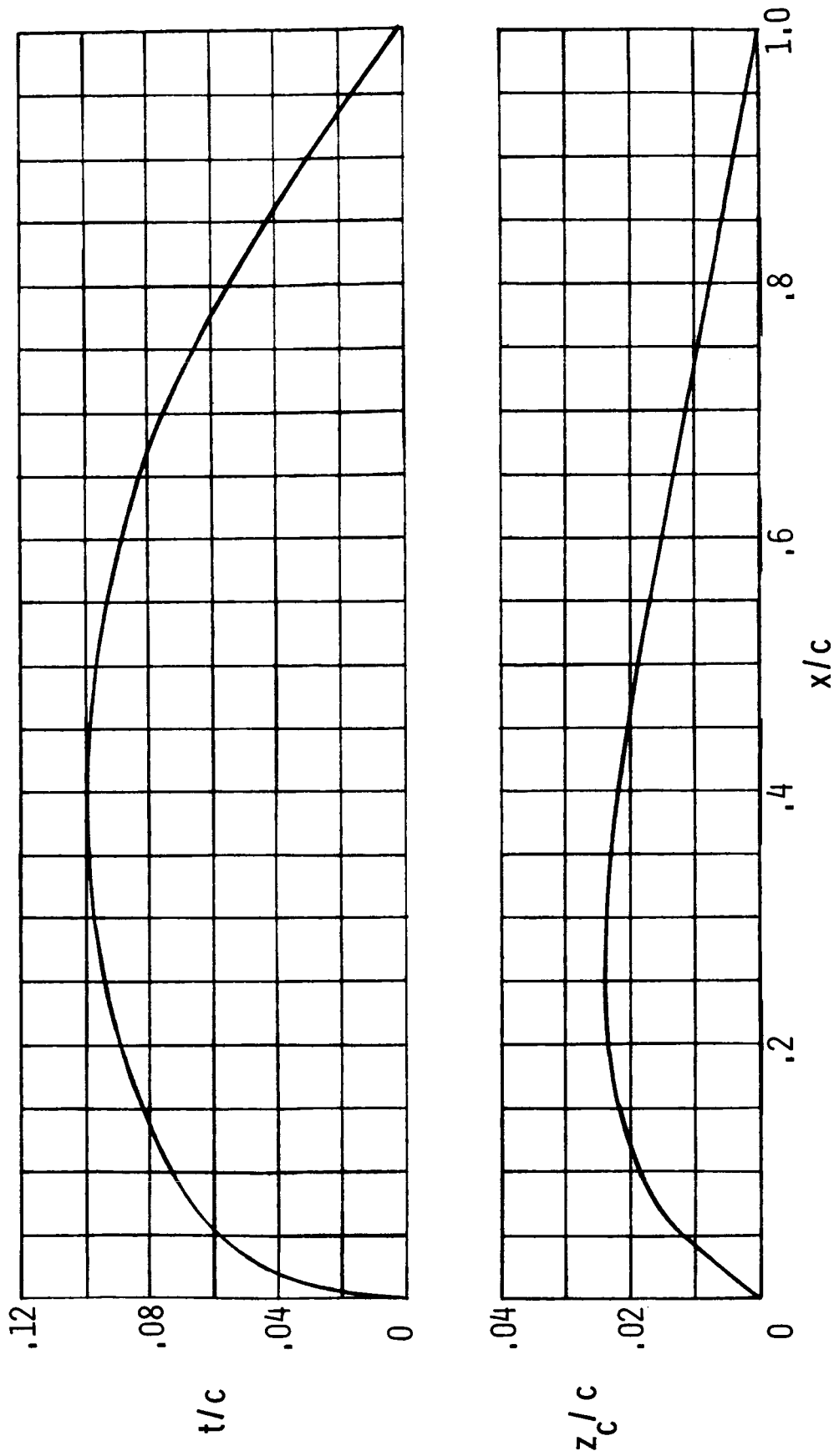


Figure 2.- RC(1)-10 thickness distribution and mean line.

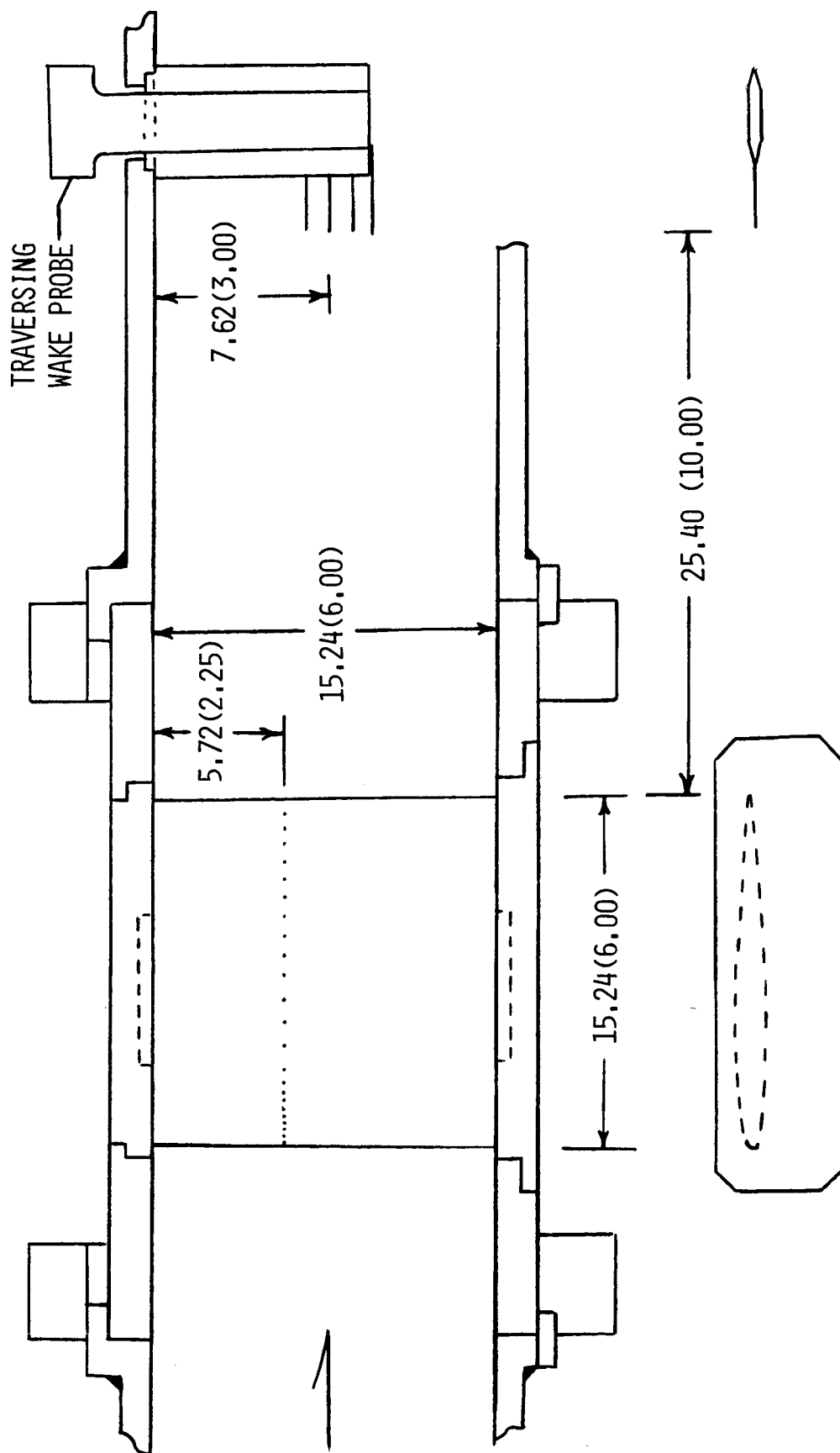


Figure 3.- Model and wake-survey probe installation in Langley 6- by 28-Inch Transonic Tunnel.  
All dimensions are in centimeters (inches).

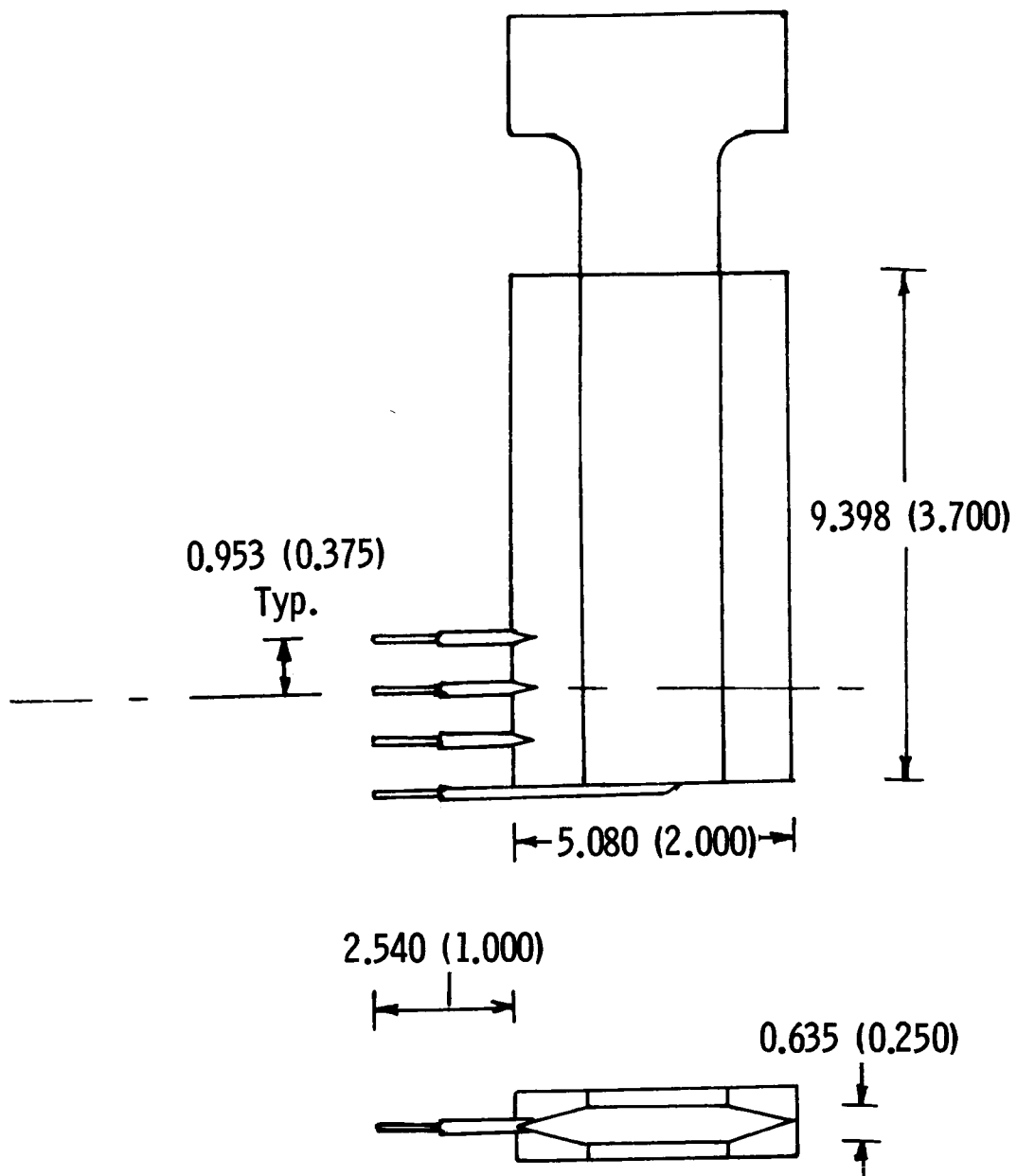
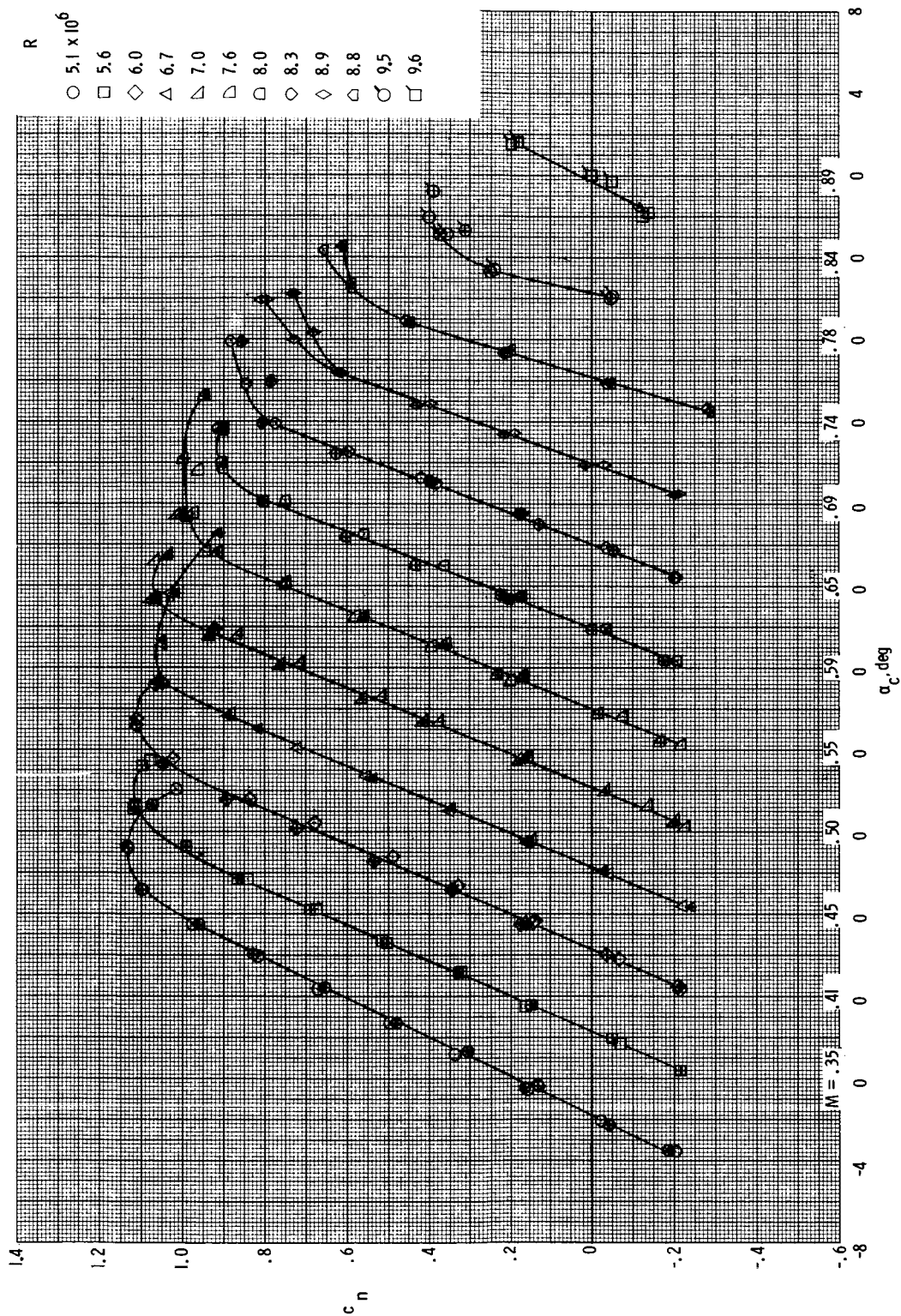


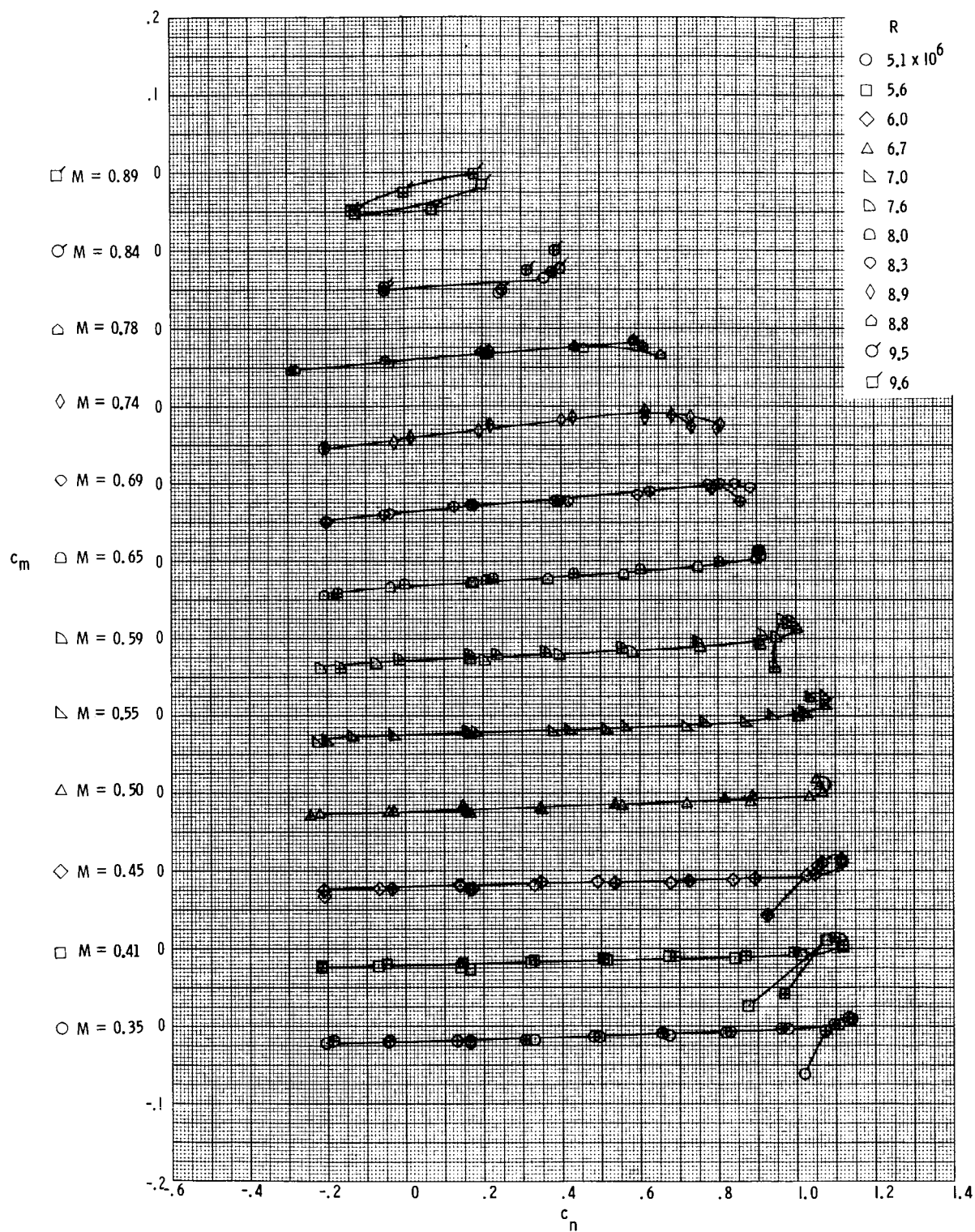
Figure 4.- Wake-survey probe used in 6- by 28-Inch Transonic Tunnel.  
All dimensions in centimeters (inches).





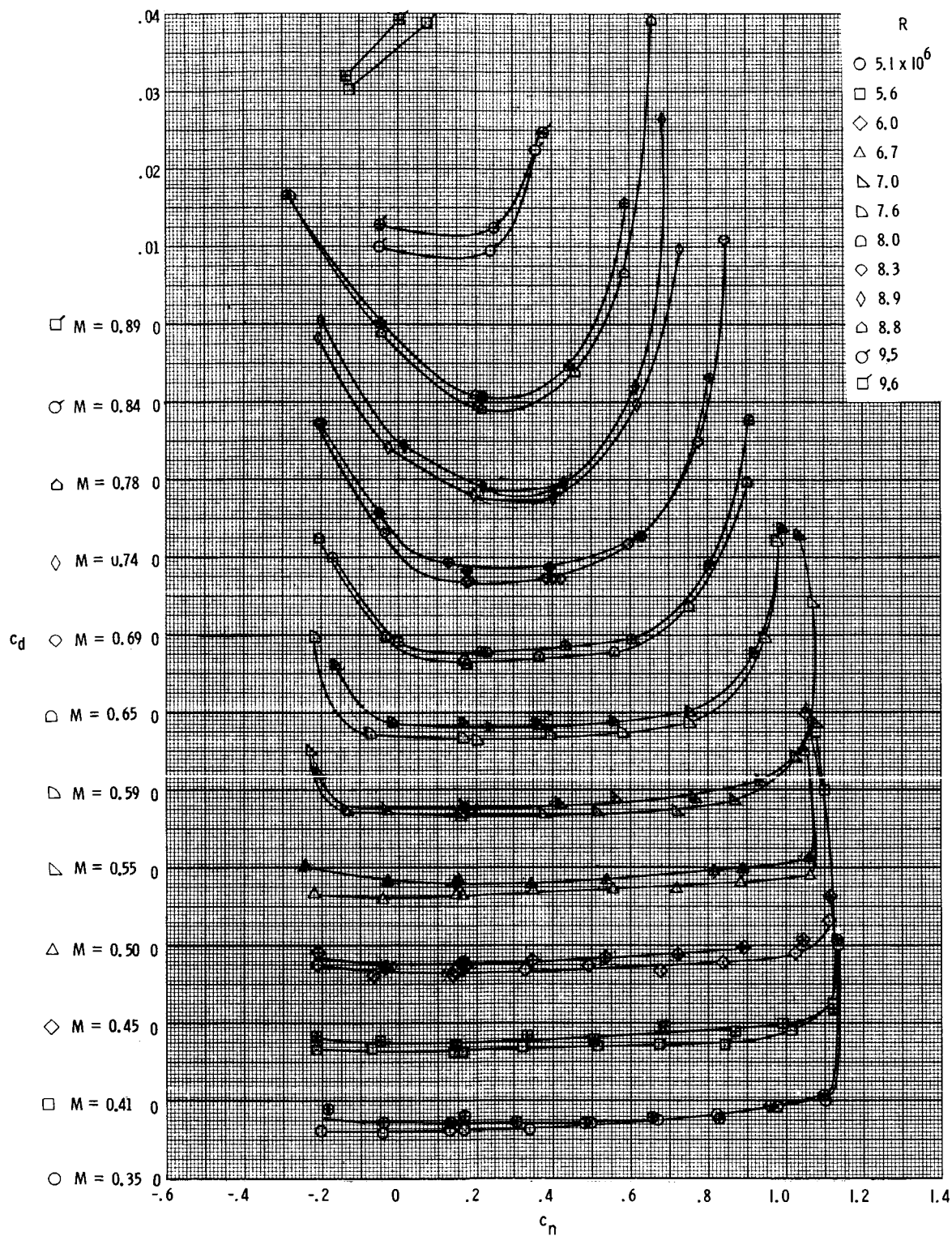
(a) Section normal-force coefficients.

Figure 5.- Aerodynamic characteristics of RC(1)-10 airfoil measured in Langley 6- by 28-Inch Transonic Tunnel. Open symbols indicate model surface smooth; centered symbols with a "+" inside indicate transition fixed.



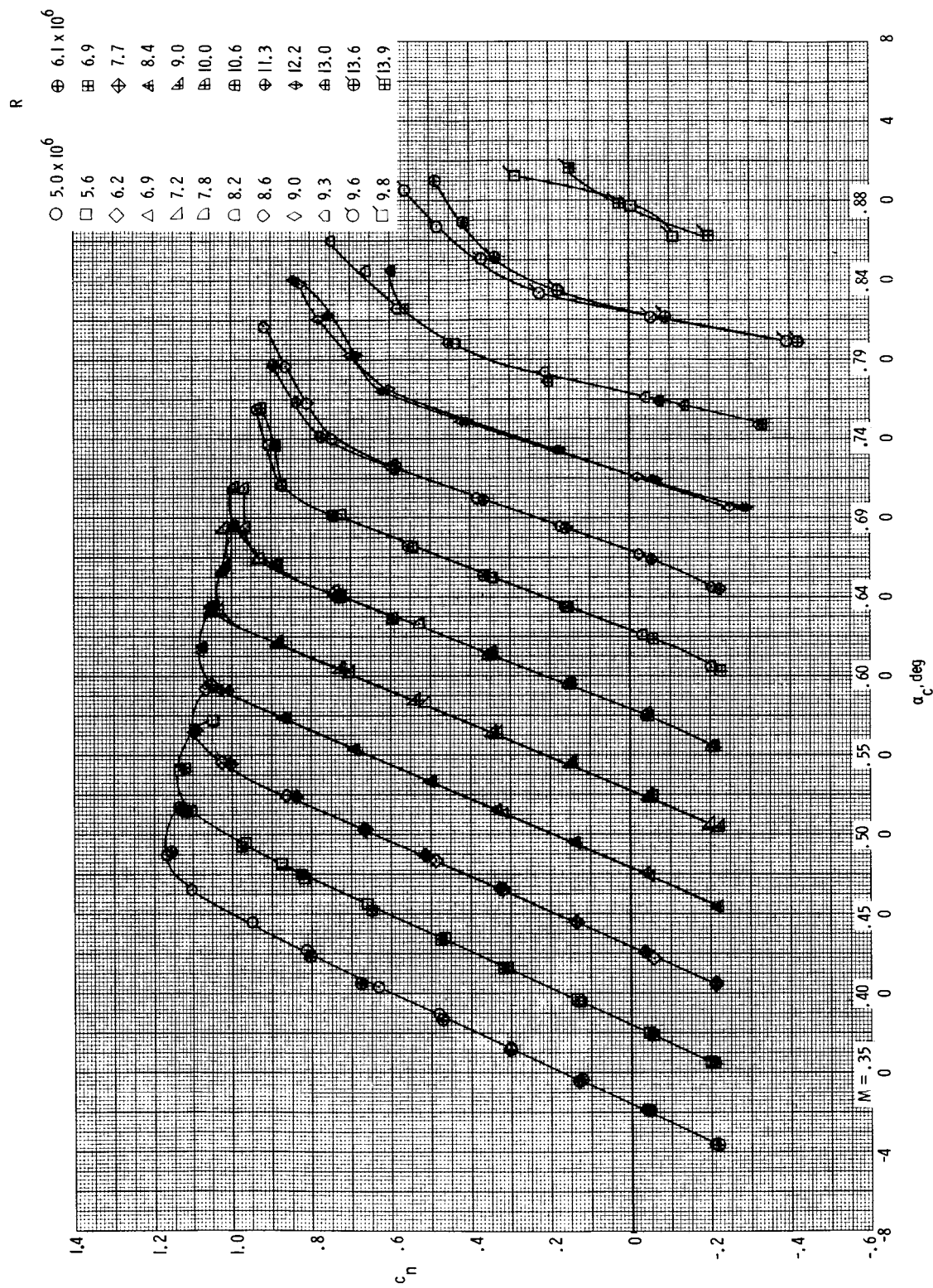
(b) Section pitching-moment coefficients.

Figure 5.- Continued.



(c) Section profile-drag coefficients.

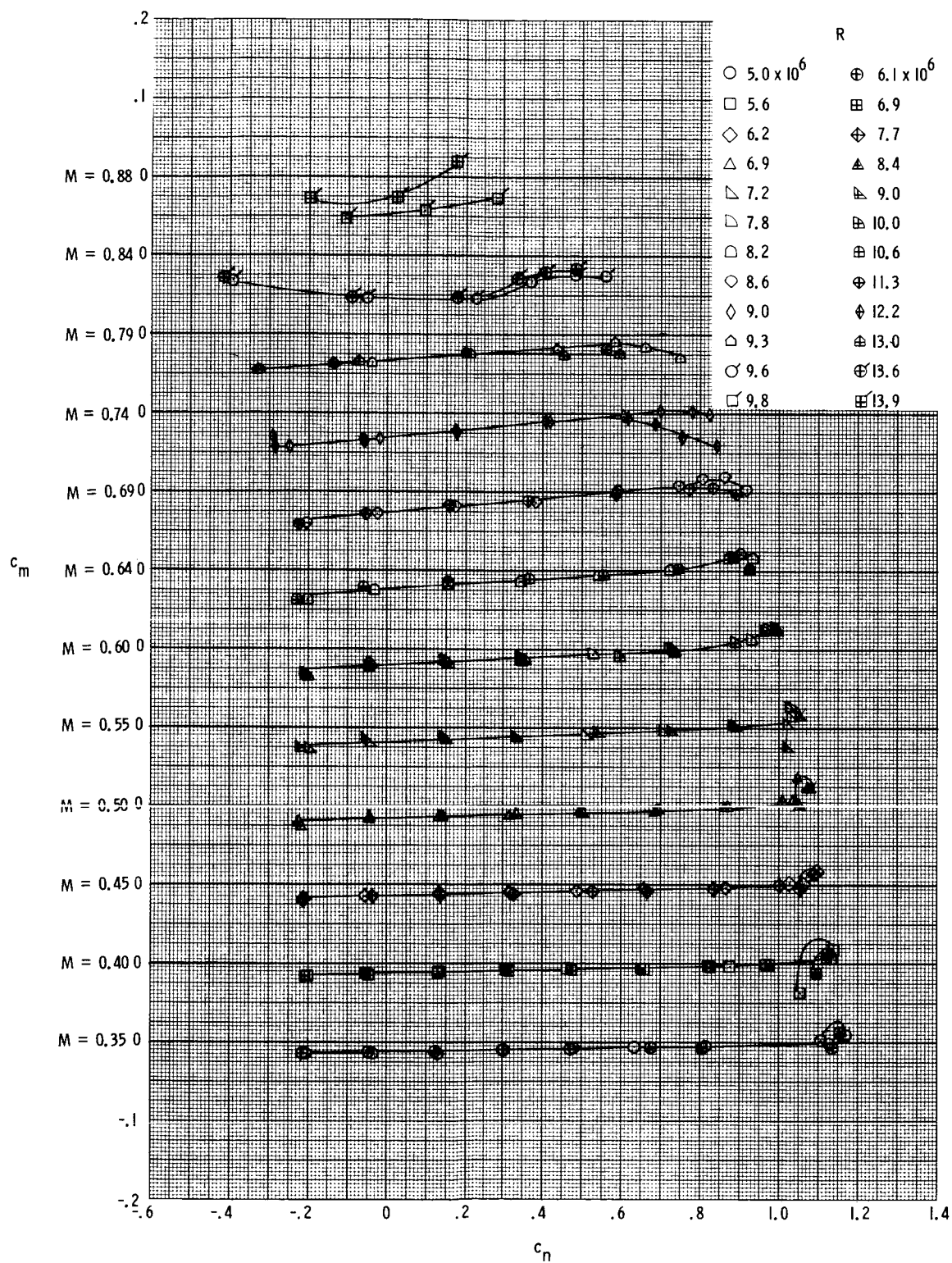
Figure 5.- Concluded.



(a) Section normal-force coefficients.

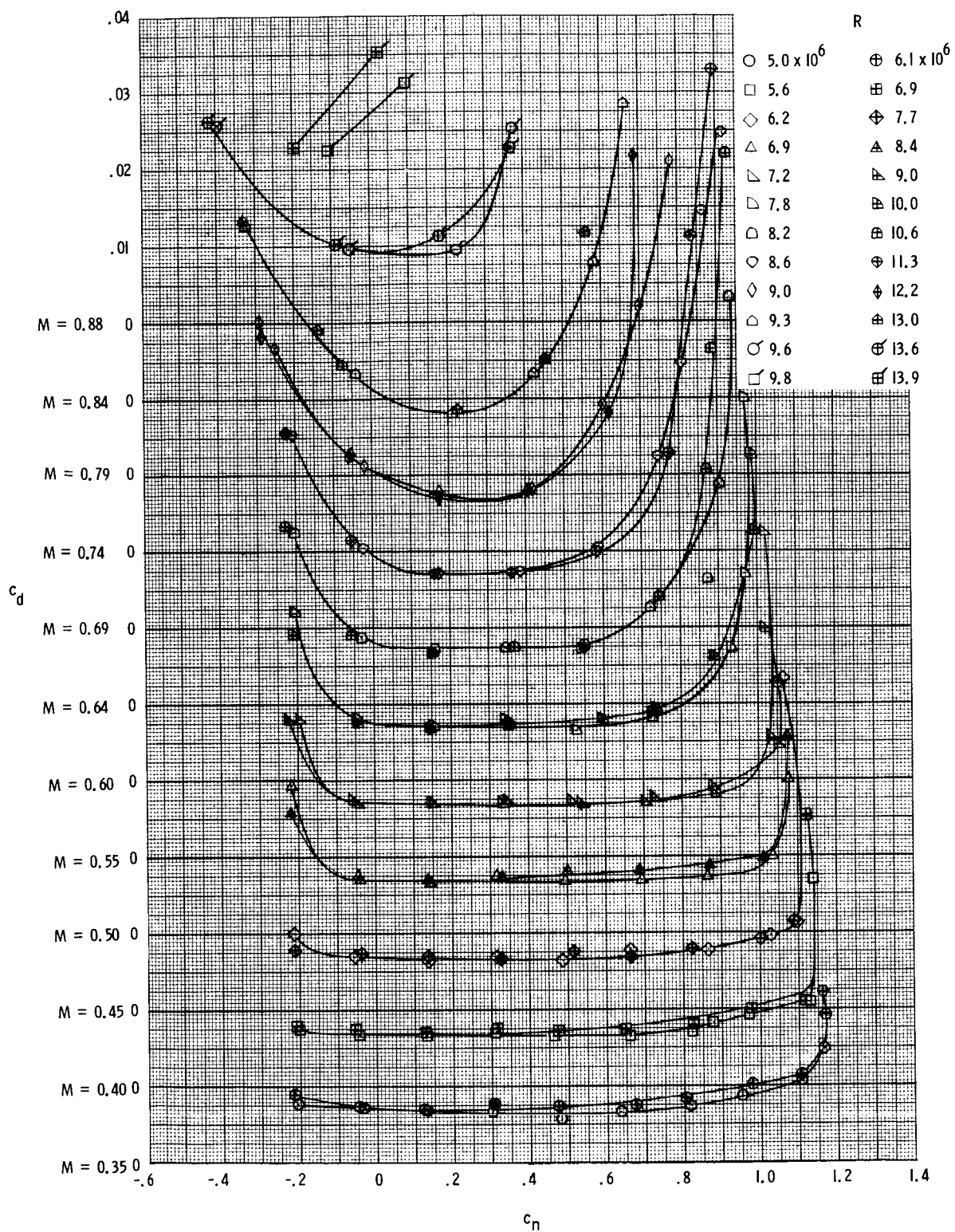
Figure 6.- Aerodynamic characteristics of RC(1)-10 Mod 1 airfoil measured in Langley 6- by 28-Inch Transonic Tunnel. Model surfaces smooth.





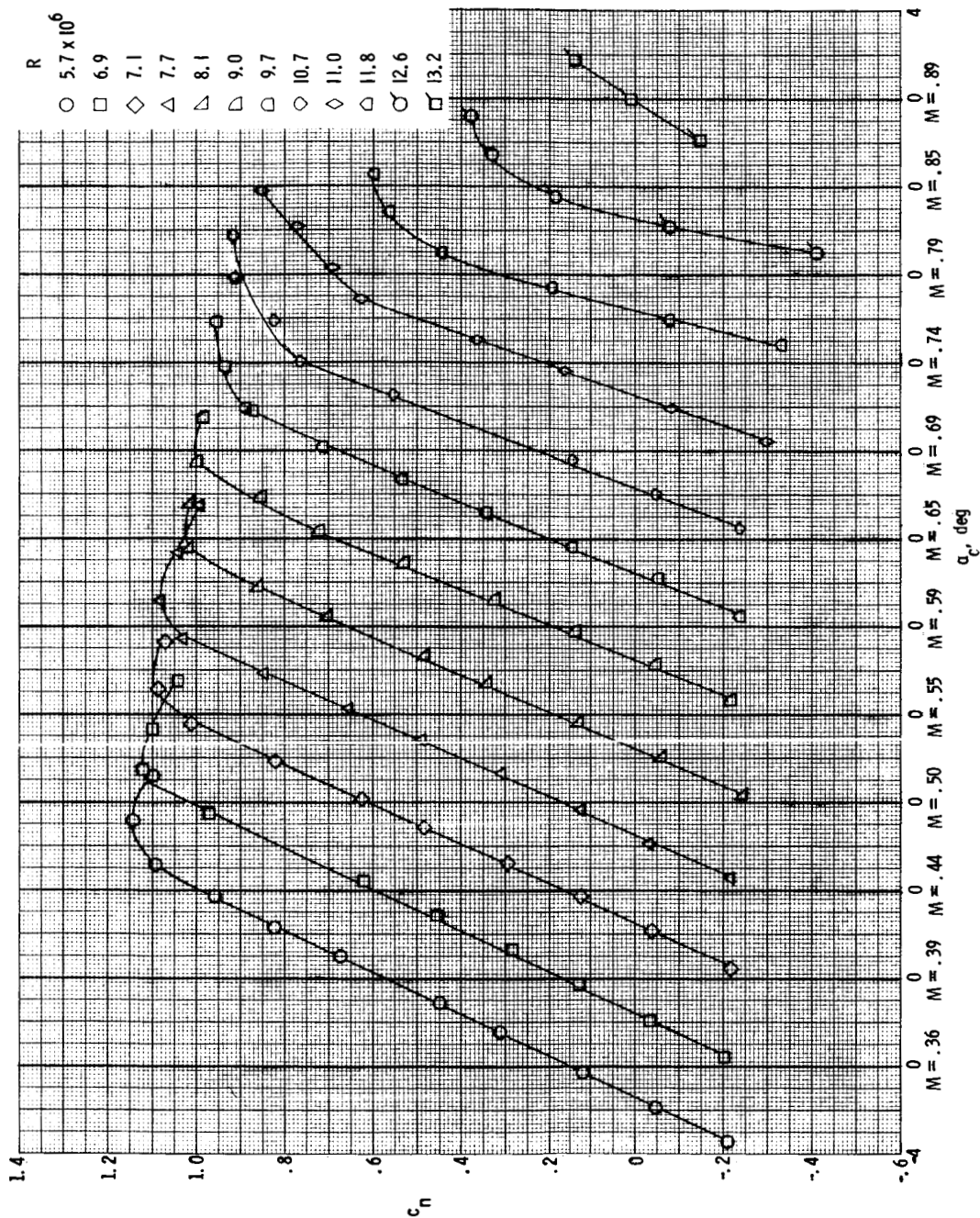
(b) Section pitching-moment coefficients.

Figure 6.- Continued.



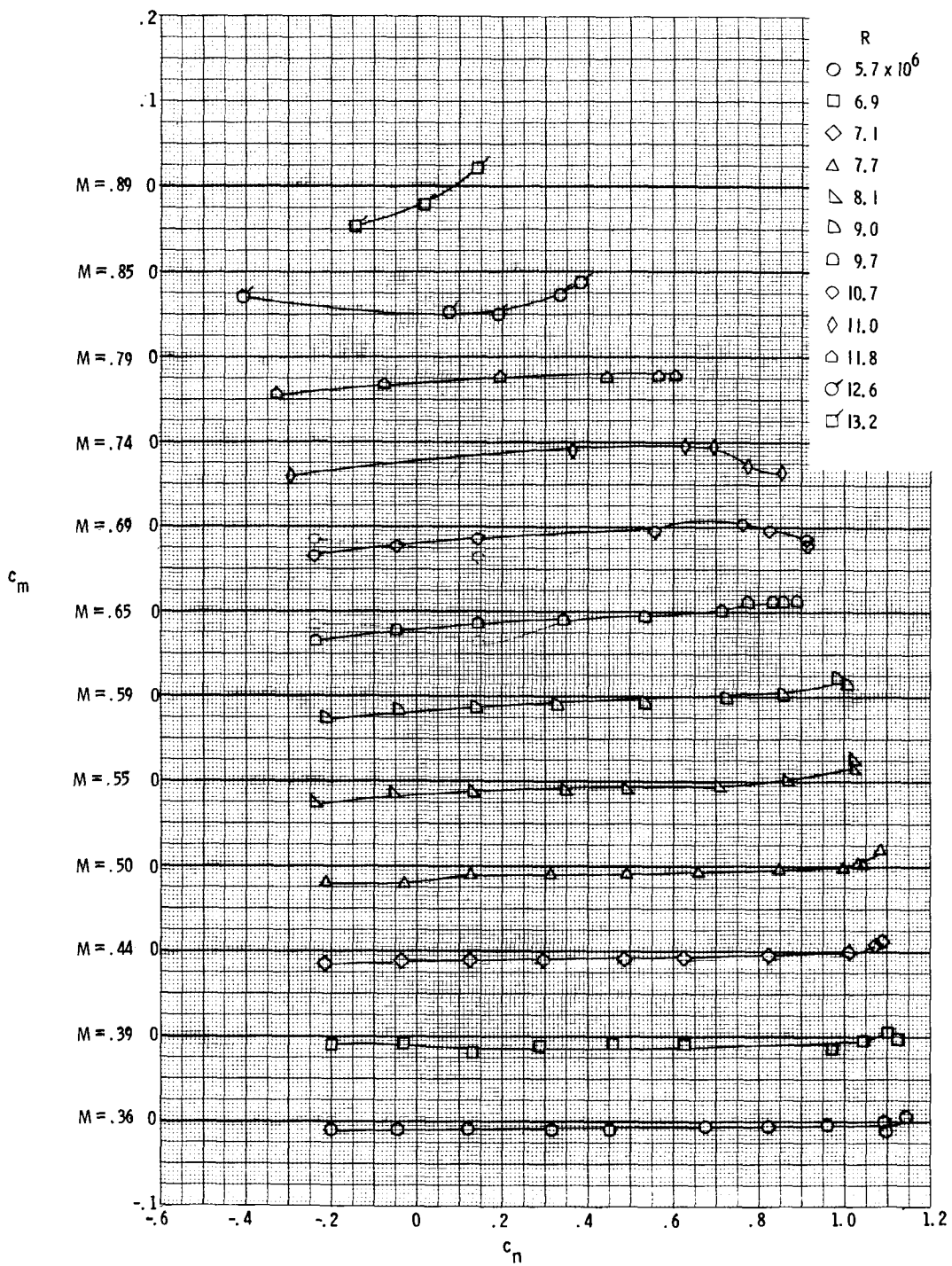
(c) Section profile-drag coefficients.

Figure 6.- Concluded.



(a) Section normal-force coefficients.

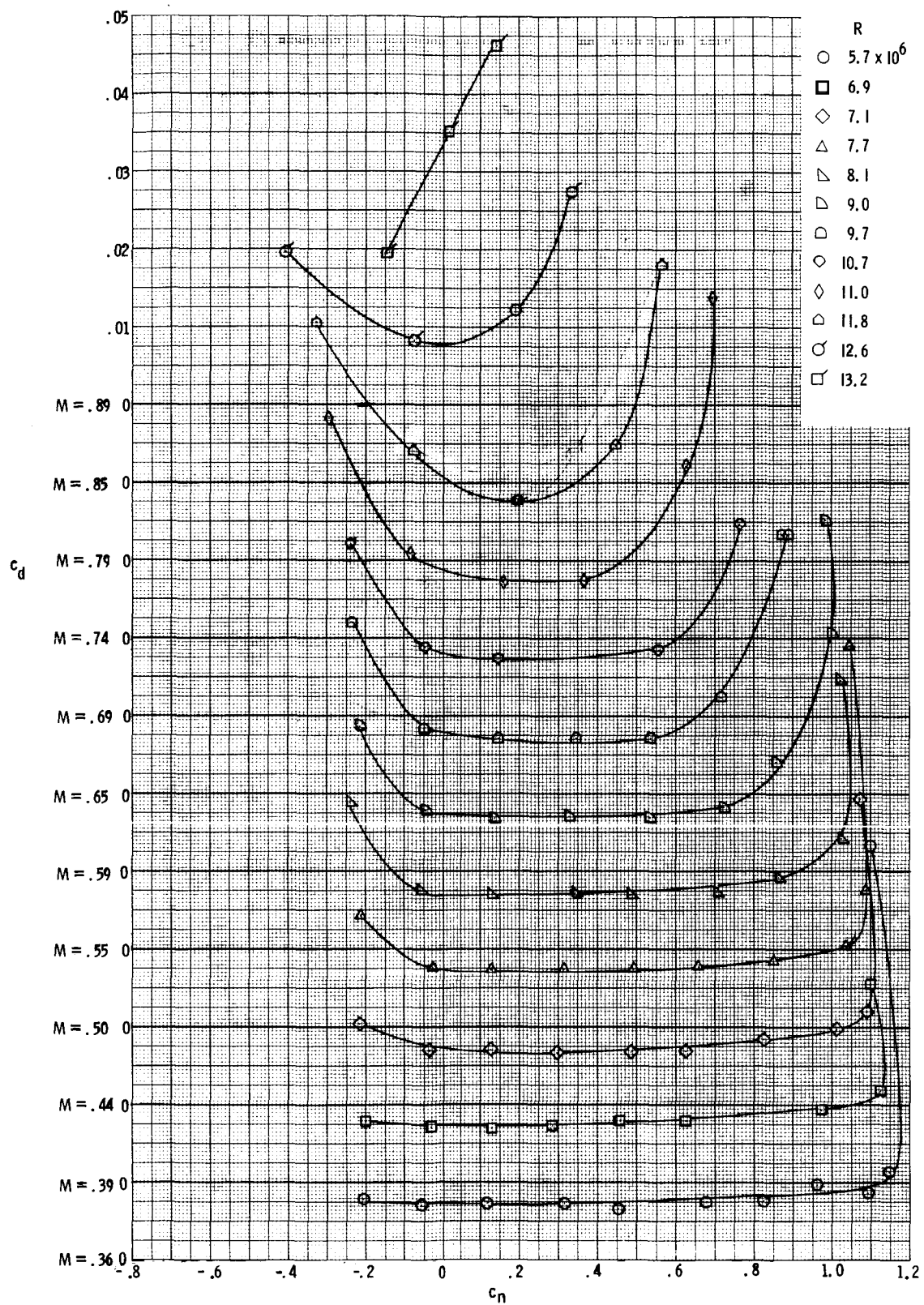
Figure 7.- Aerodynamic characteristics of RC(1)-10 Mod 2 airfoil measured in Langley 6- by 28-Inch Transonic Tunnel. Model surfaces smooth.



(b) Section pitching-moment coefficients.

Figure 7.- Continued.





(c) Section profile-drag coefficients.

Figure 7.- Concluded.

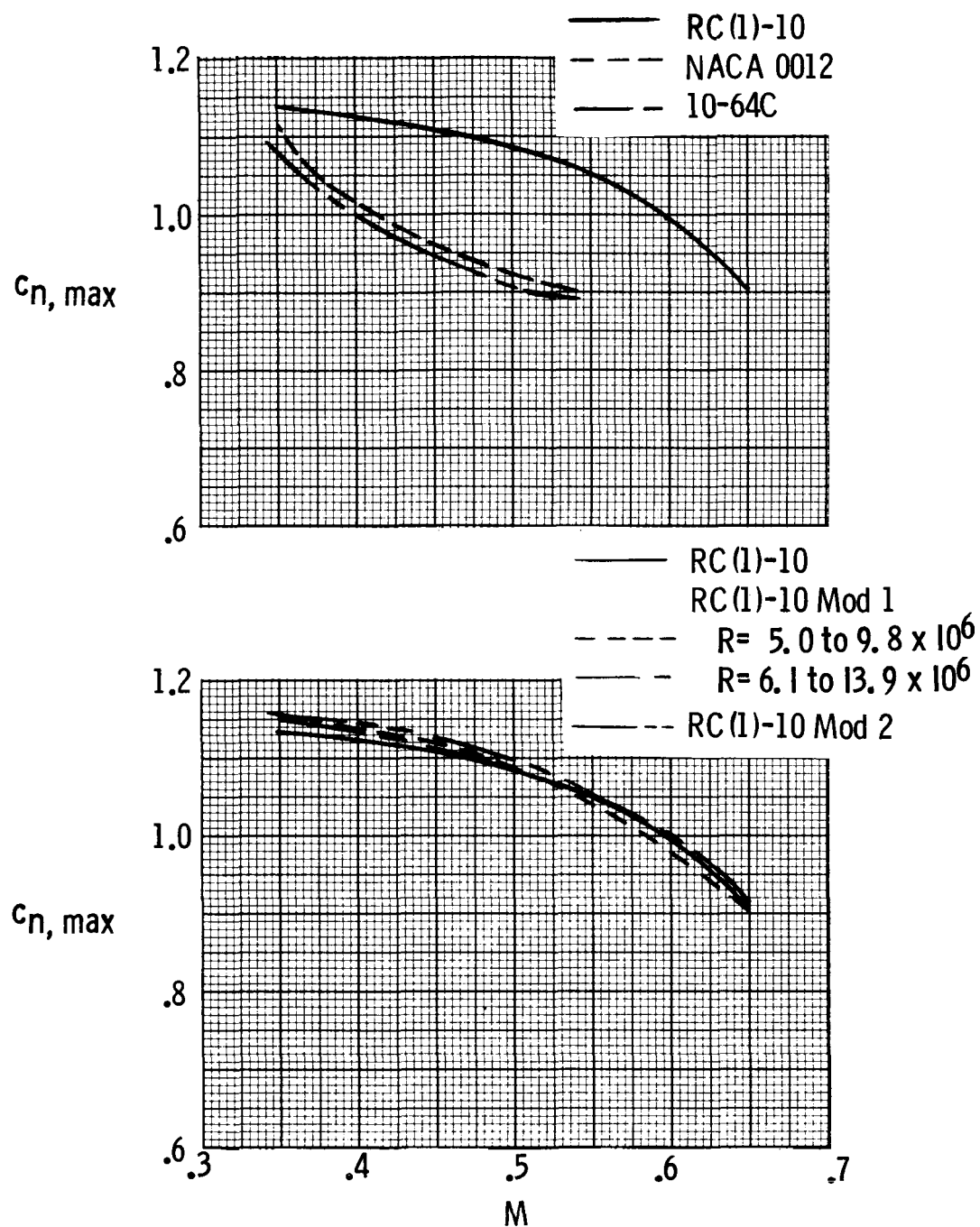


Figure 8.- Variation of maximum section normal-force coefficient with Mach number for several airfoils as measured in Langley 6- by 28-Inch Transonic Tunnel.

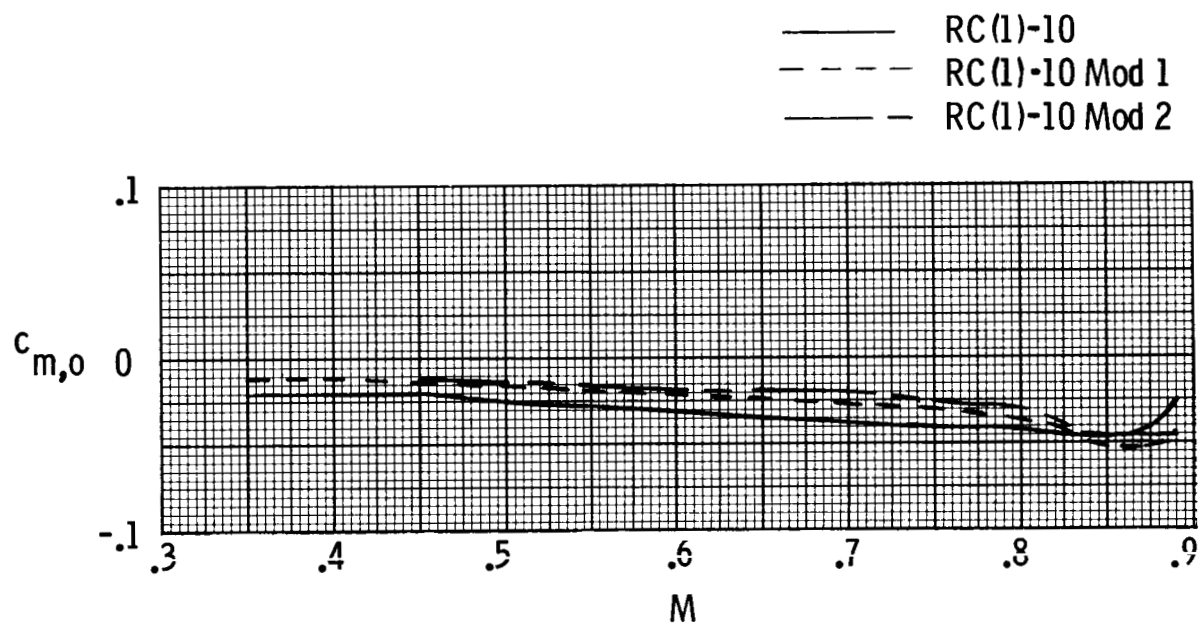


Figure 9.- Variation in section pitching-moment coefficient at zero normal-force coefficient with Mach number.

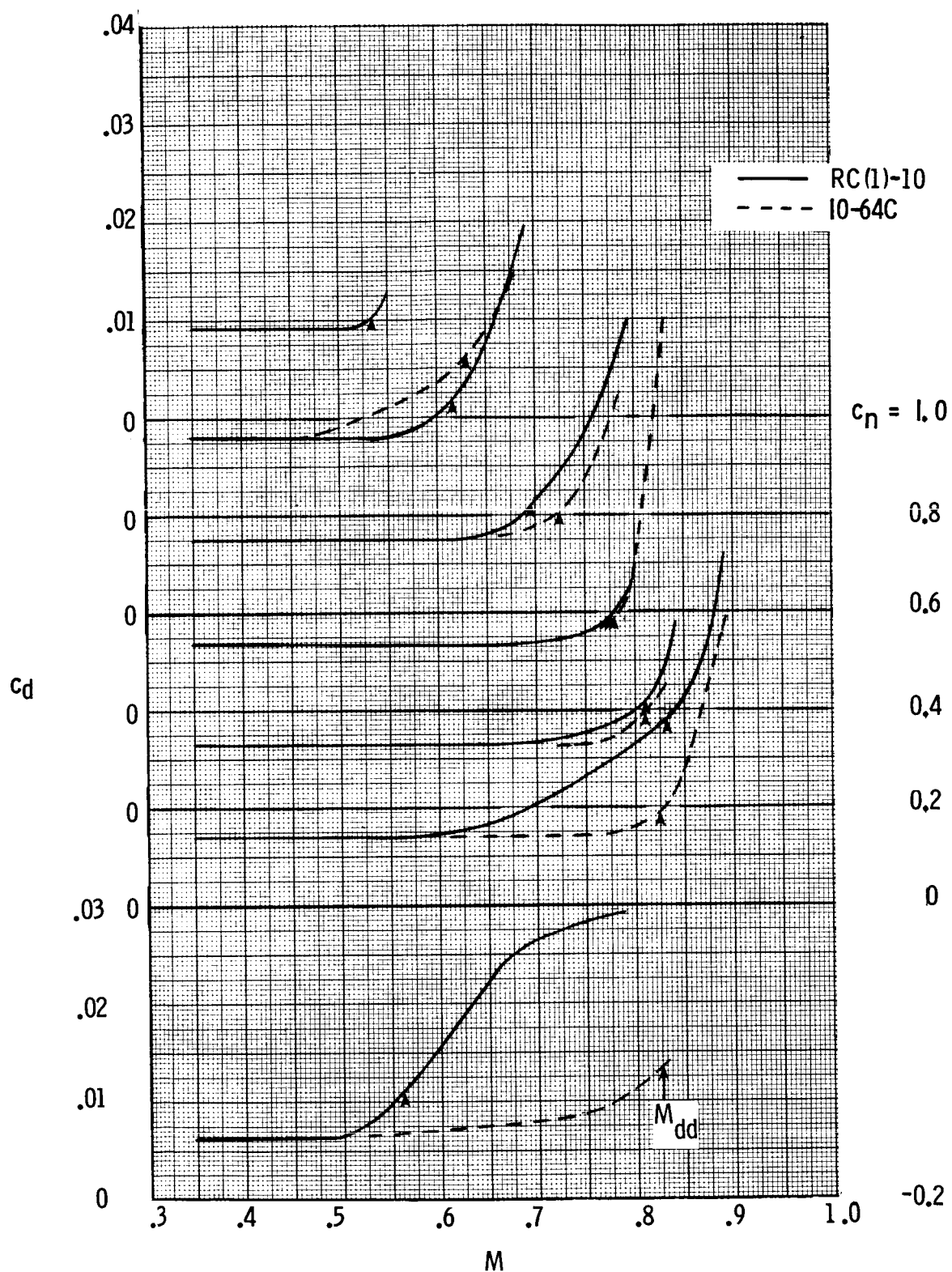


Figure 10.- Variation in section profile-drag coefficient with Mach number for RC(1)-10 and 10-64C airfoils. Model surfaces smooth.

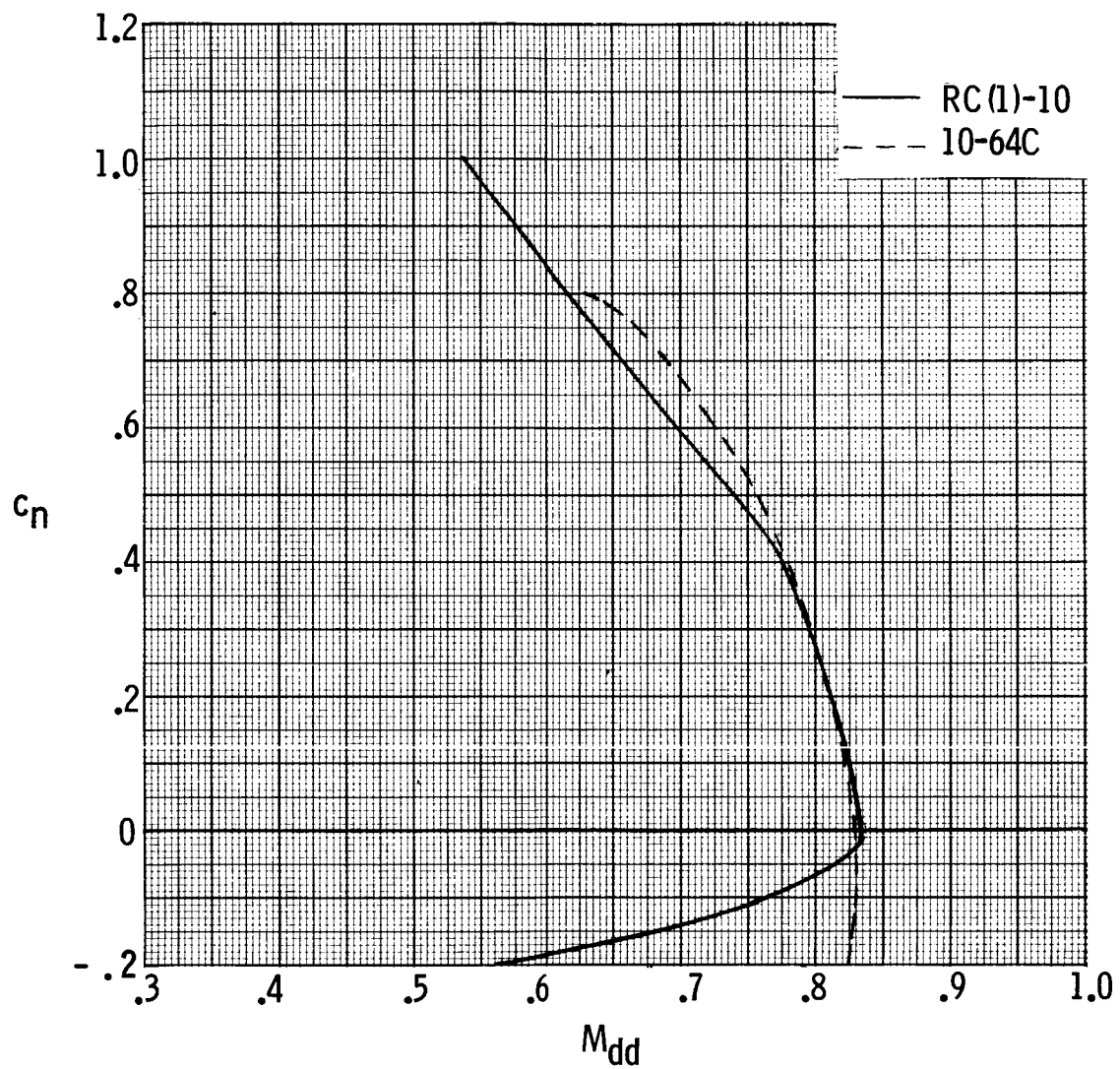


Figure 11.- Comparison of RC(1)-10 and 10-64C airfoil section normal-force coefficient at drag-divergence Mach number.

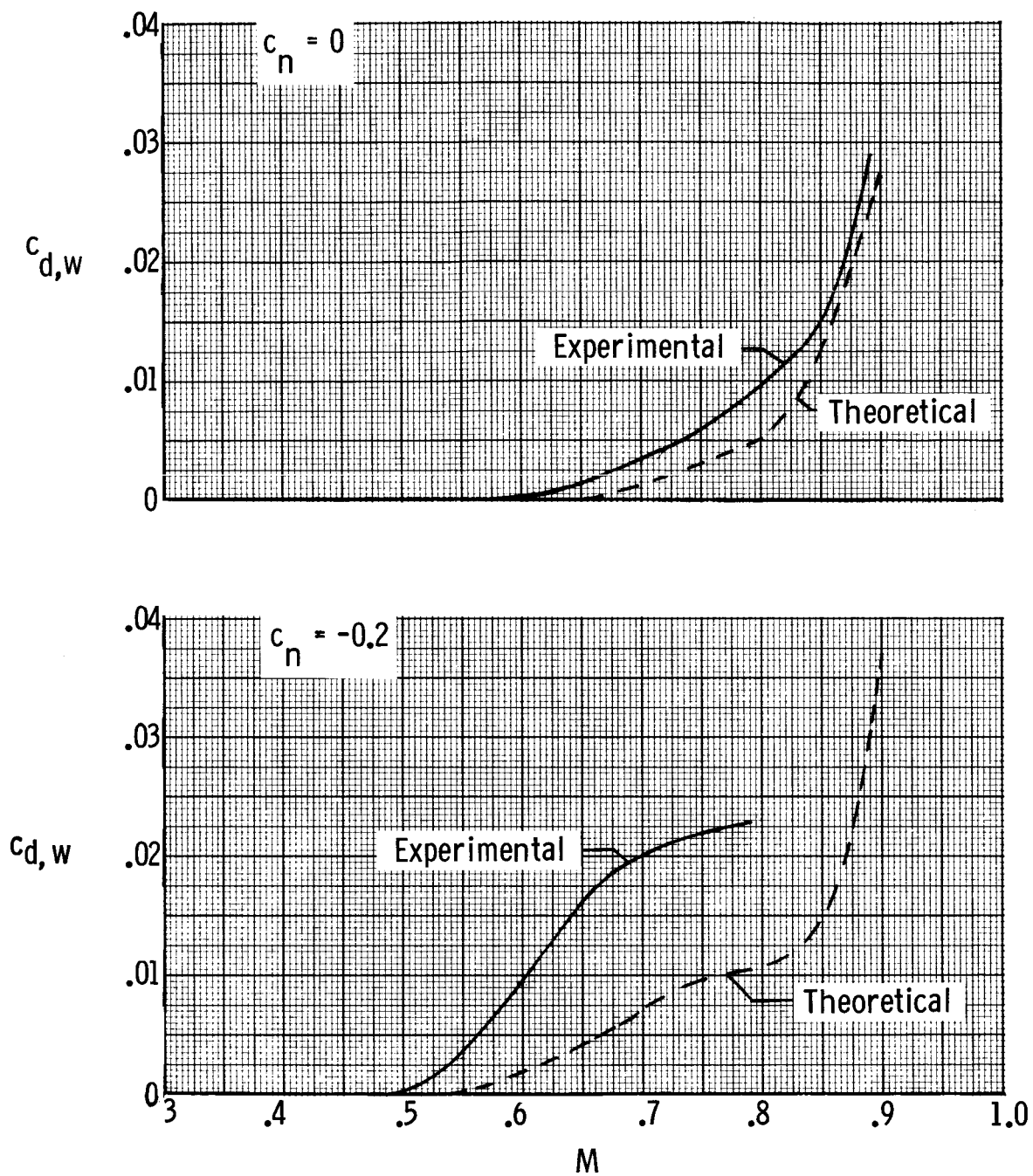


Figure 12.- Variation of experimental and theoretical section wave-drag coefficient with Mach number for RC(1)-10 airfoil.

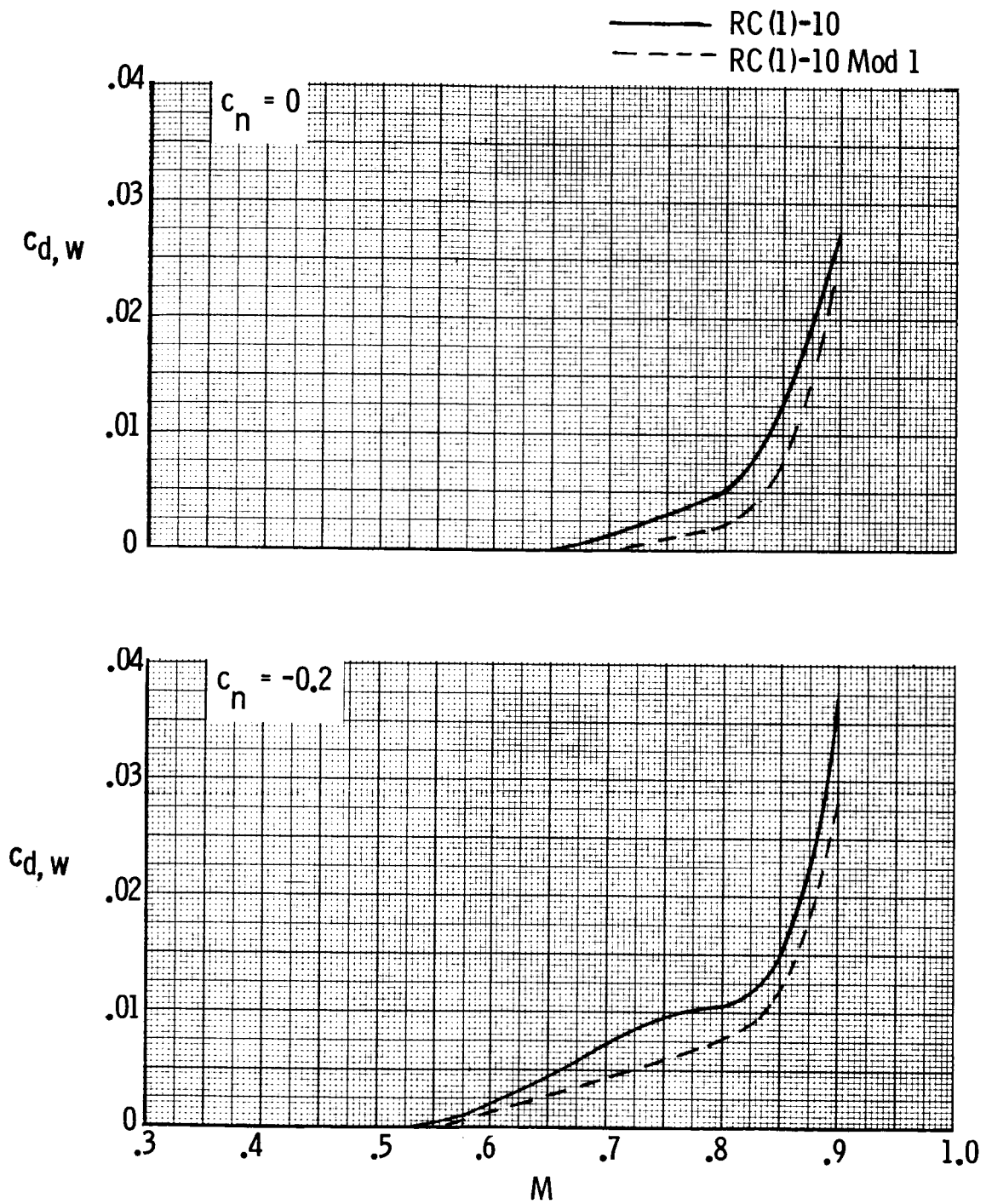


Figure 13.- Variation in theoretical section wave-drag coefficient with Mach number for RC(1)-10 and RC(1)-10 Mod 1 airfoils.

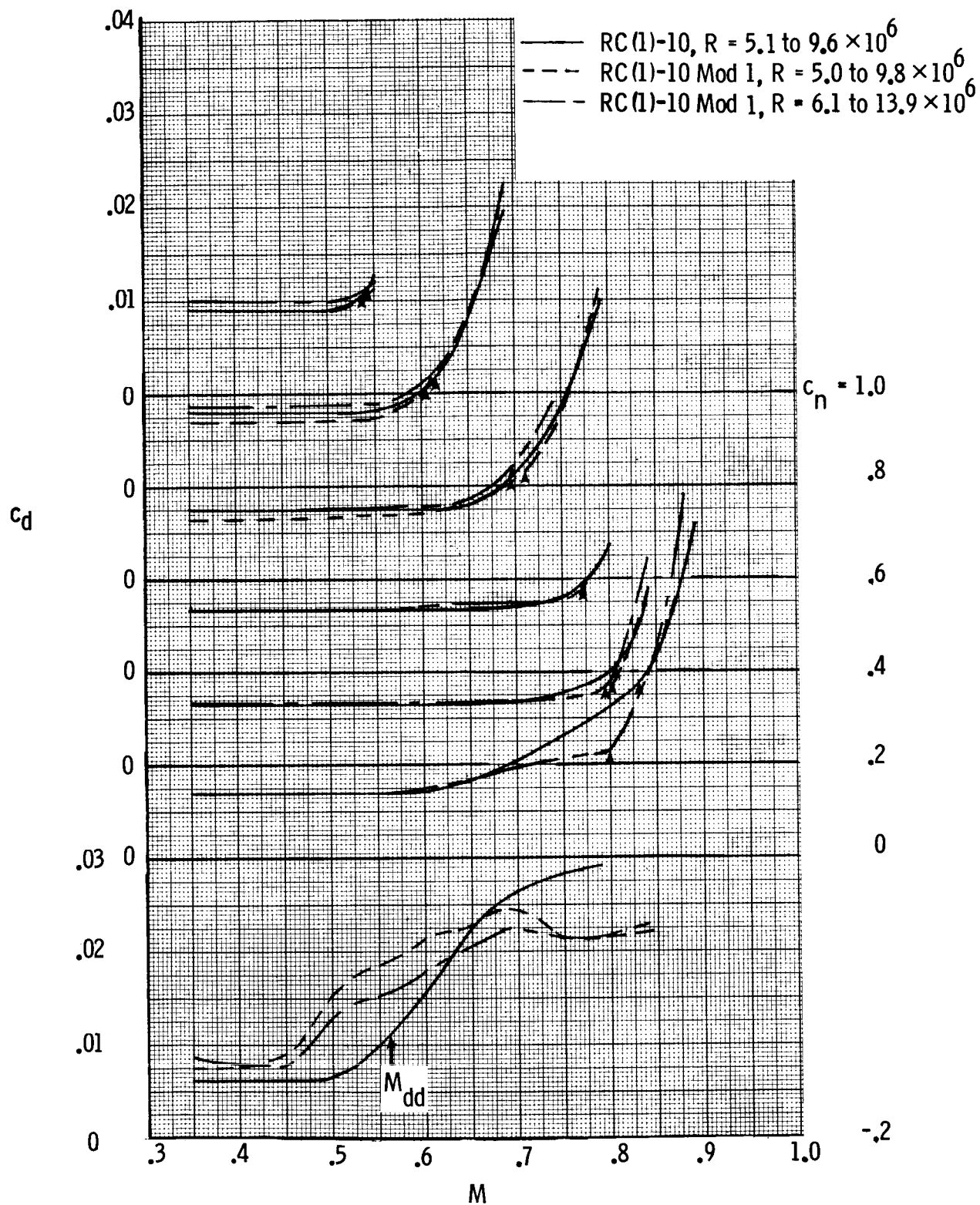


Figure 14.- Variation in section profile-drag coefficient with Mach number for RC(1)-10 and RC(1)-10 Mod 1 airfoils.



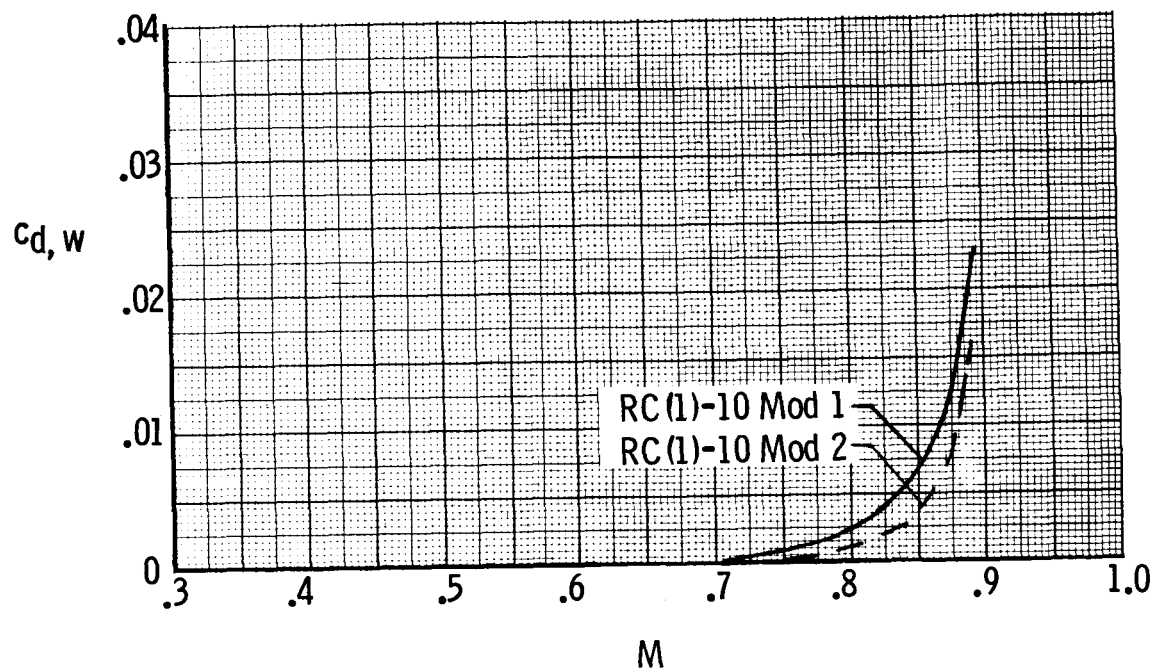


Figure 15.- Variation in section wave-drag coefficient with Mach number for RC(1)-10 Mod 1 and RC(1)-10 Mod 2 airfoils.  $c_n = 0$ .

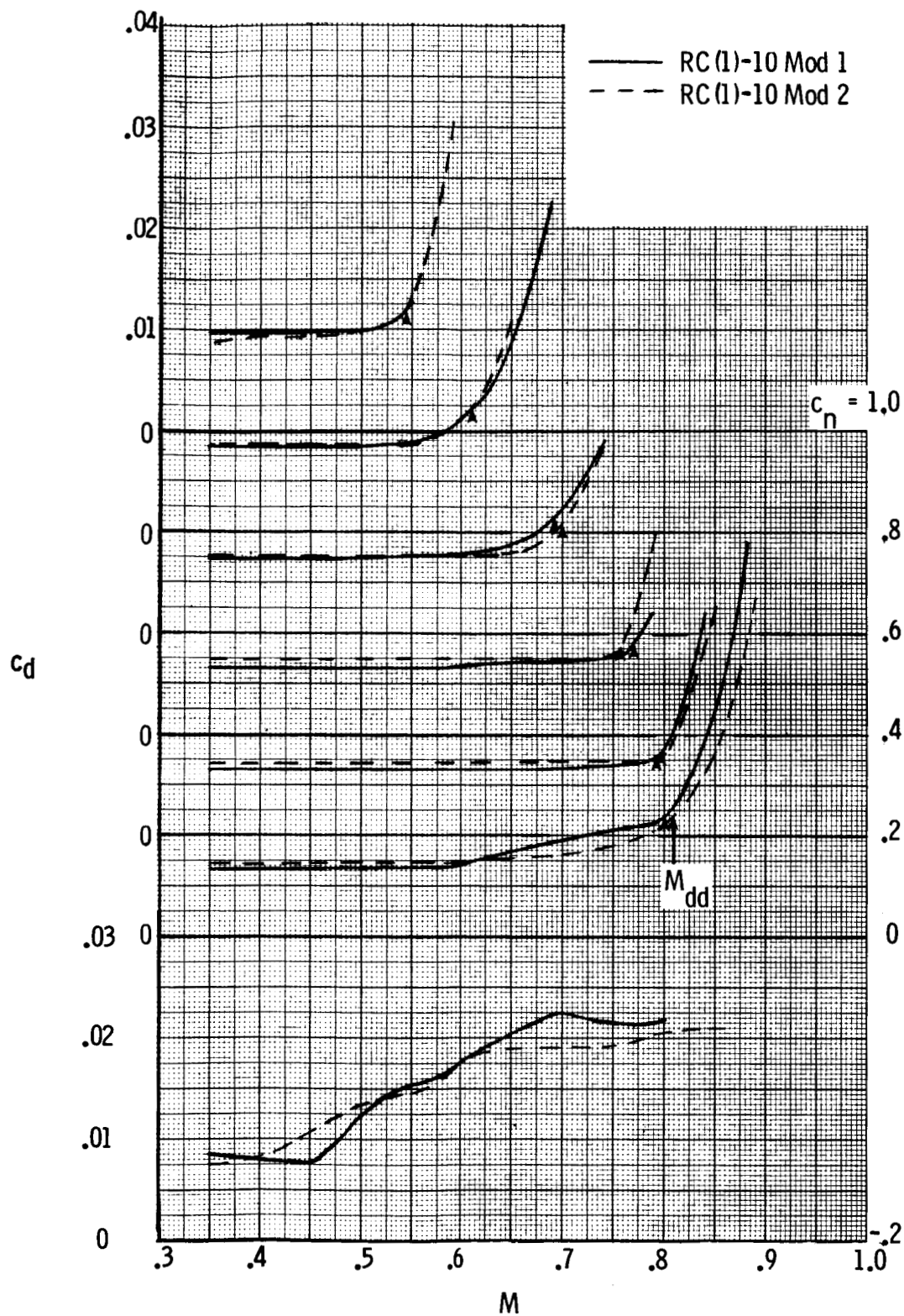
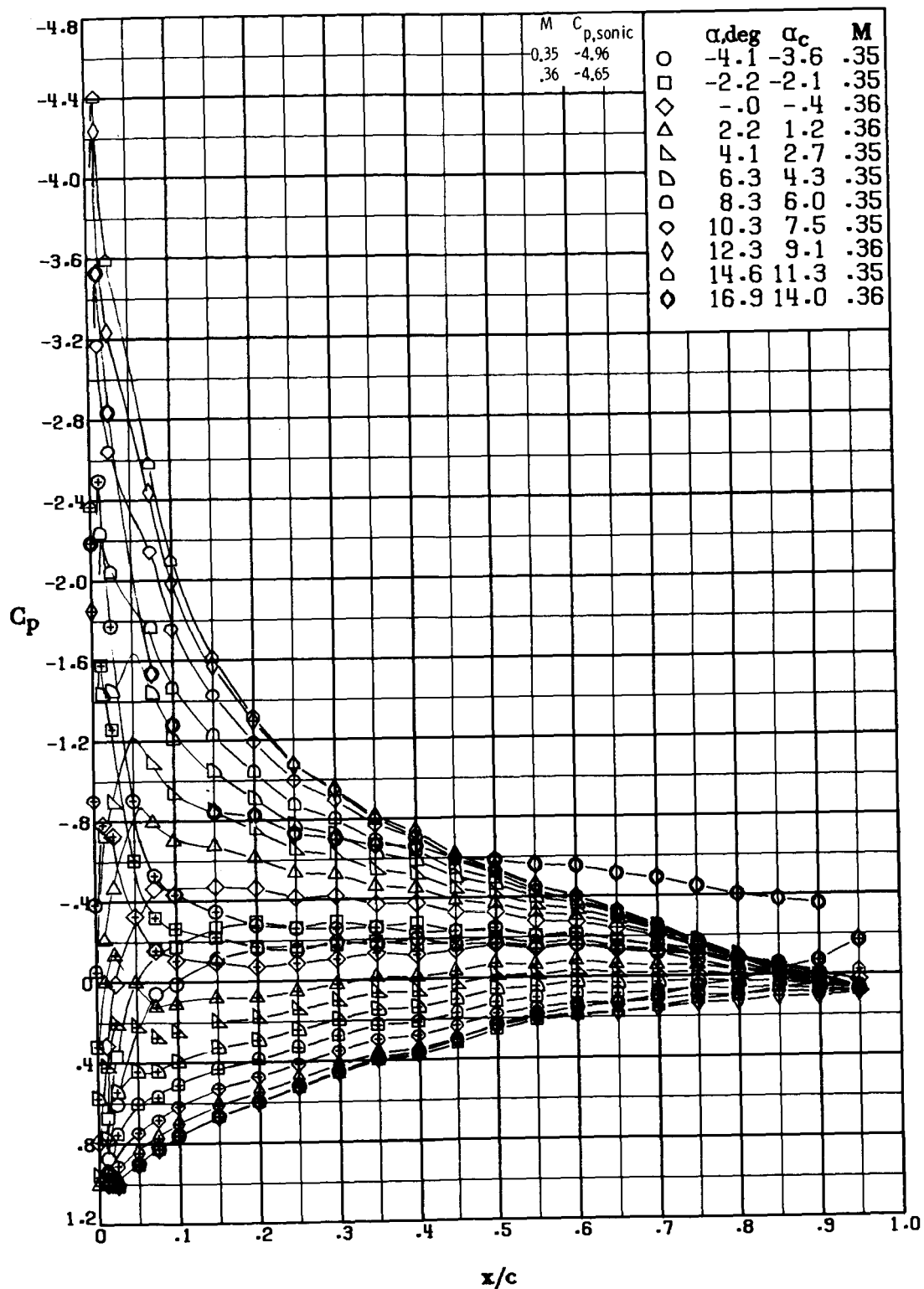
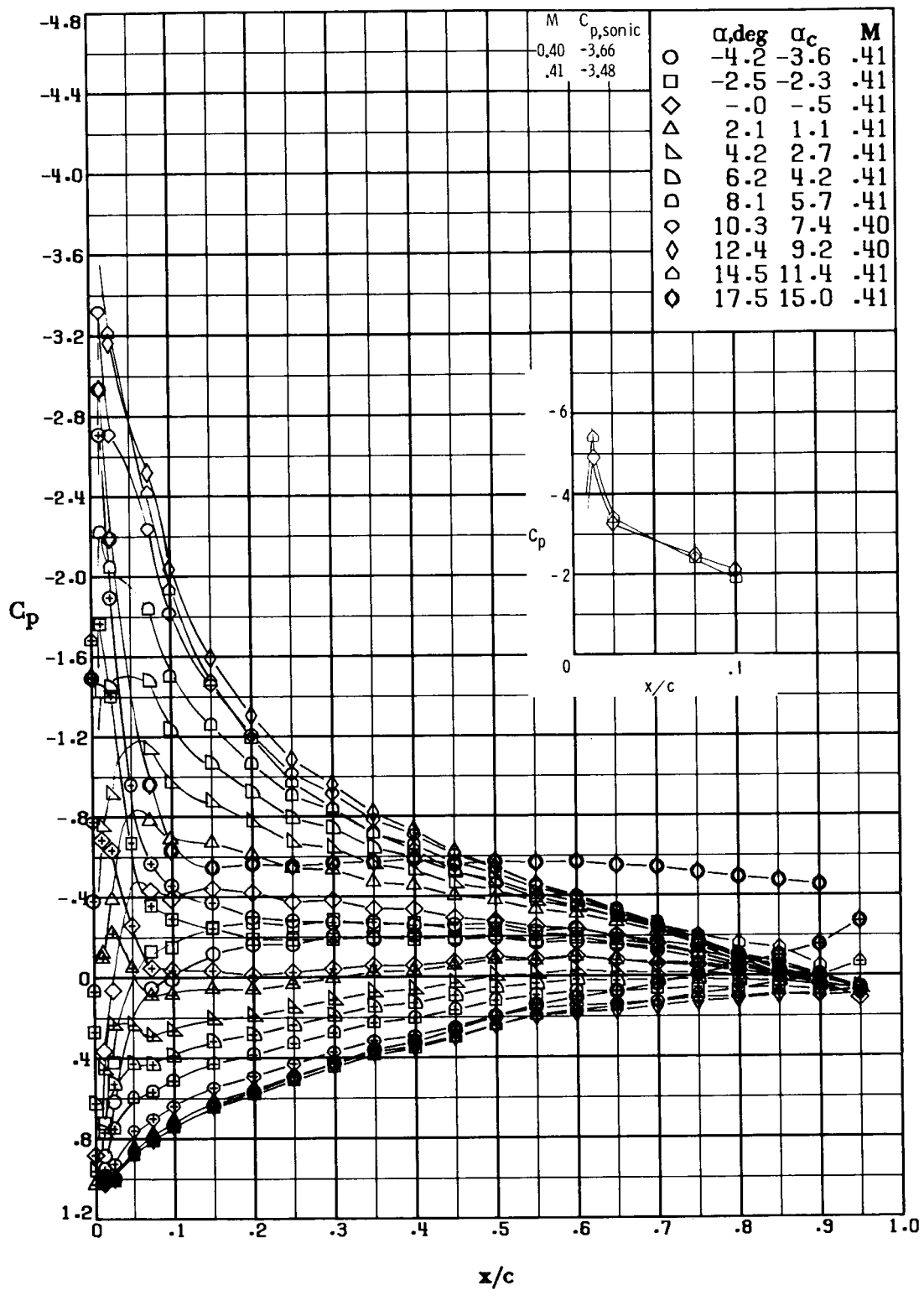


Figure 16.- Variation in section drag coefficient with Mach number for RC(1)-10 Mod 1 and RC(1)-10 Mod 2 airfoils.



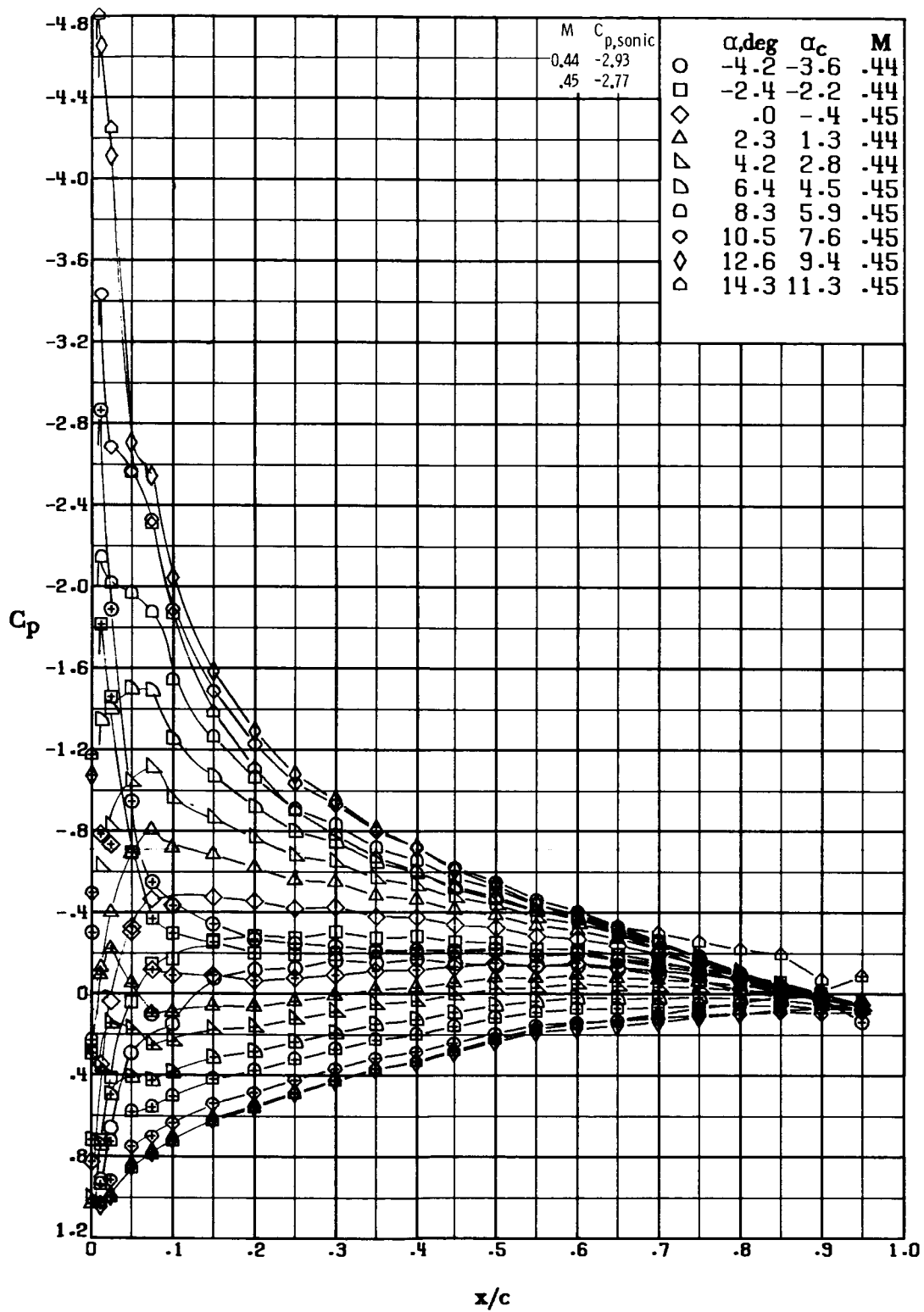
(a)  $M \approx 0.35$ ;  $R \approx 5.1 \times 10^6$ .

Figure 17.- Pressure distribution over RC(1)-10 airfoil.  
Symbols with "+" inside indicate lower surface.



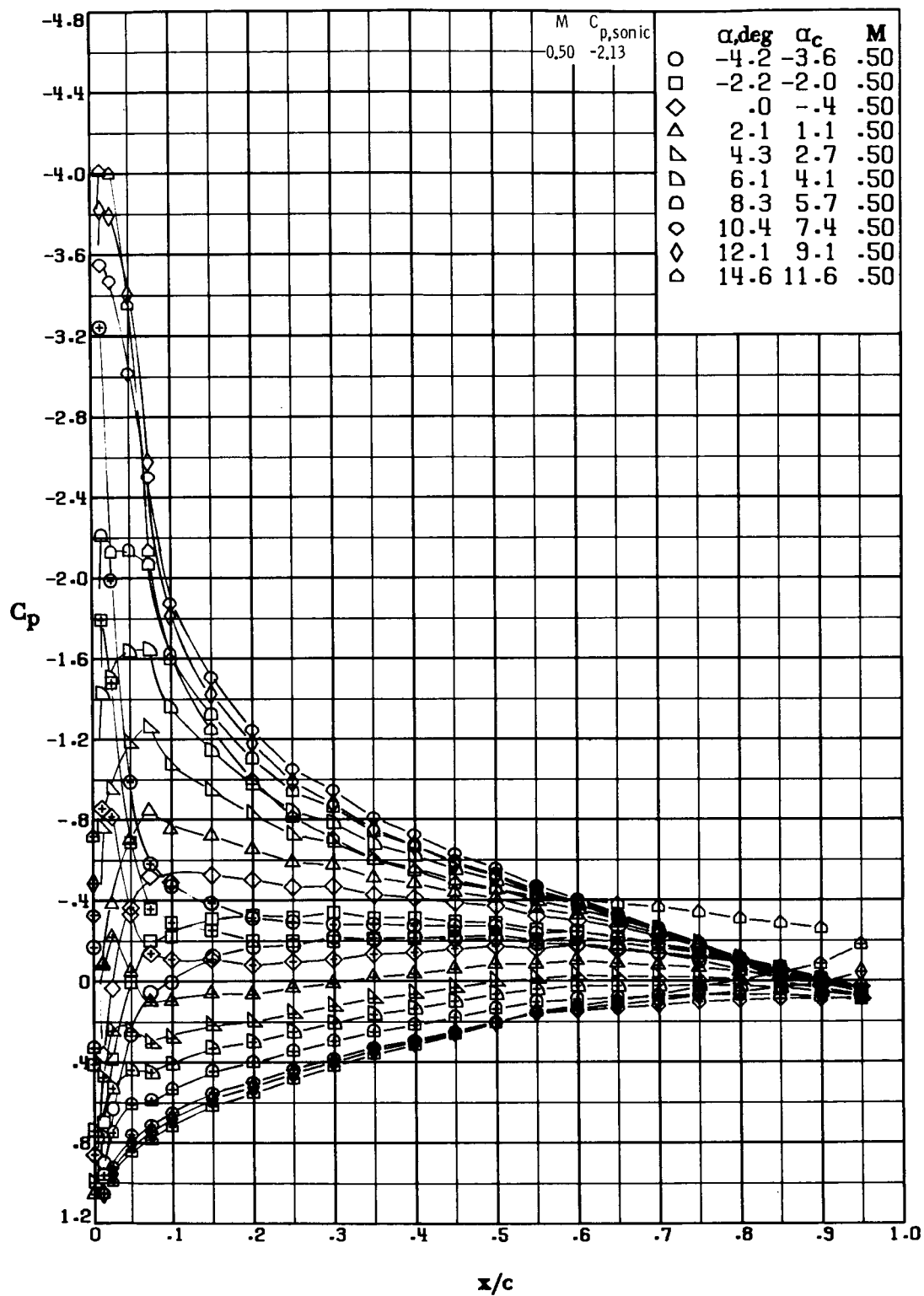
(b)  $M \approx 0.41$ ;  $R \approx 5.8 \times 10^6$ .

Figure 17.- Continued.



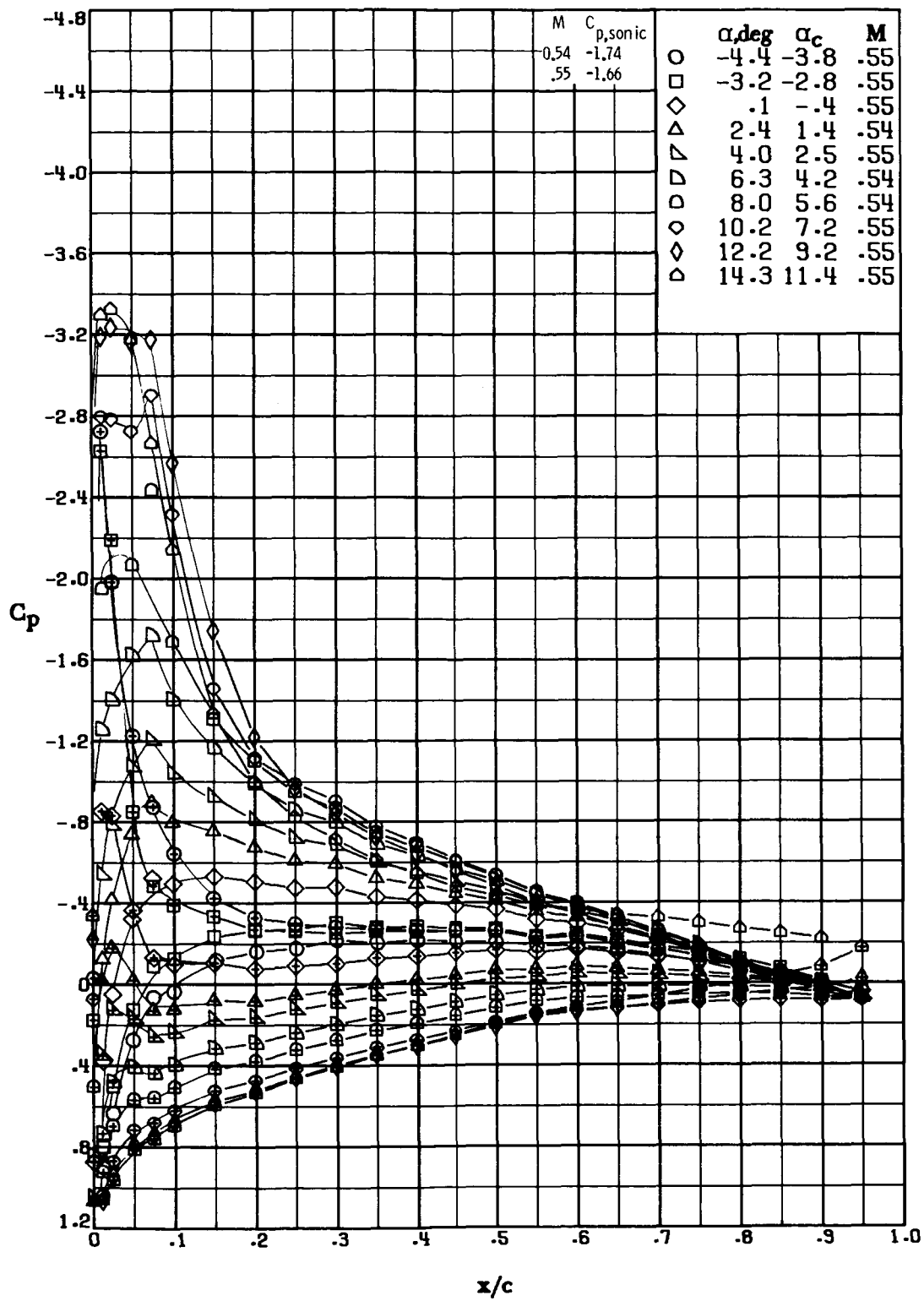
(c)  $M \approx 0.45$ ;  $R \approx 6.0 \times 10^6$ .

Figure 17.- Continued.



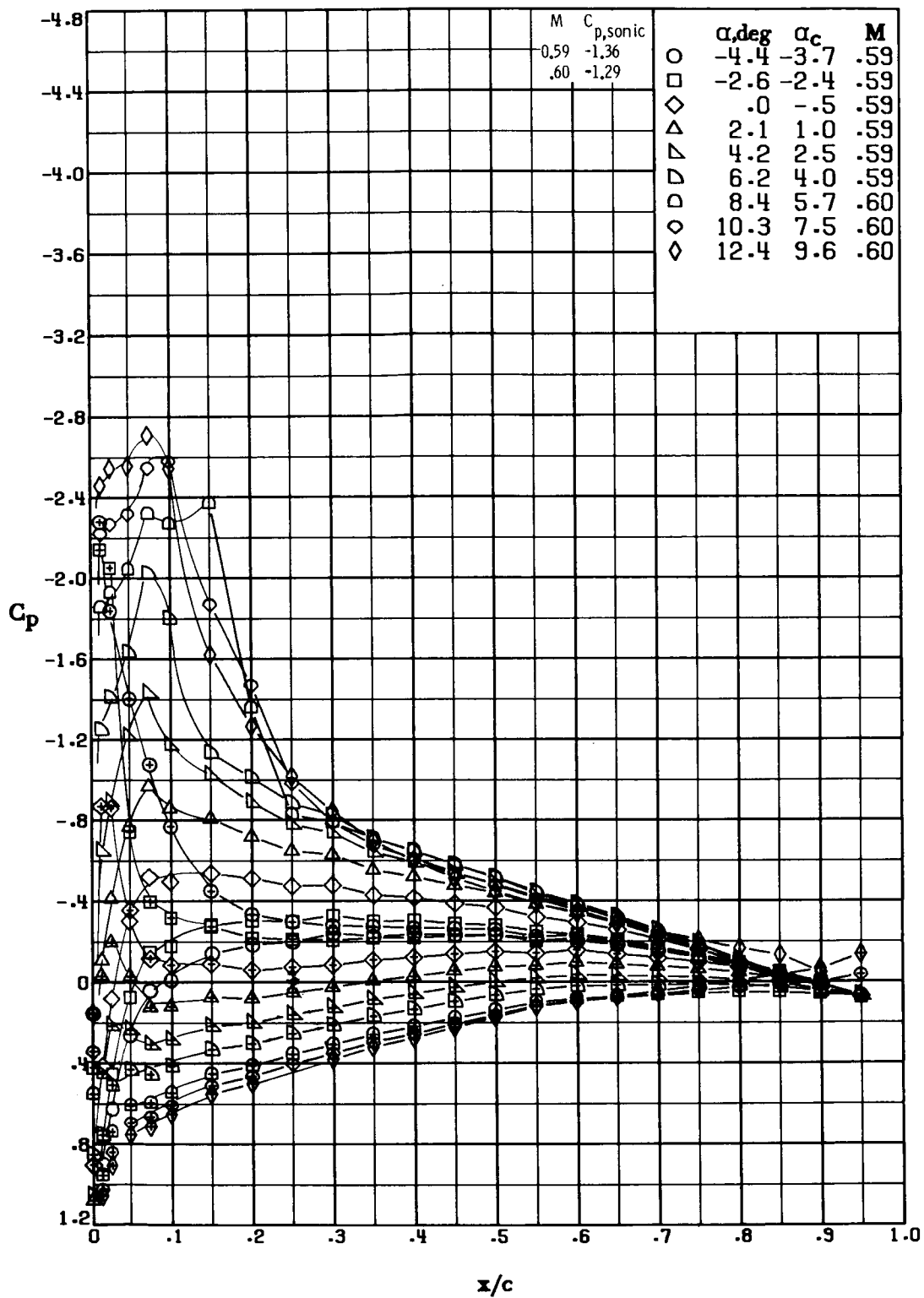
(d)  $M \approx 0.50$ ;  $R \approx 6.7 \times 10^6$ .

Figure 17.- Continued.



(e)  $M \approx 0.55$ ;  $R \approx 7.0 \times 10^6$ .

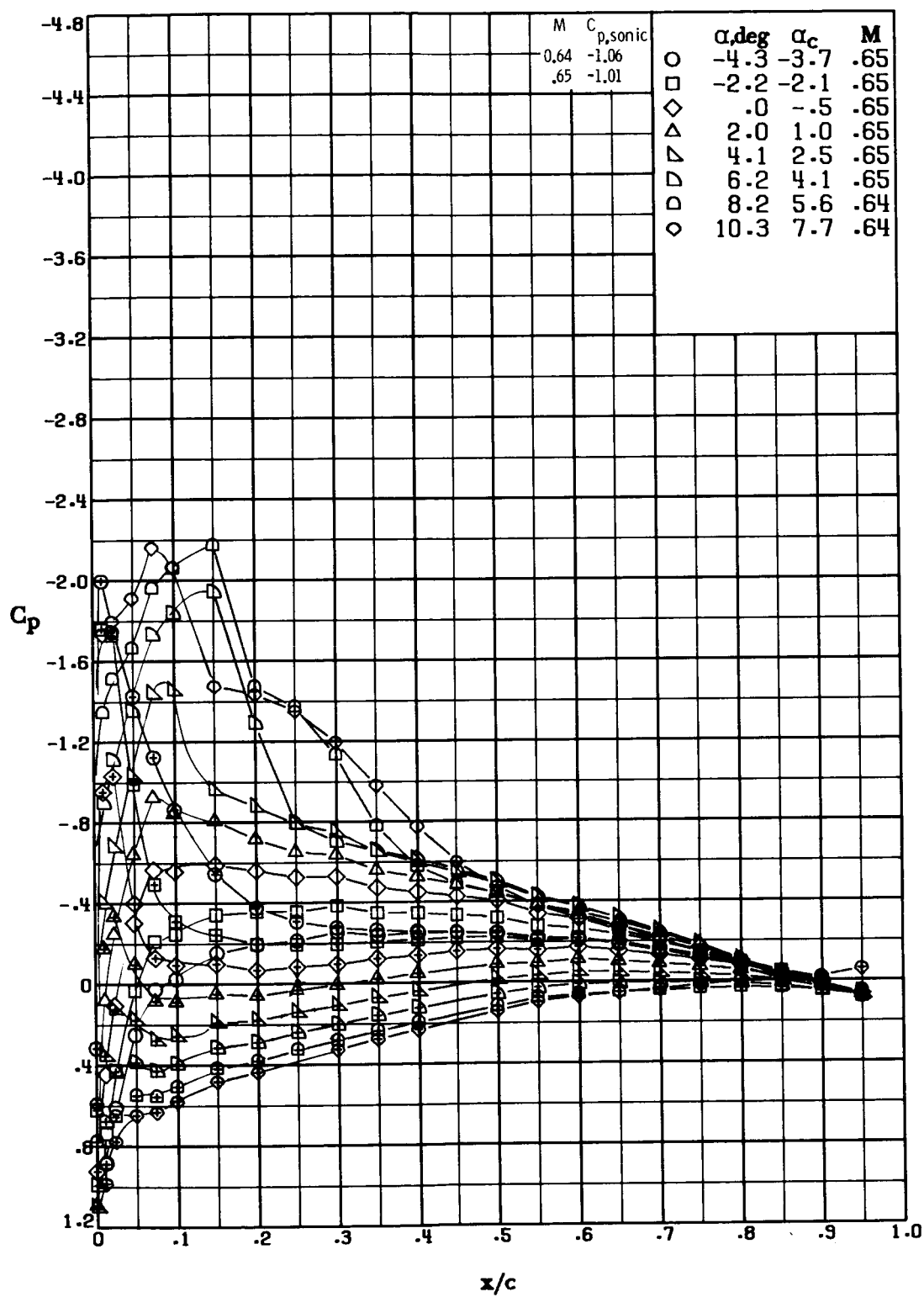
Figure 17.- Continued.



(f)  $M \approx 0.59$ ;  $R \approx 7.6 \times 10^6$ .

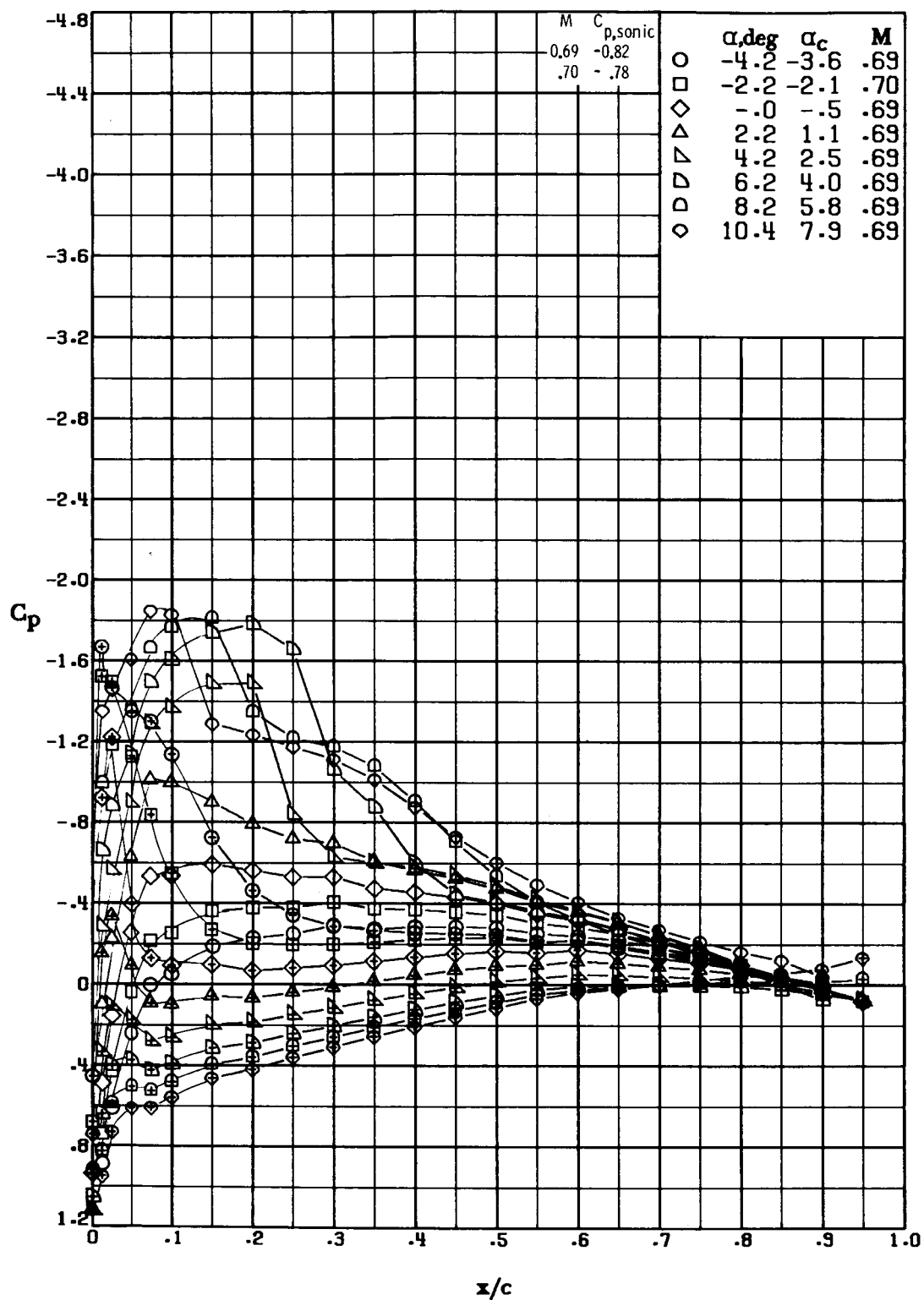
Figure 17.- Continued.





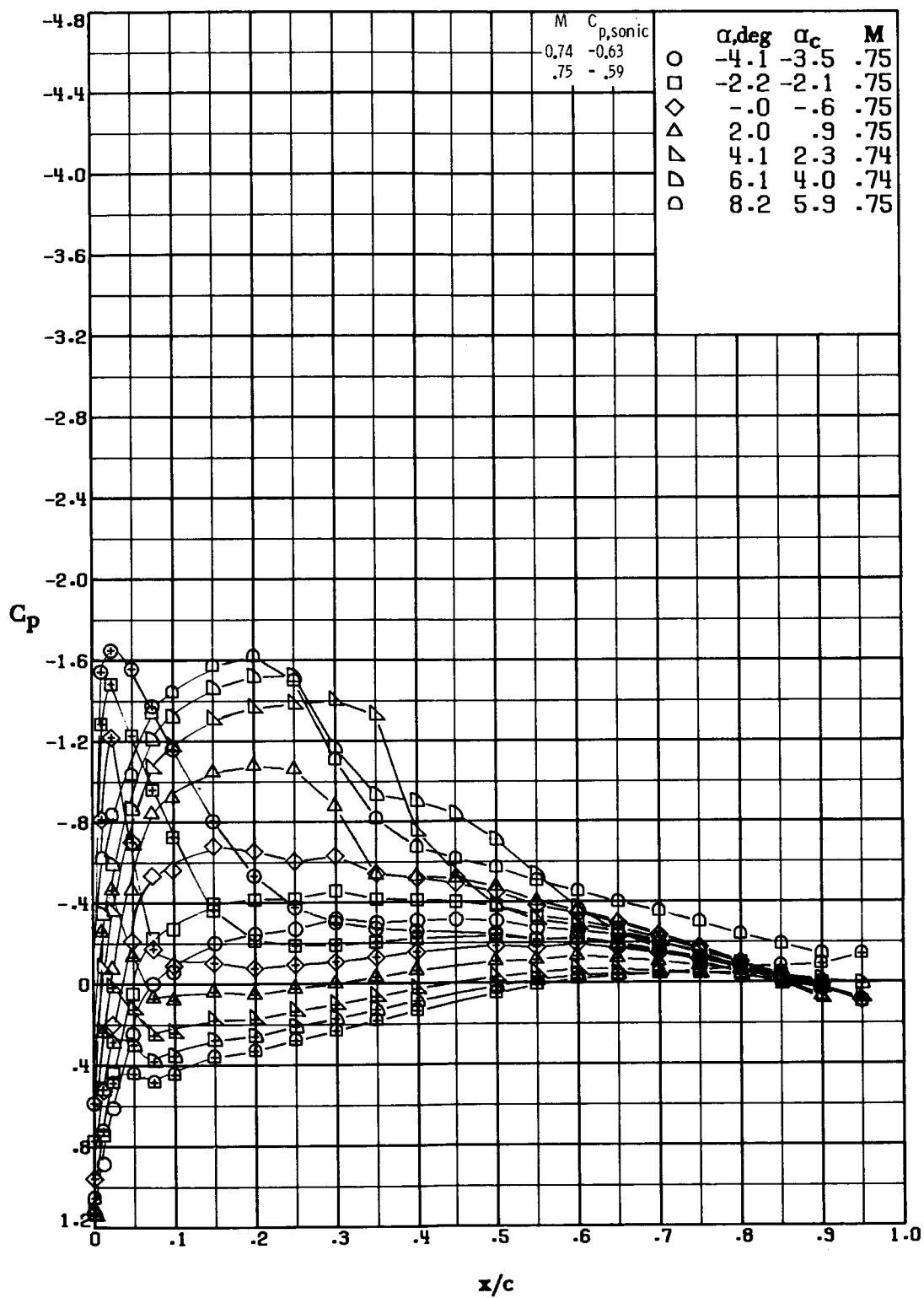
(g)  $M \approx 0.65$ ;  $R \approx 8.0 \times 10^6$ .

Figure 17.- Continued.



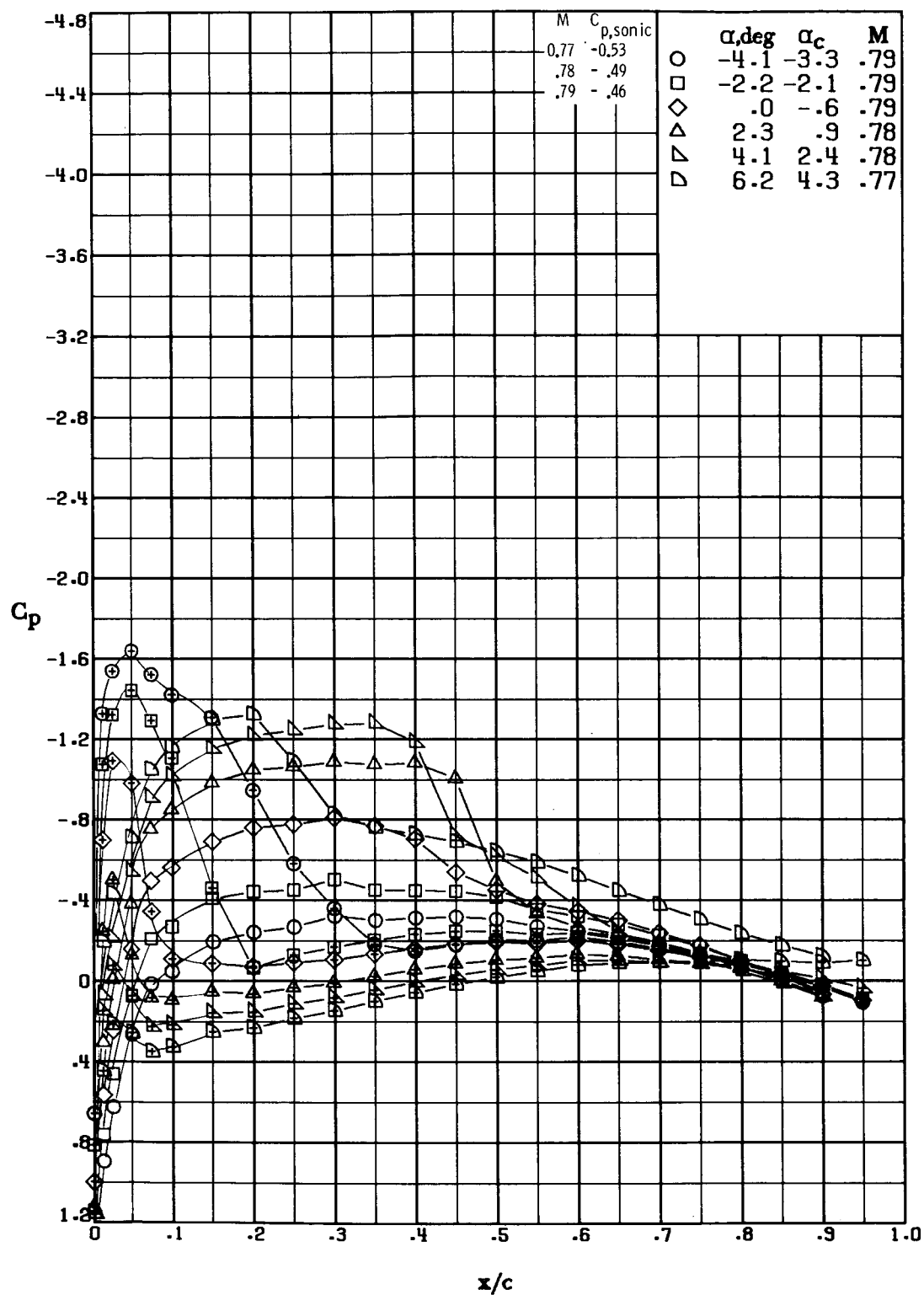
(h)  $M \approx 0.69$ ;  $R \approx 8.3 \times 10^6$ .

Figure 17.- Continued.



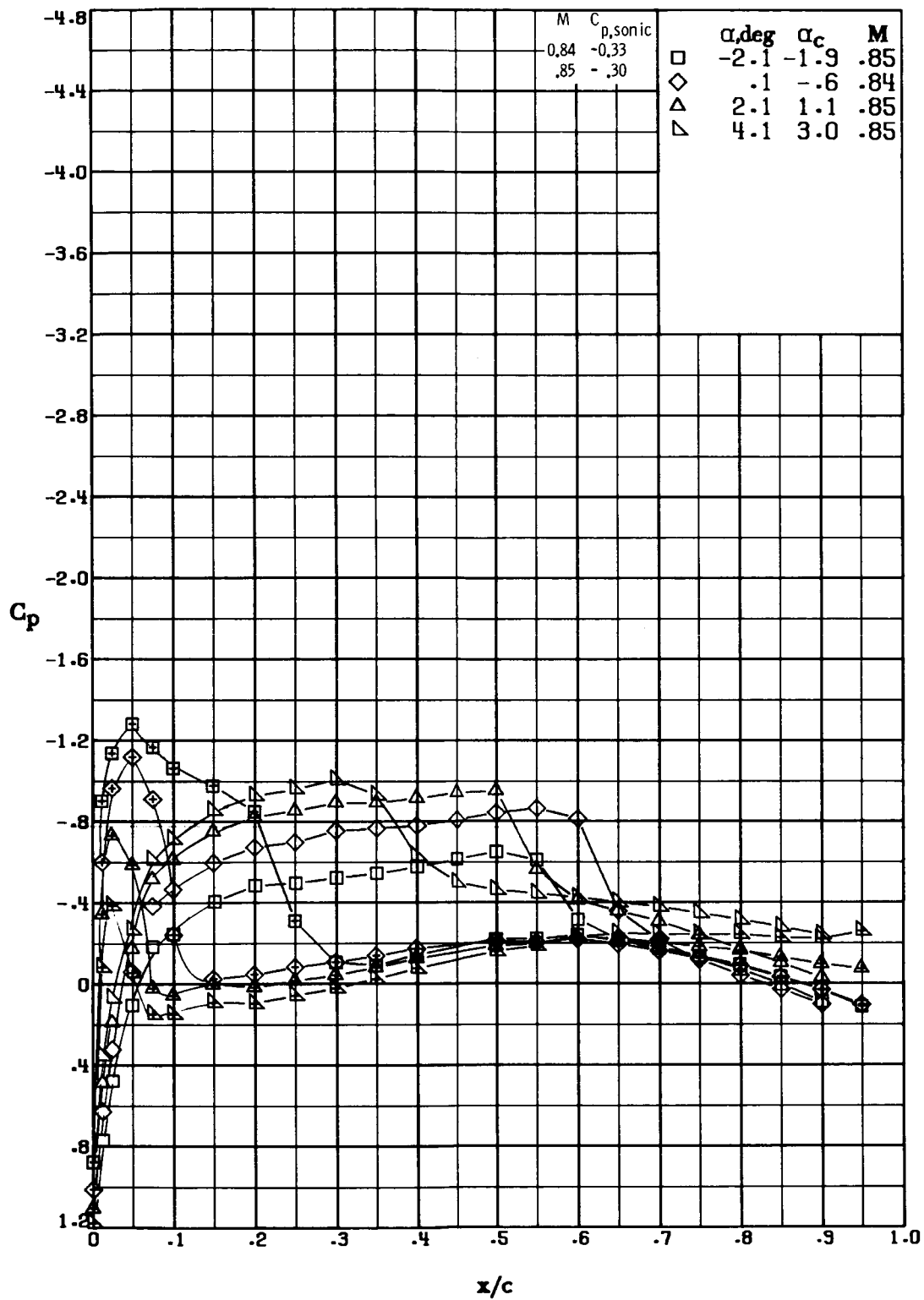
(i)  $M \approx 0.74$ ;  $R \approx 8.9 \times 10^6$ .

Figure 17.- Continued.



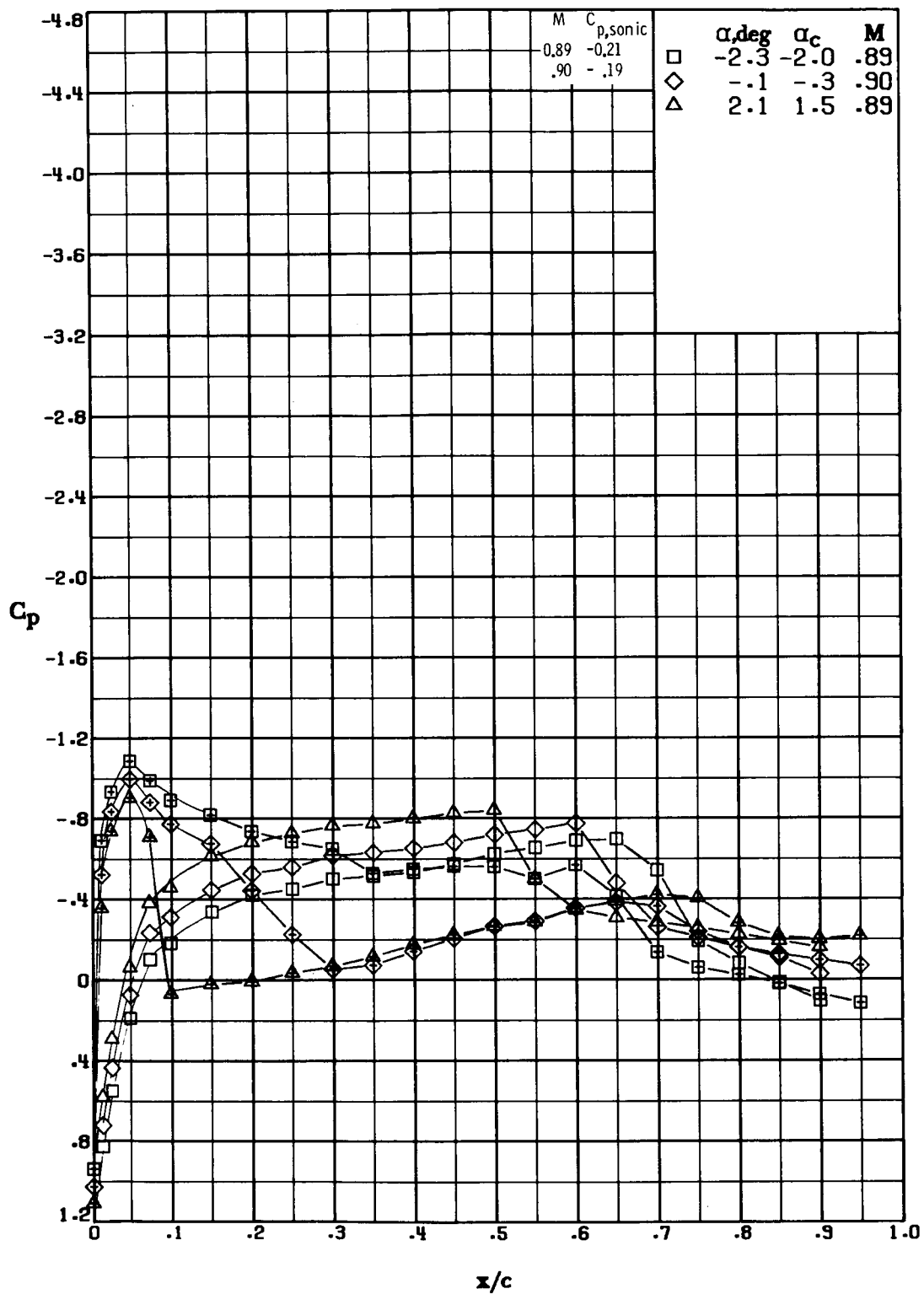
(j)  $M \approx 0.78$ ;  $R \approx 8.8 \times 10^6$ .

Figure 17.- Continued.



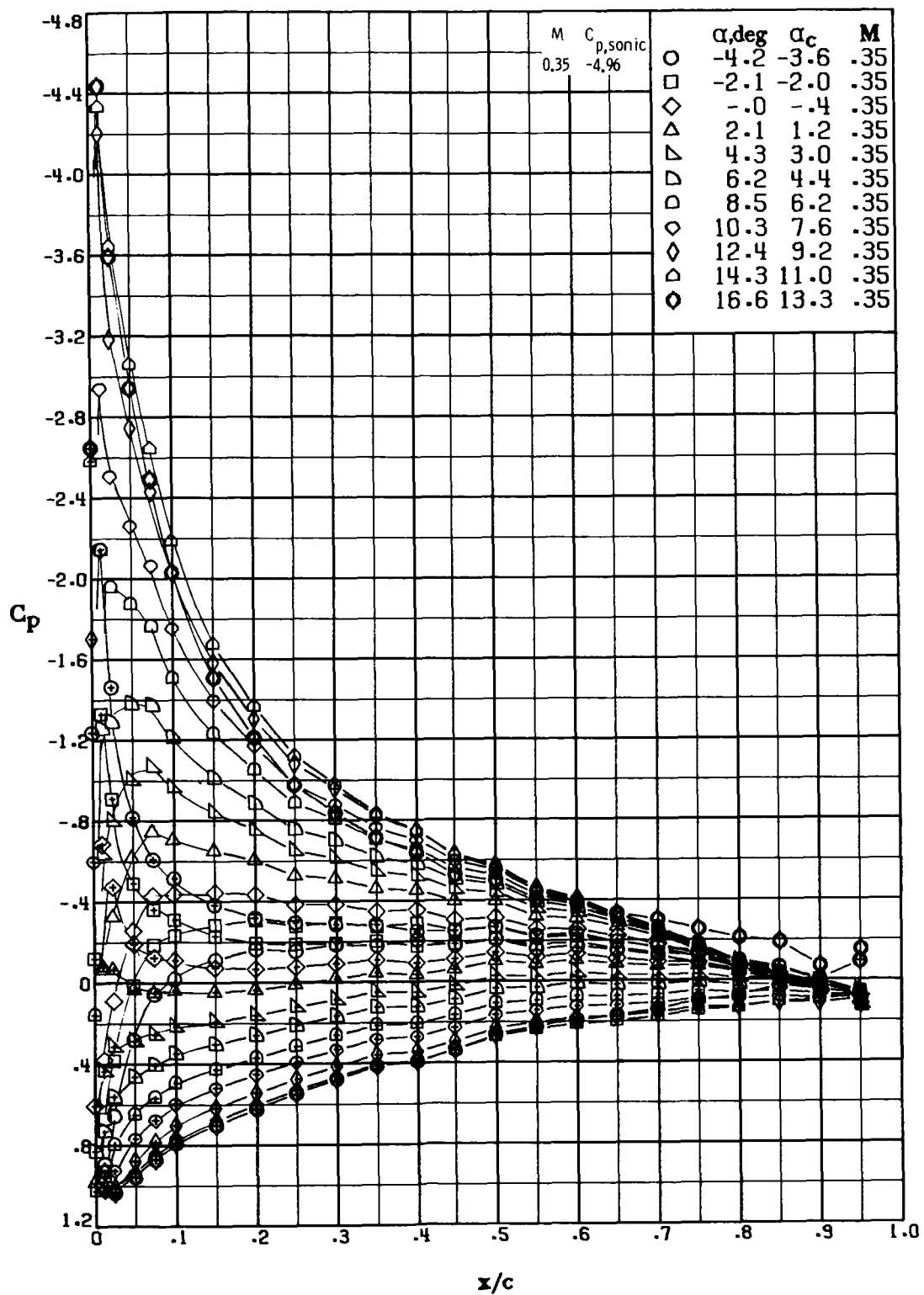
(k)  $M \approx 0.84$ ;  $R \approx 9.5 \times 10^6$ .

Figure 17.- Continued.



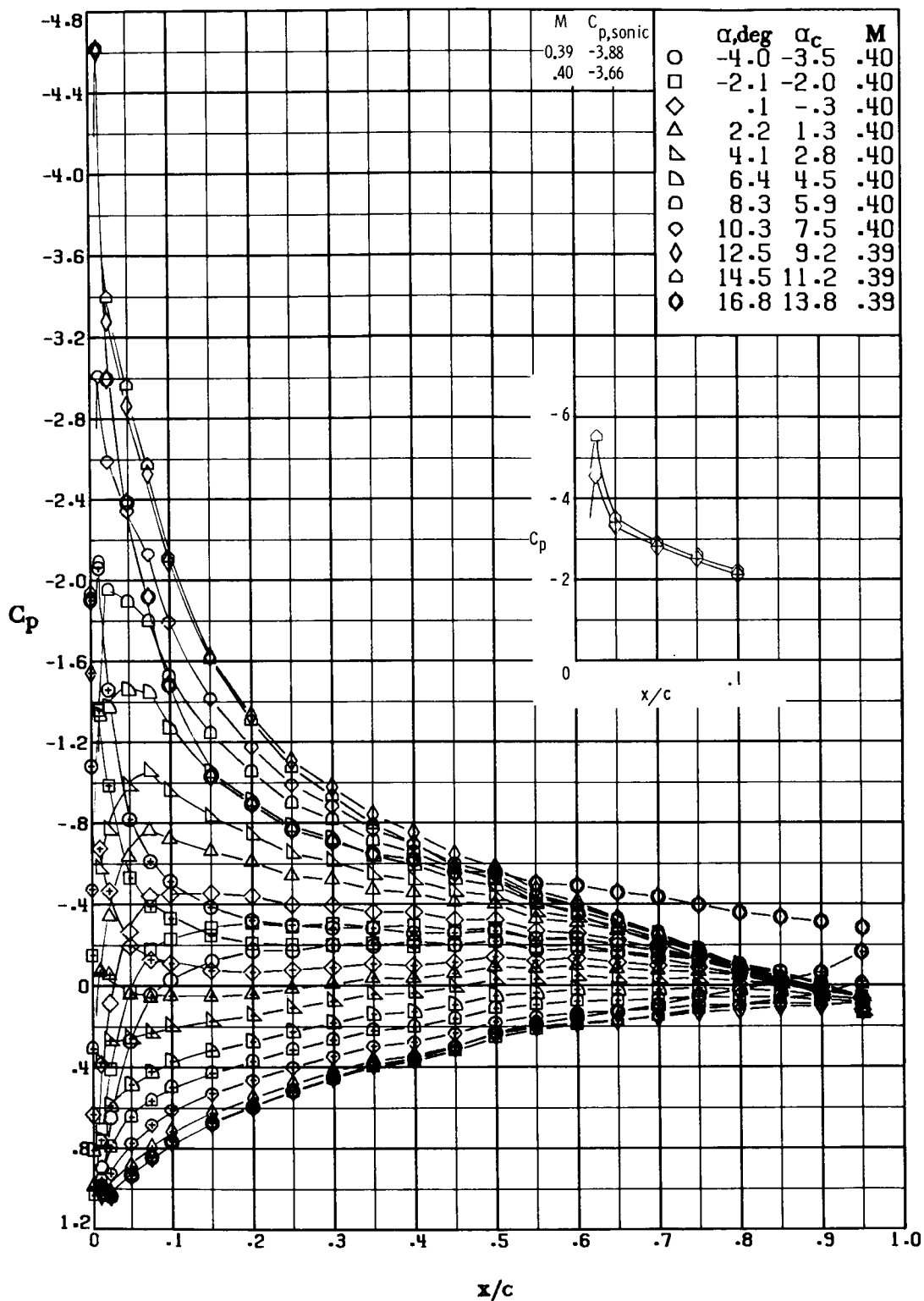
(1)  $M \approx 0.89$ ;  $R \approx 9.6 \times 10^6$ .

Figure 17.- Concluded.



(a)  $M \approx 0.35$ ;  $R \approx 5.0 \times 10^6$ .

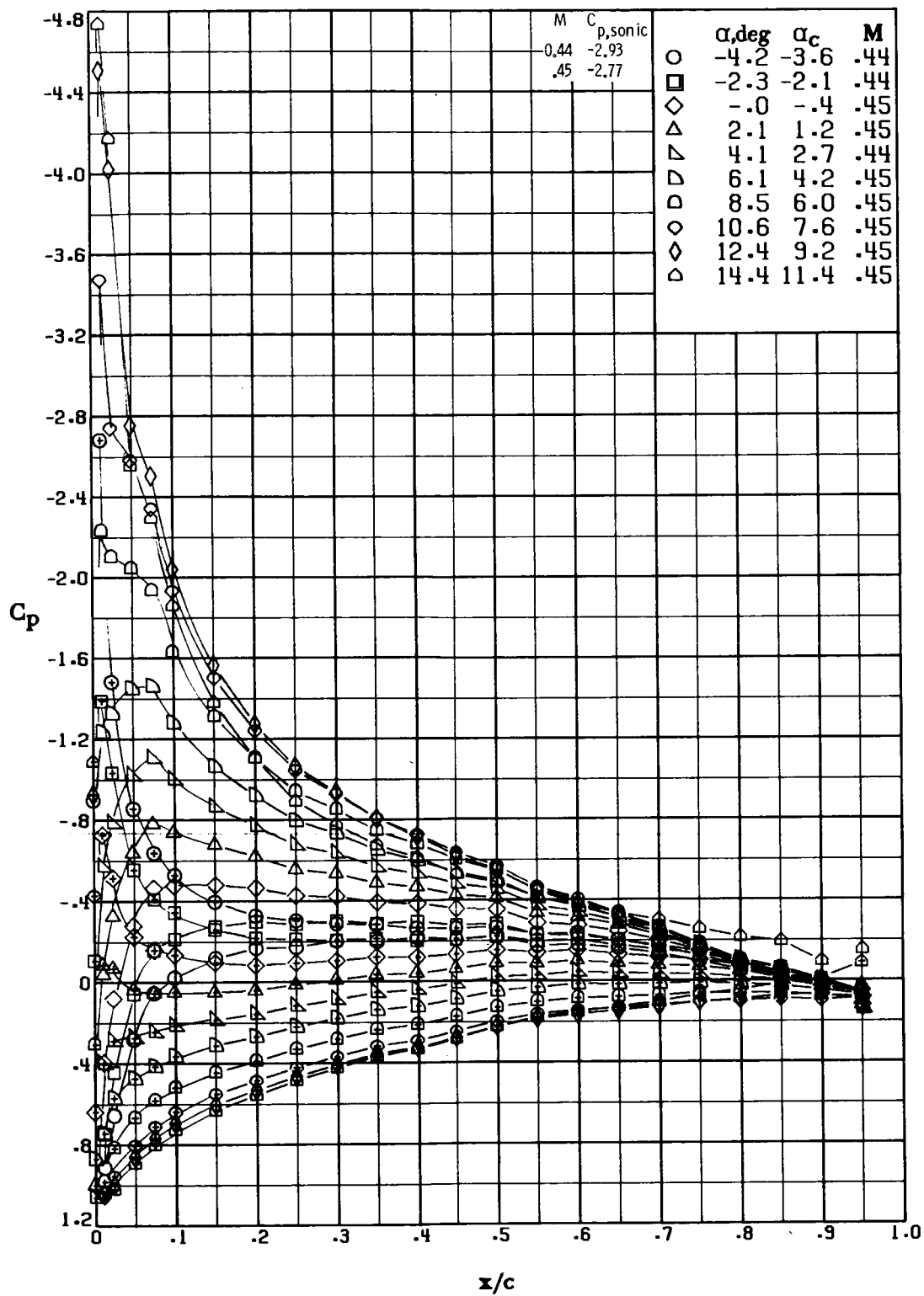
Figure 18.- Pressure distribution over RC(1)-10 Mod 1 airfoil.  
Symbols with "+" inside indicate lower surface.



(b)  $M \approx 0.40$ ;  $R \approx 5.8 \times 10^6$ .

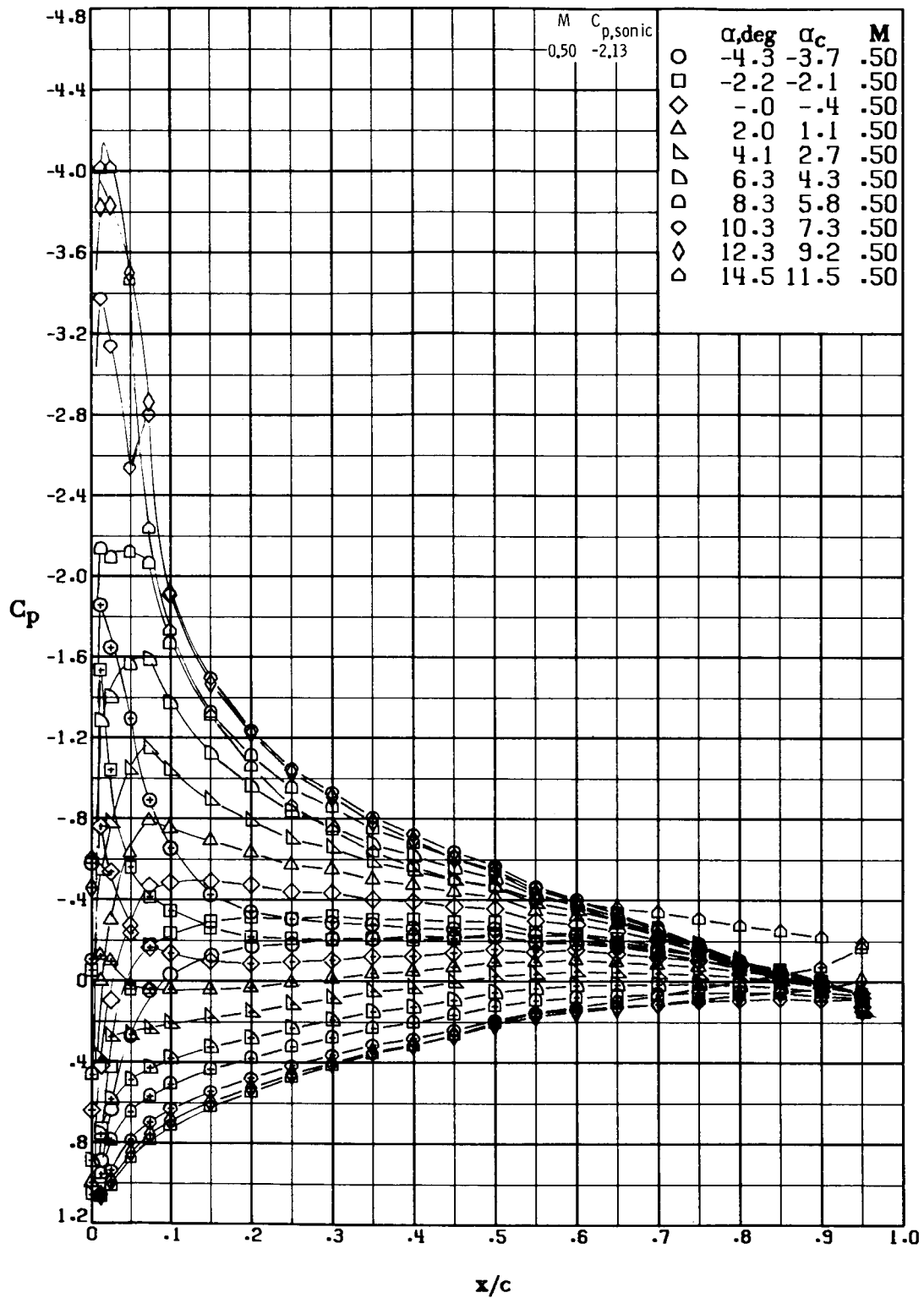
Figure 18.- Continued.





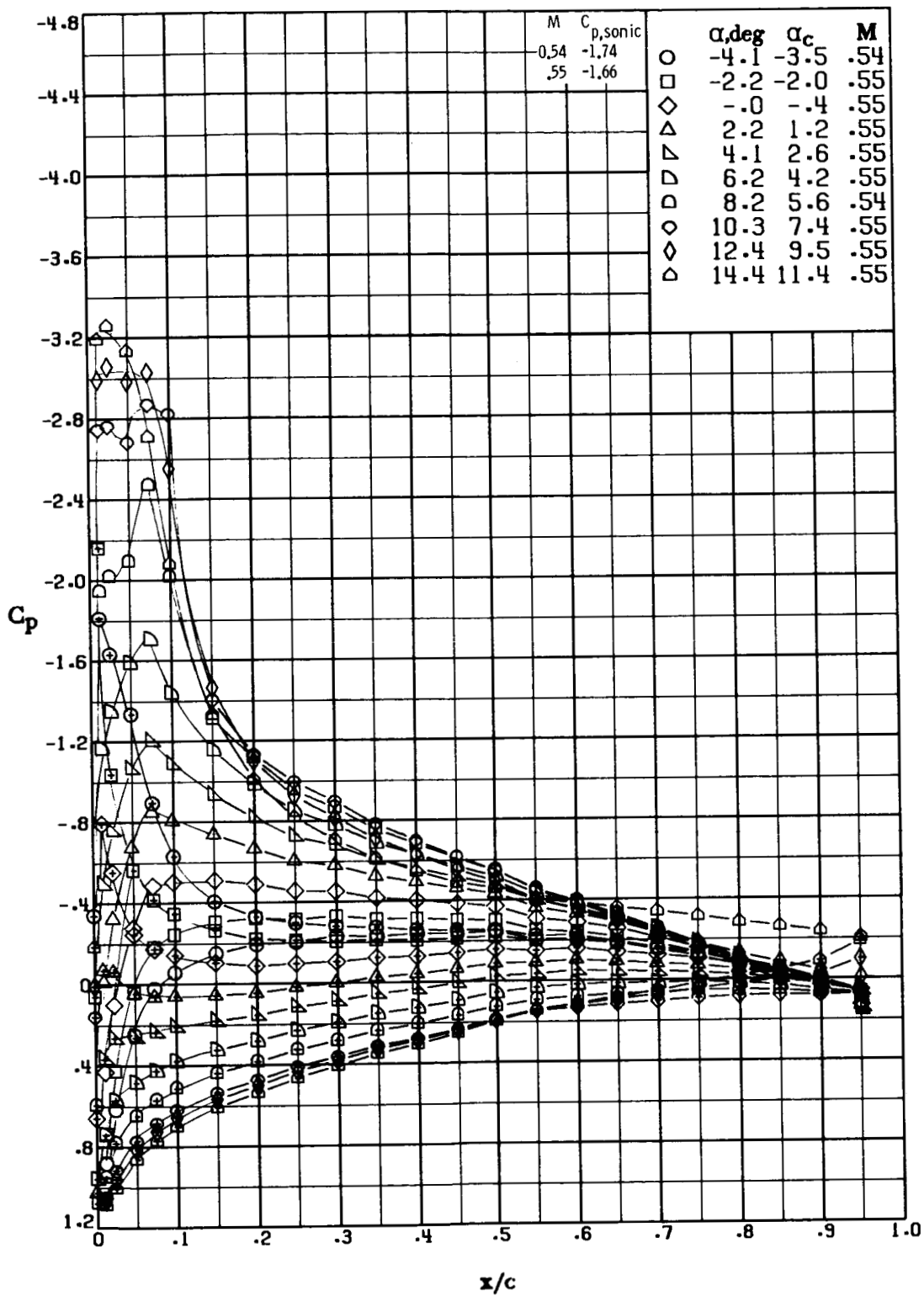
(c)  $M \approx 0.45$ ;  $R \approx 6.2 \times 10^6$ .

Figure 18.- Continued.



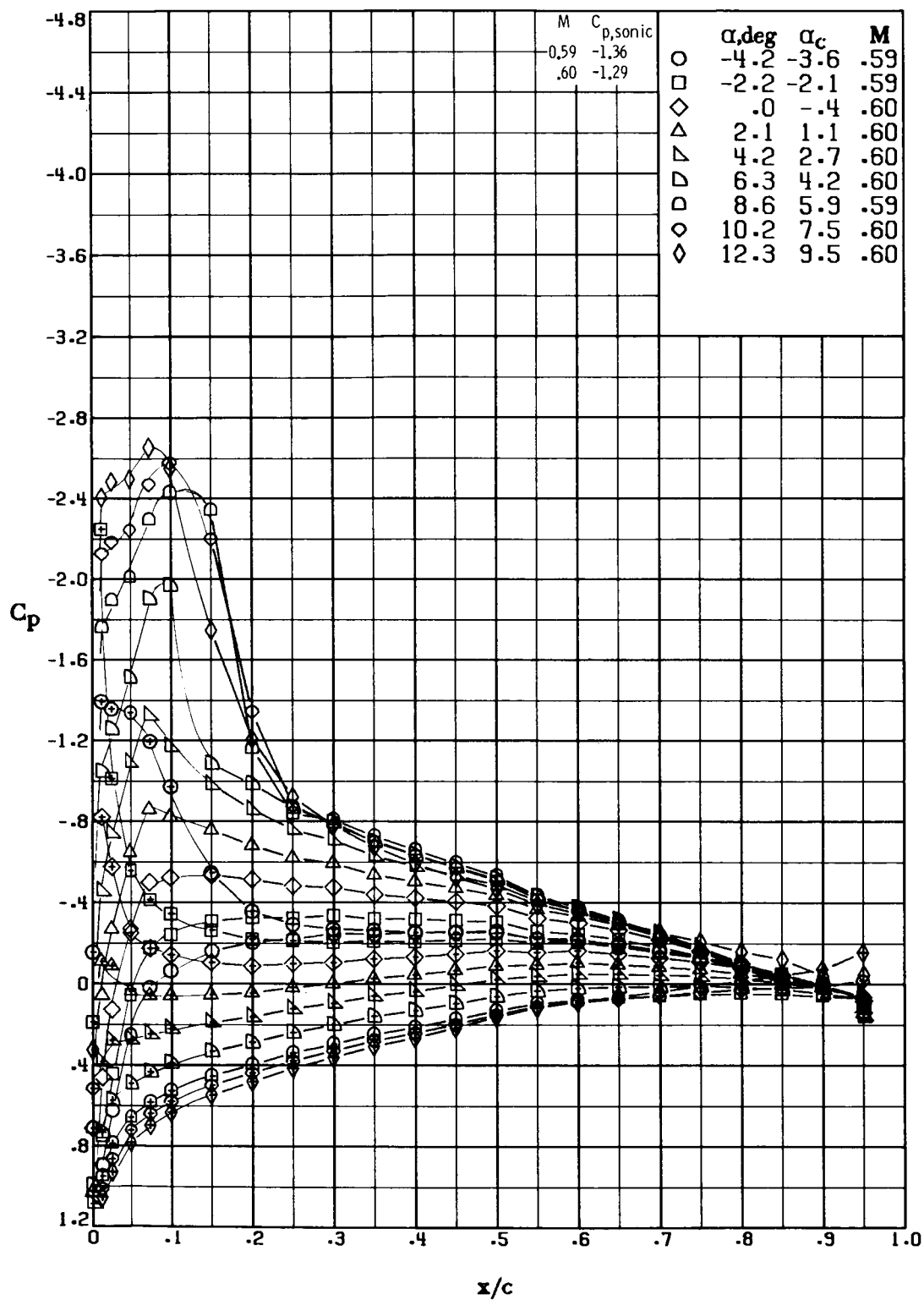
(d)  $M \approx 0.50$ ;  $R \approx 6.9 \times 10^6$ .

Figure 18.- Continued.



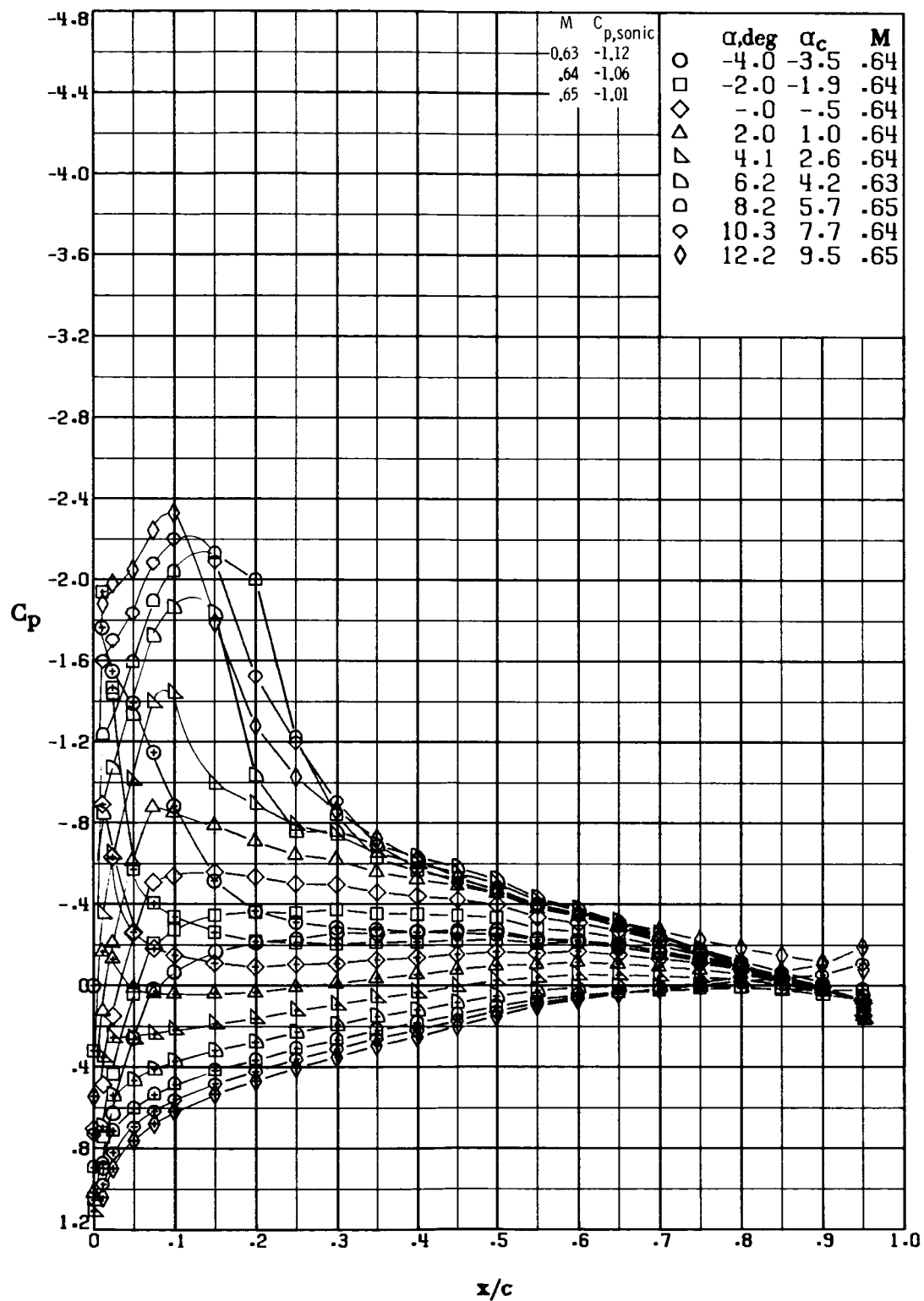
(e)  $M \approx 0.55$ ;  $R \approx 7.2 \times 10^6$ .

Figure 18.- Continued.



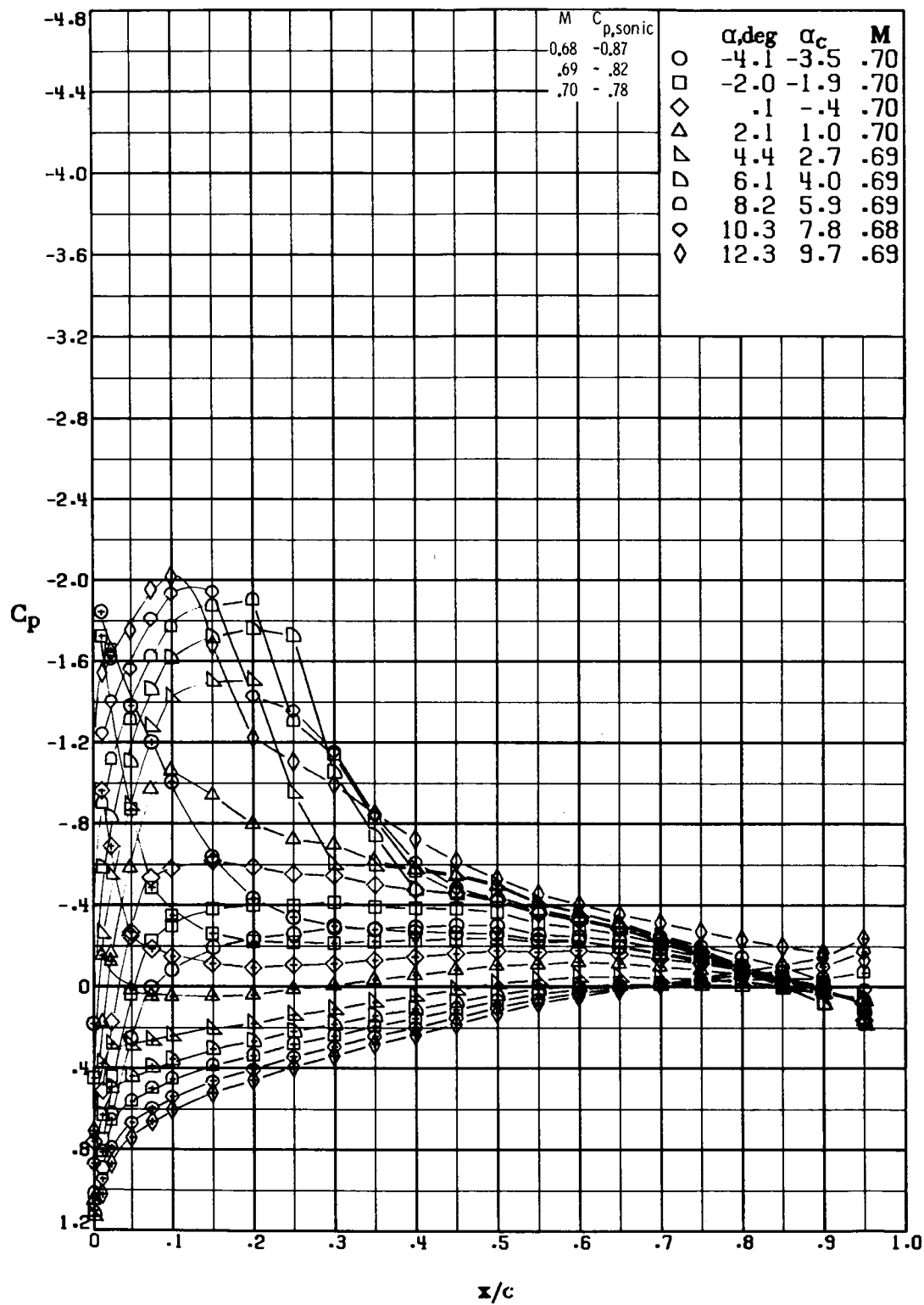
(f)  $M \approx 0.60$ ;  $R \approx 7.8 \times 10^6$ .

Figure 18.- Continued.



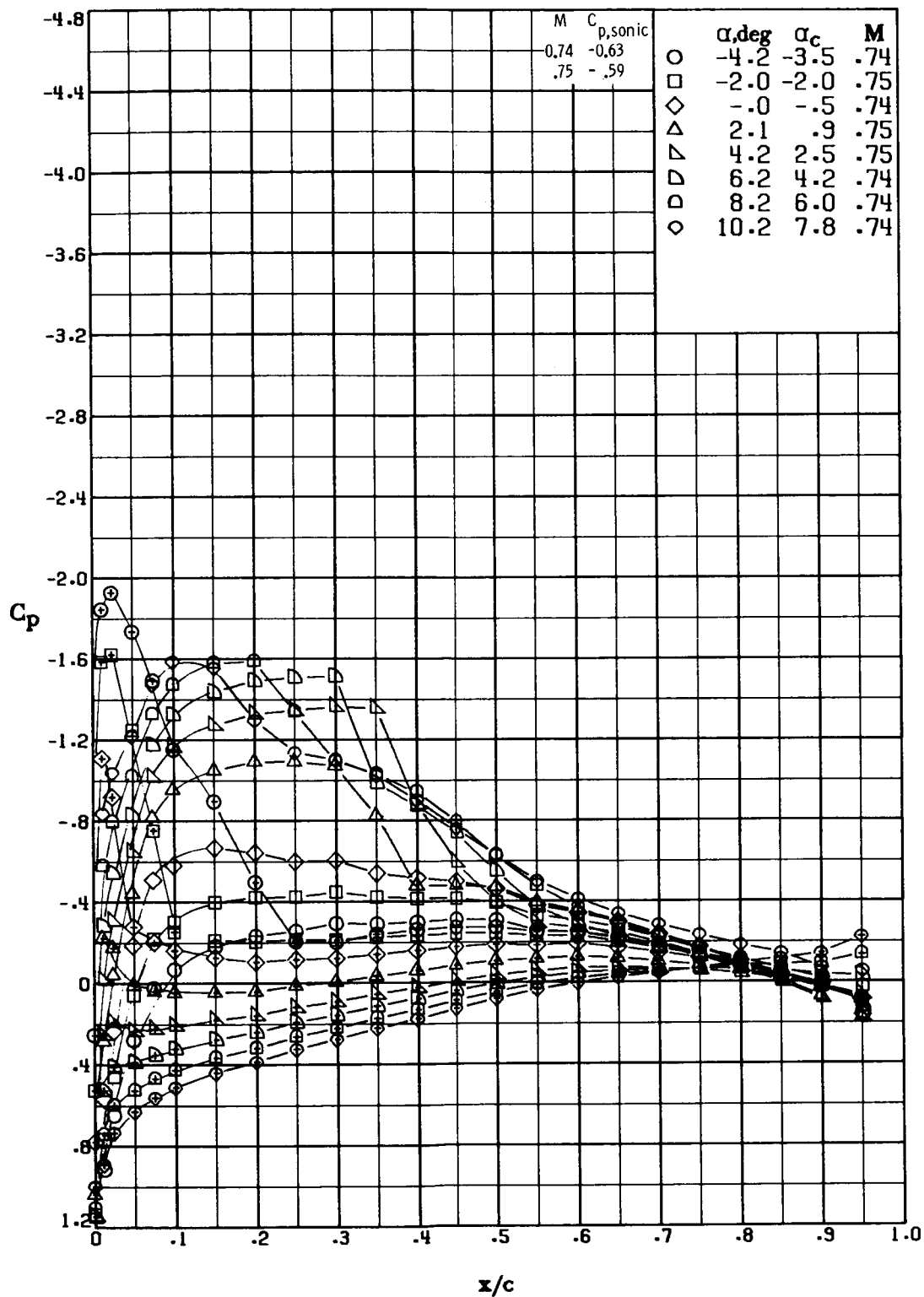
(g)  $M \approx 0.64$ ;  $R \approx 8.2 \times 10^6$ .

Figure 18.- Continued.



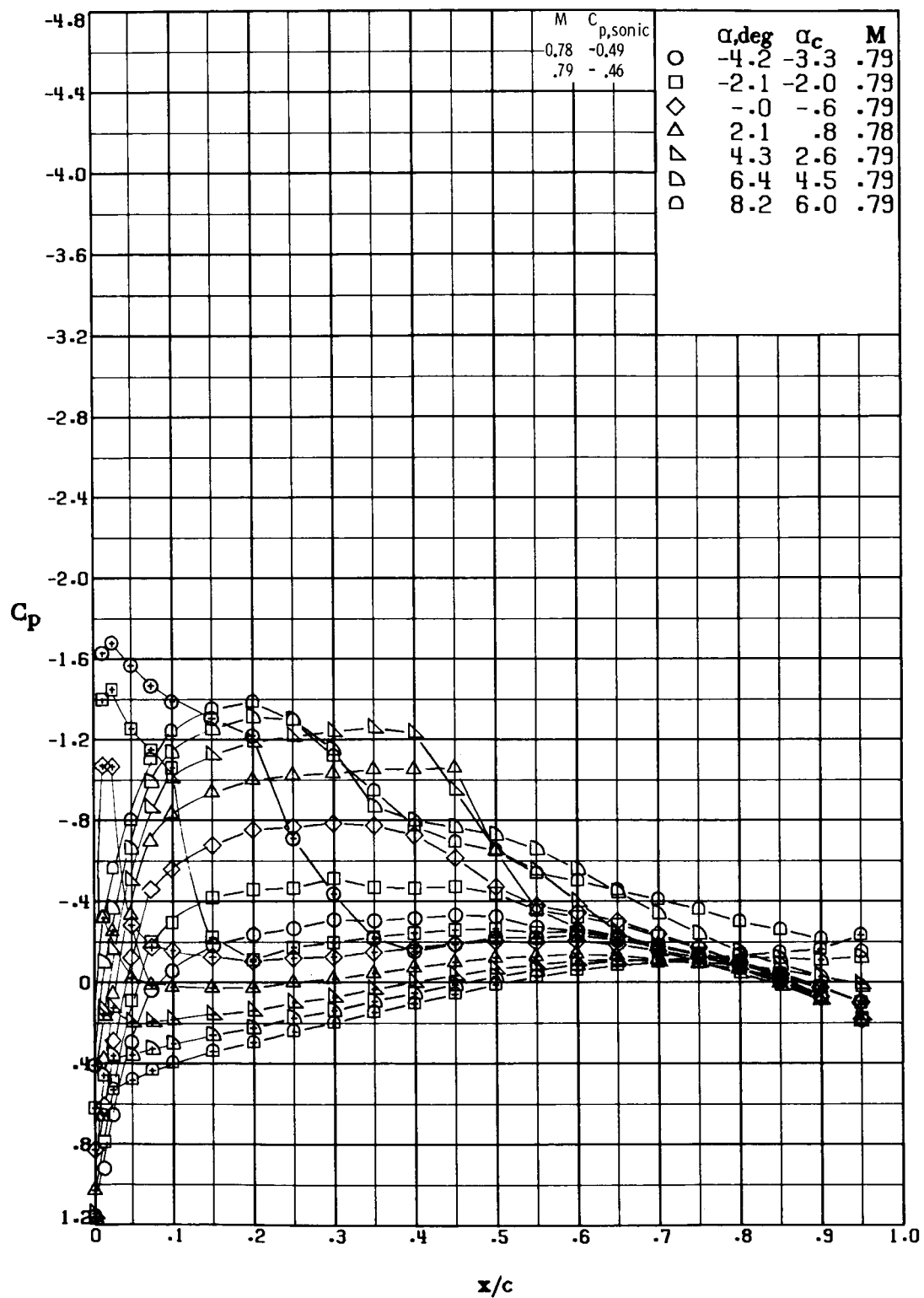
(h)  $M \approx 0.69$ ;  $R \approx 8.6 \times 10^6$ .

Figure 18.- Continued.



(i)  $M \approx 0.74$ ;  $R \approx 9.0 \times 10^6$ .

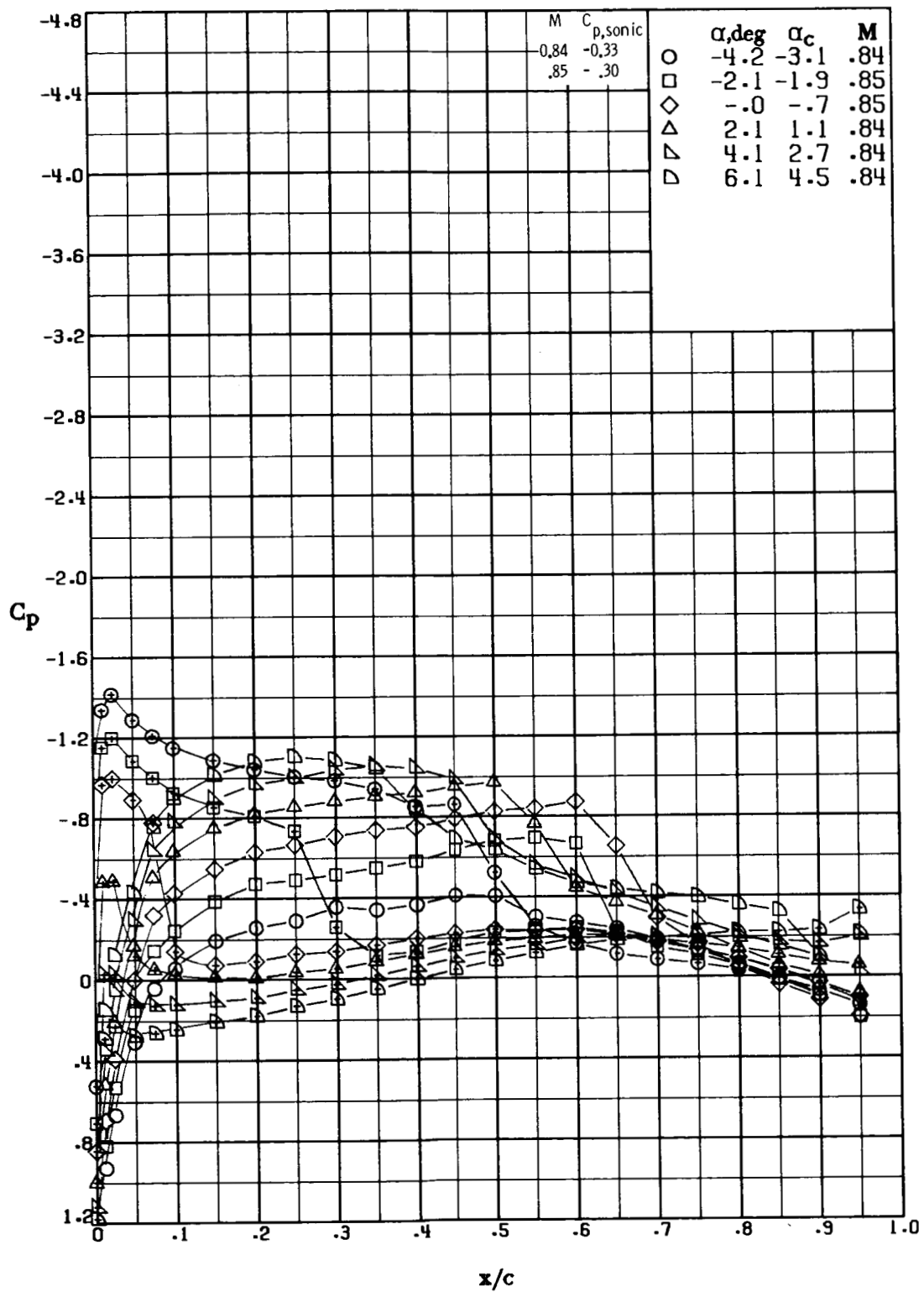
Figure 18.- Continued.



(j)  $M \approx 0.79$ ;  $R \approx 9.3 \times 10^6$ .

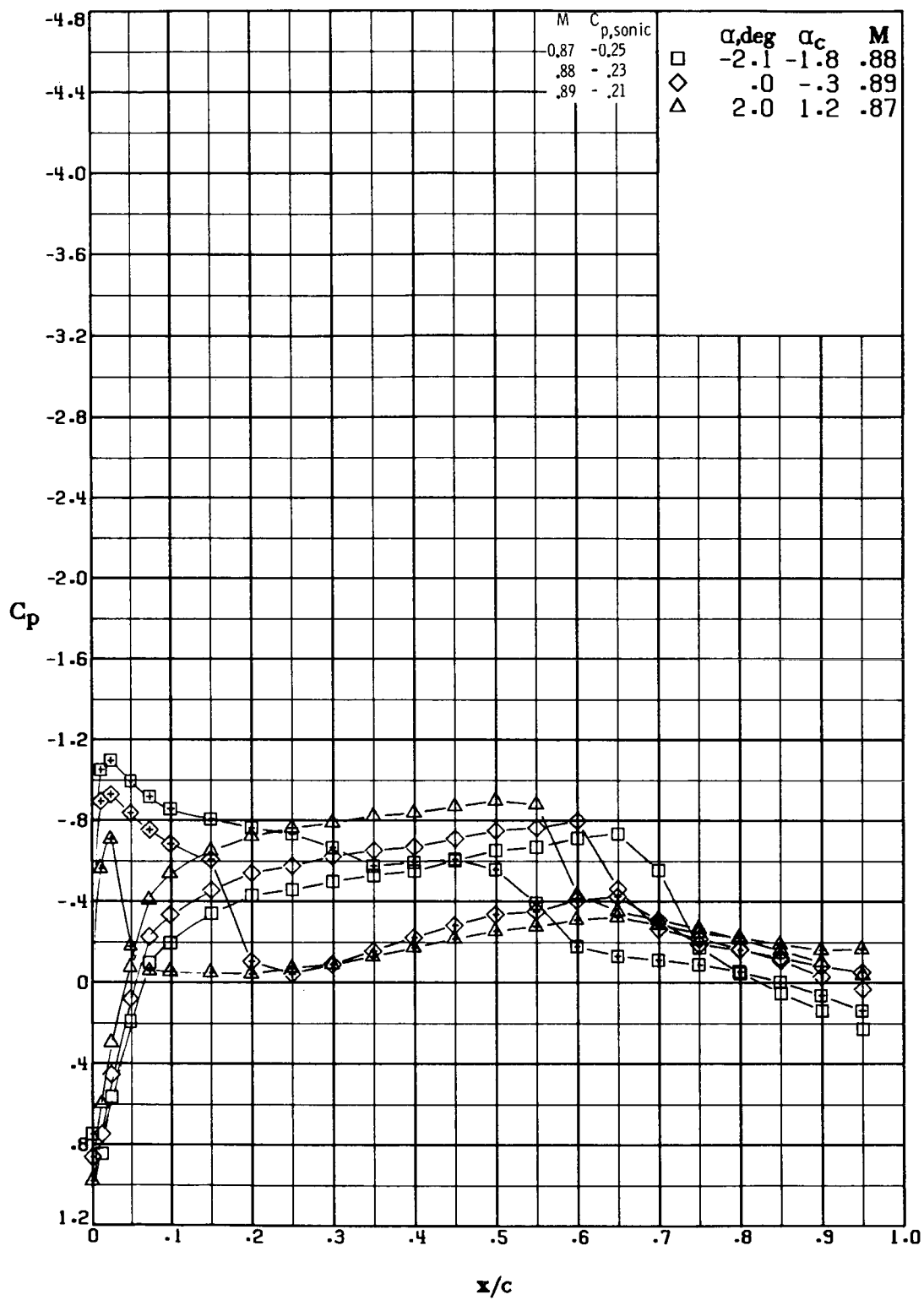
Figure 18.- Continued.





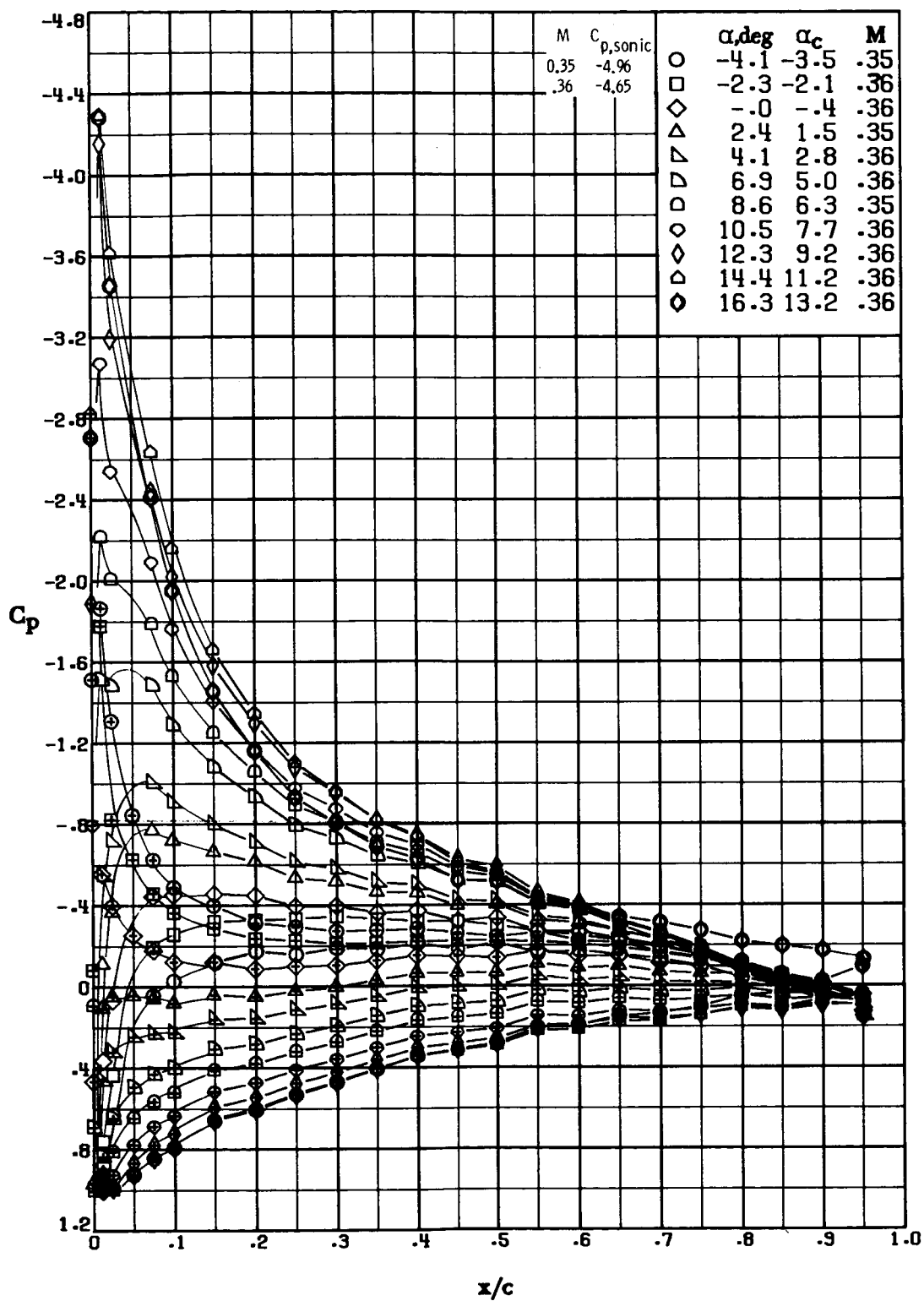
(k)  $M \approx 0.84$ ;  $R \approx 9.6 \times 10^6$ .

Figure 18.- Continued.



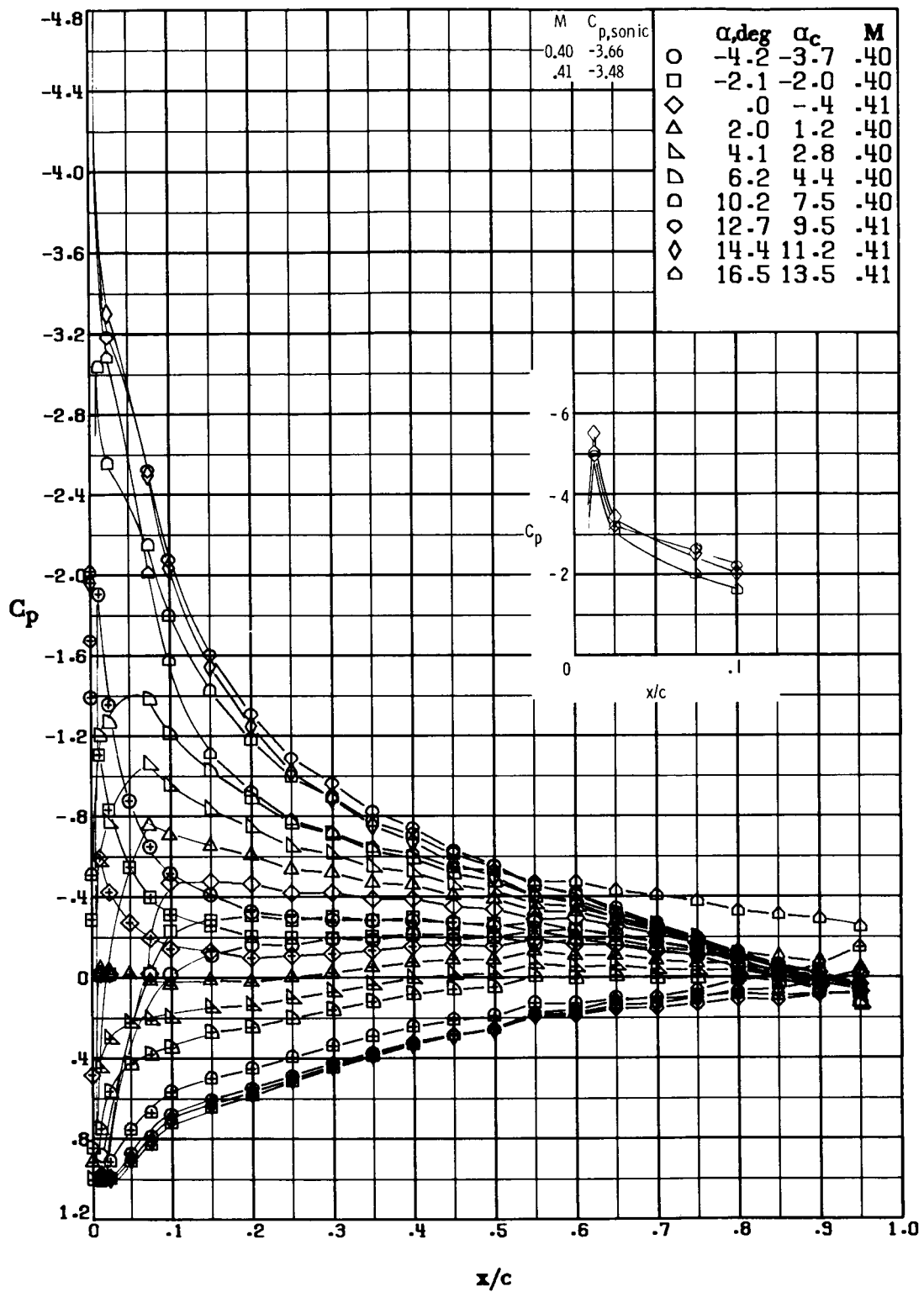
(1)  $M \approx 0.89$ ;  $R \approx 9.8 \times 10^6$ .

Figure 18.- Concluded.



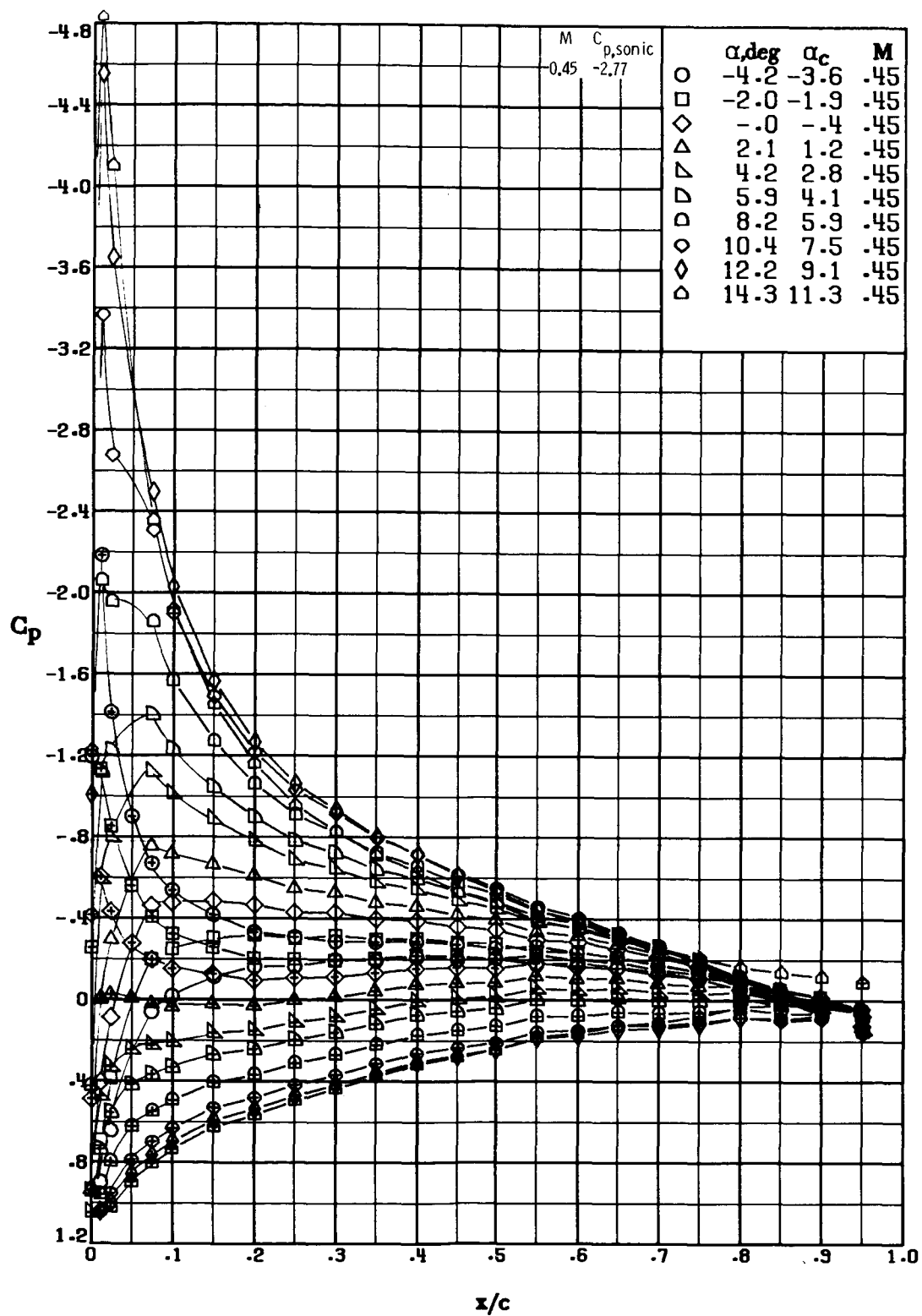
(a)  $M \approx 0.36$ ;  $R \approx 5.7 \times 10^6$ .

Figure 19.- Pressure distribution over RC(1)-10 Mod 2 airfoil.  
Symbols with "+" inside indicate lower surface.



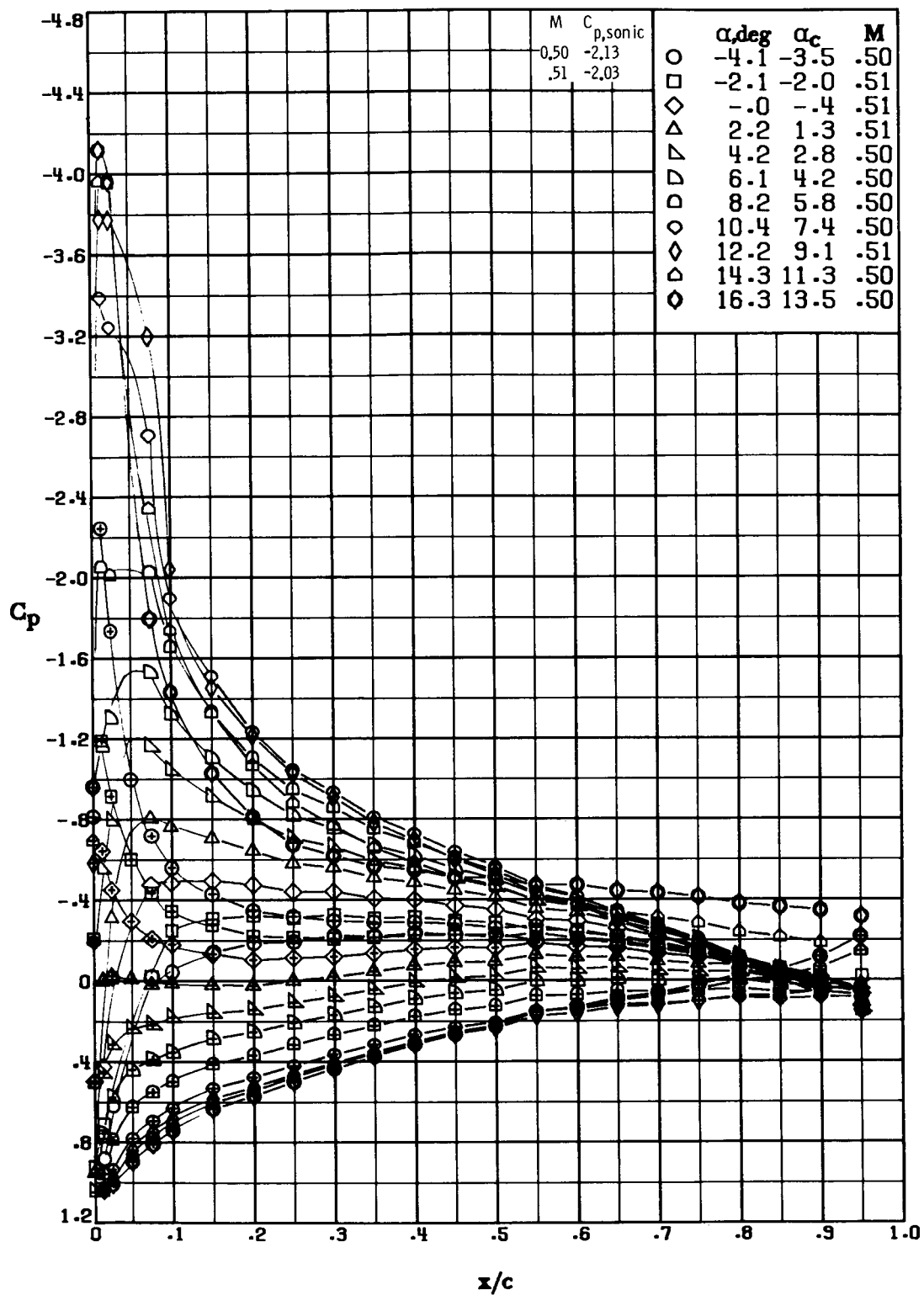
(b)  $M \approx 0.40$ ;  $R \approx 6.9 \times 10^6$ .

Figure 19.- Continued.



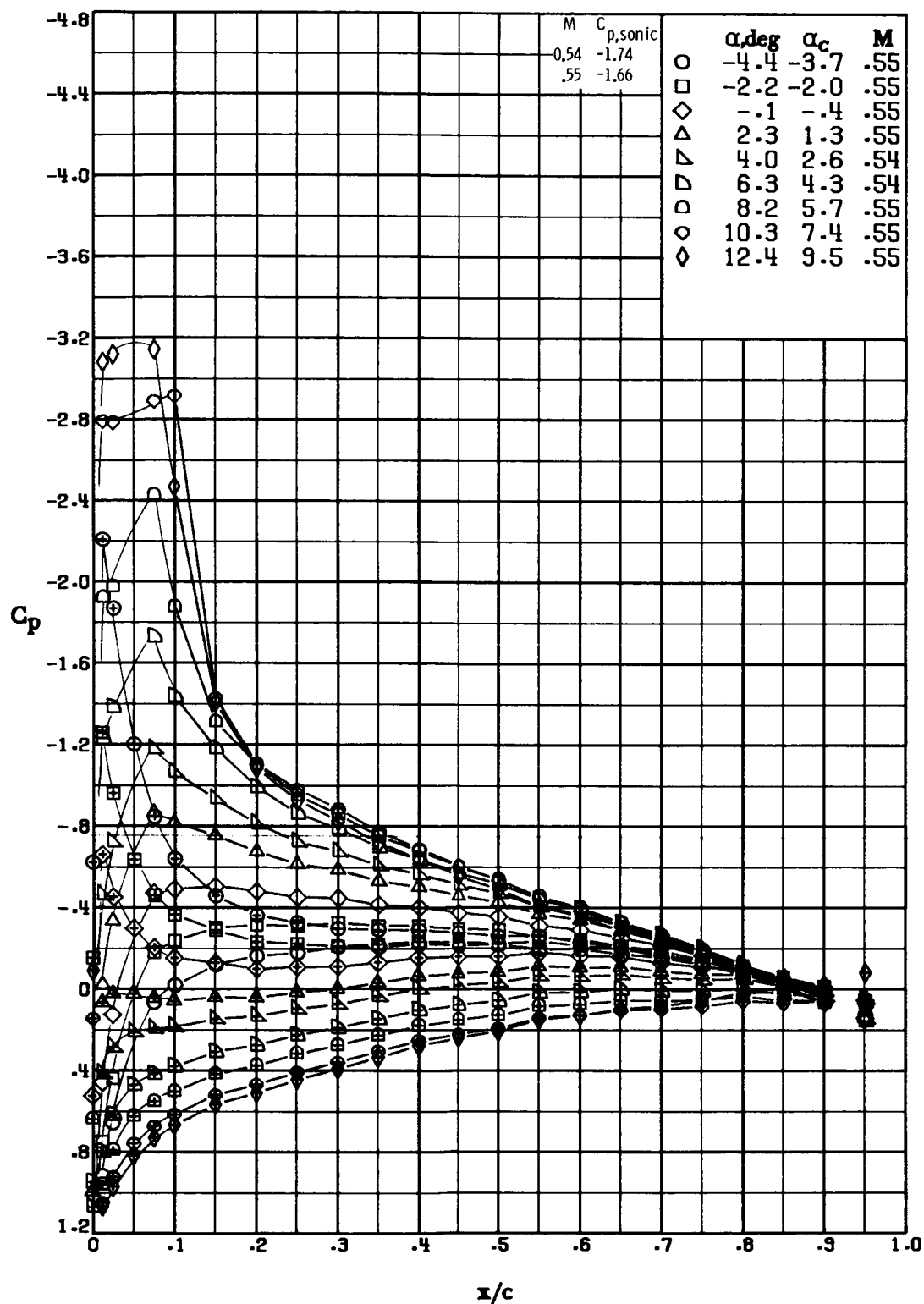
(c)  $M \approx 0.45$ ;  $R \approx 7.1 \times 10^6$ .

Figure 19.- Continued.



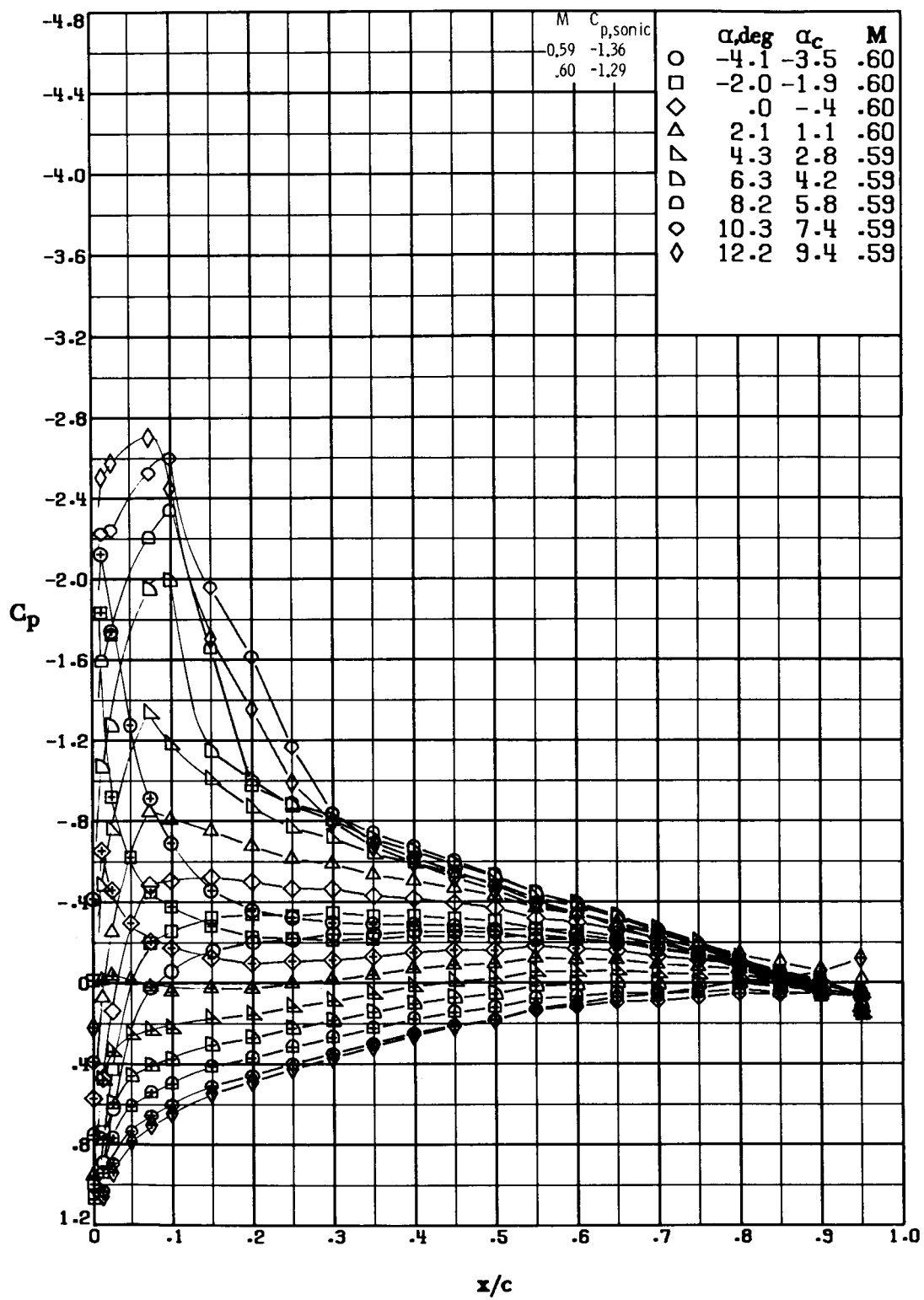
(d)  $M \approx 0.50$ ;  $R \approx 7.7 \times 10^6$ .

Figure 19.- Continued.



(e)  $M \approx 0.55$ ;  $R \approx 8.1 \times 10^6$ .

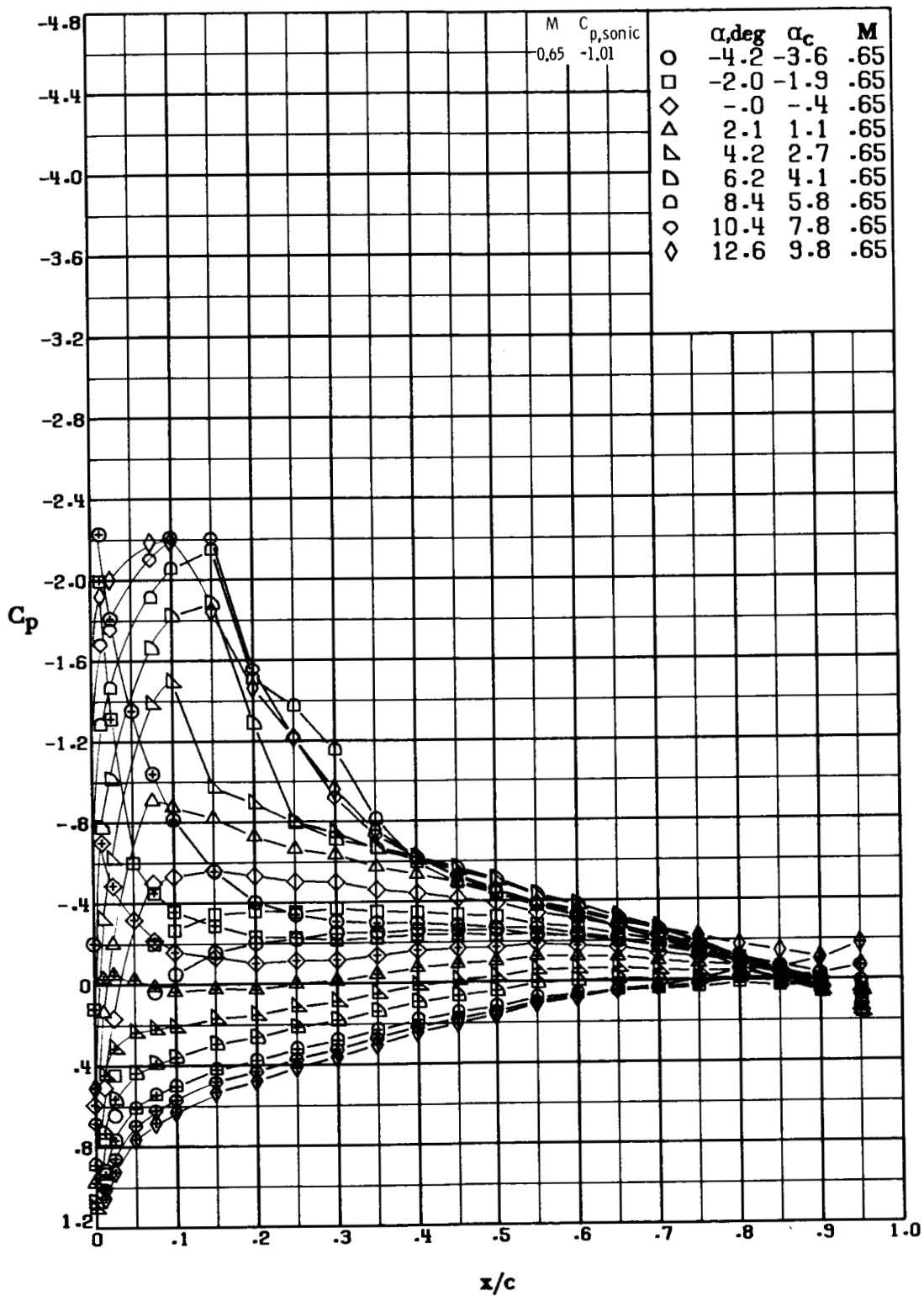
Figure 19.- Continued.



(f)  $M \approx 0.59$ ;  $R \approx 9.0 \times 10^6$ .

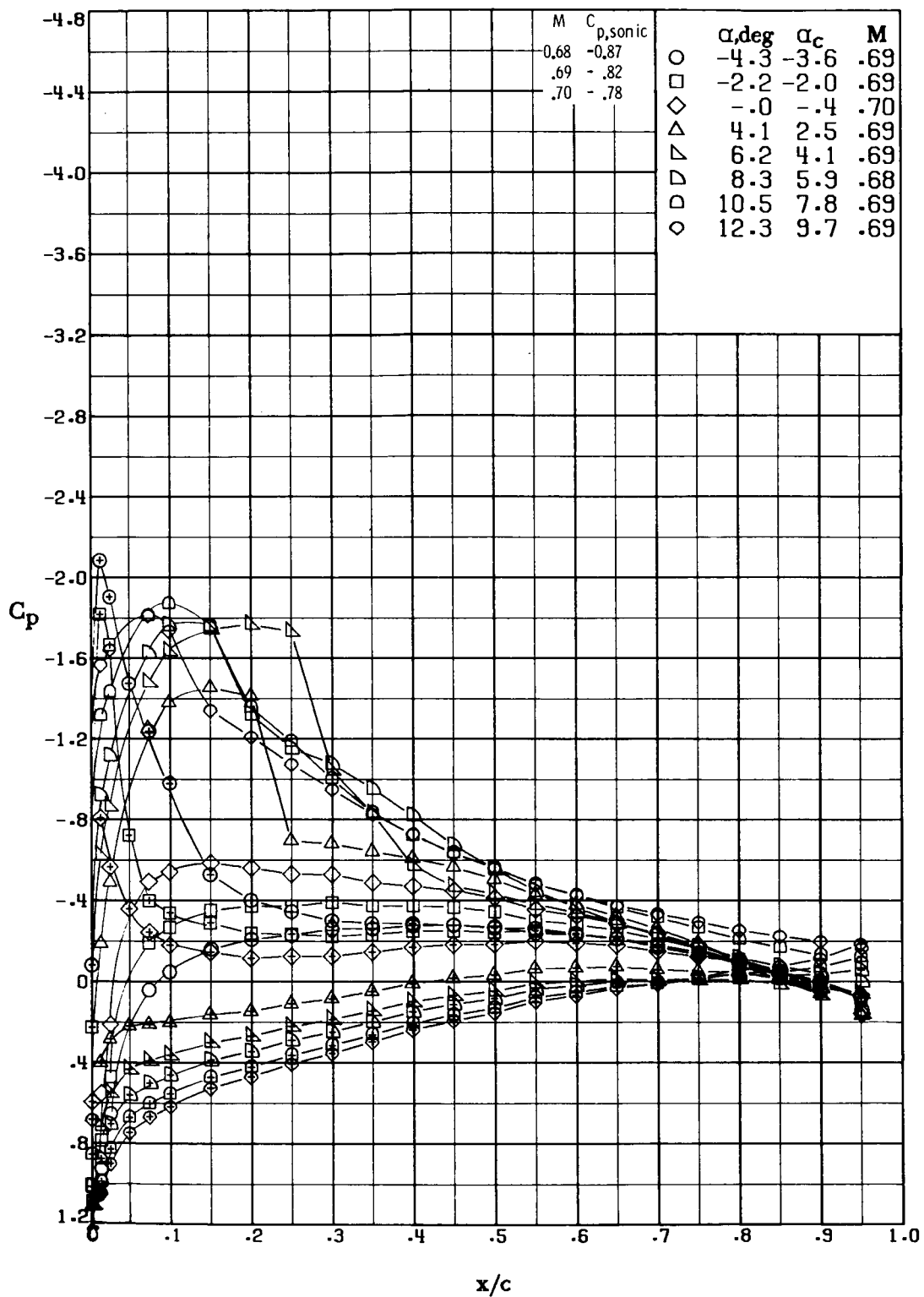
Figure 19.- Continued.





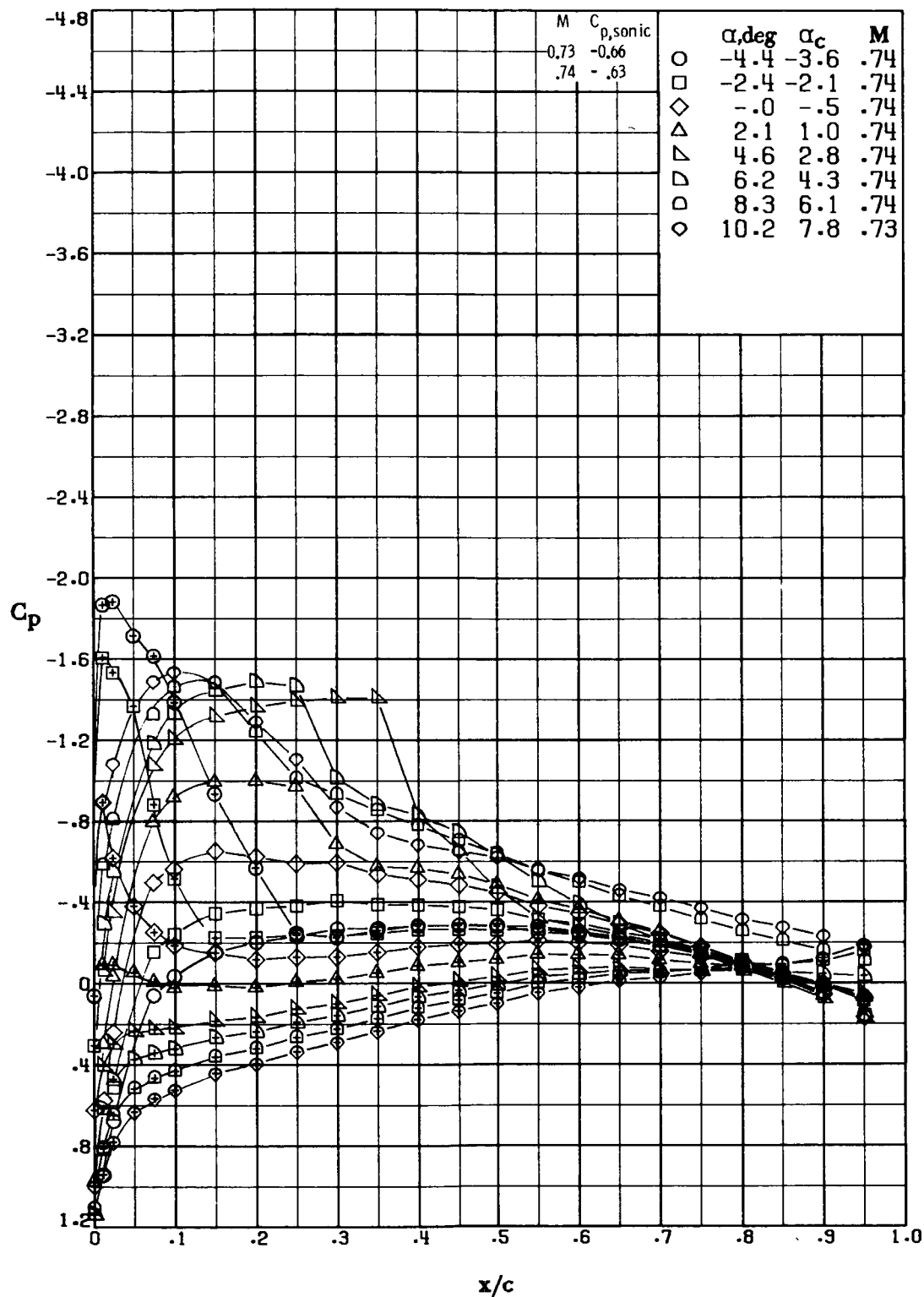
(g)  $M \approx 0.65$ ;  $R \approx 9.7 \times 10^6$ .

Figure 19.- Continued.



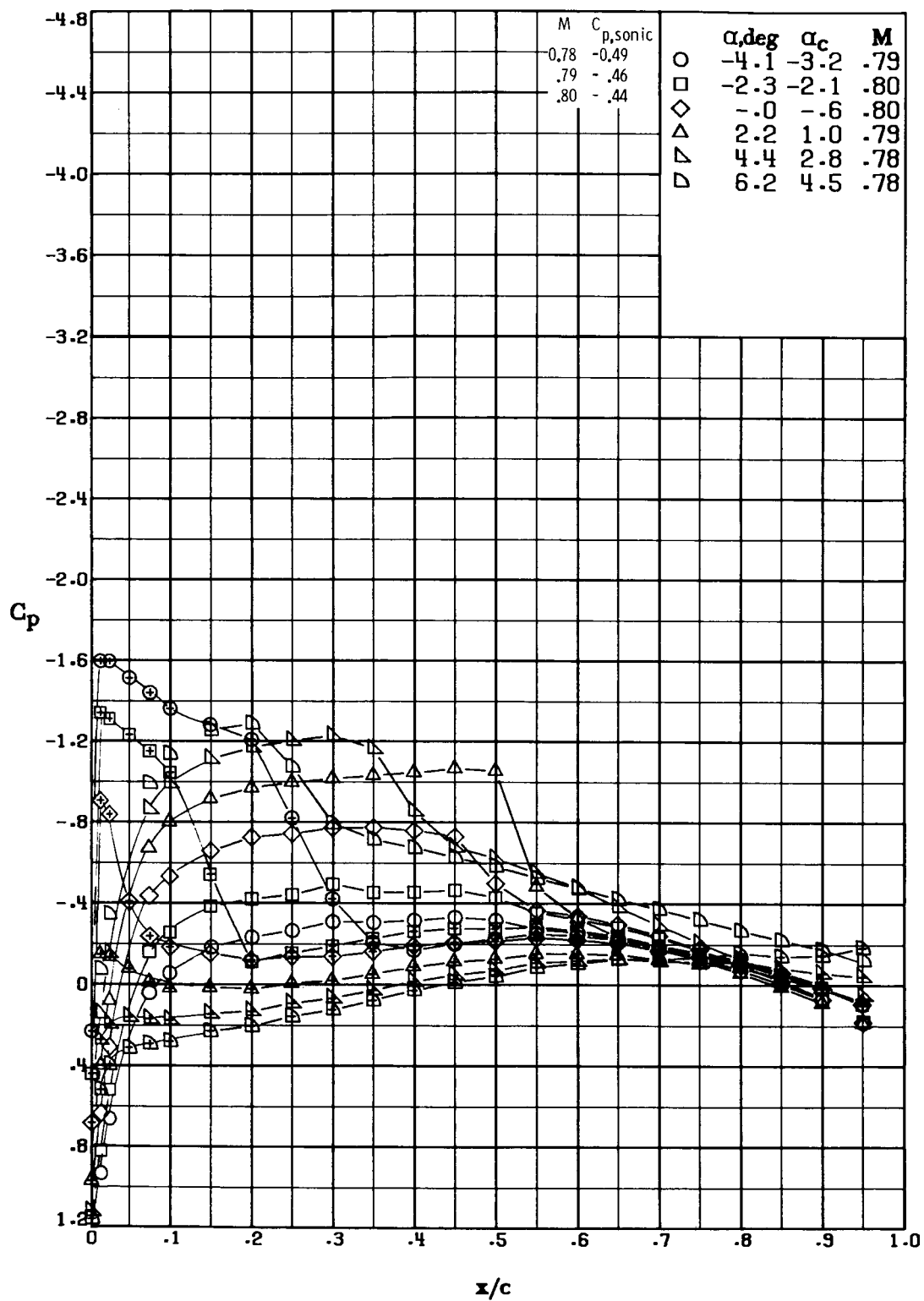
(h)  $M \approx 0.69$ ;  $R \approx 10.7 \times 10^6$ .

Figure 19.- Continued.



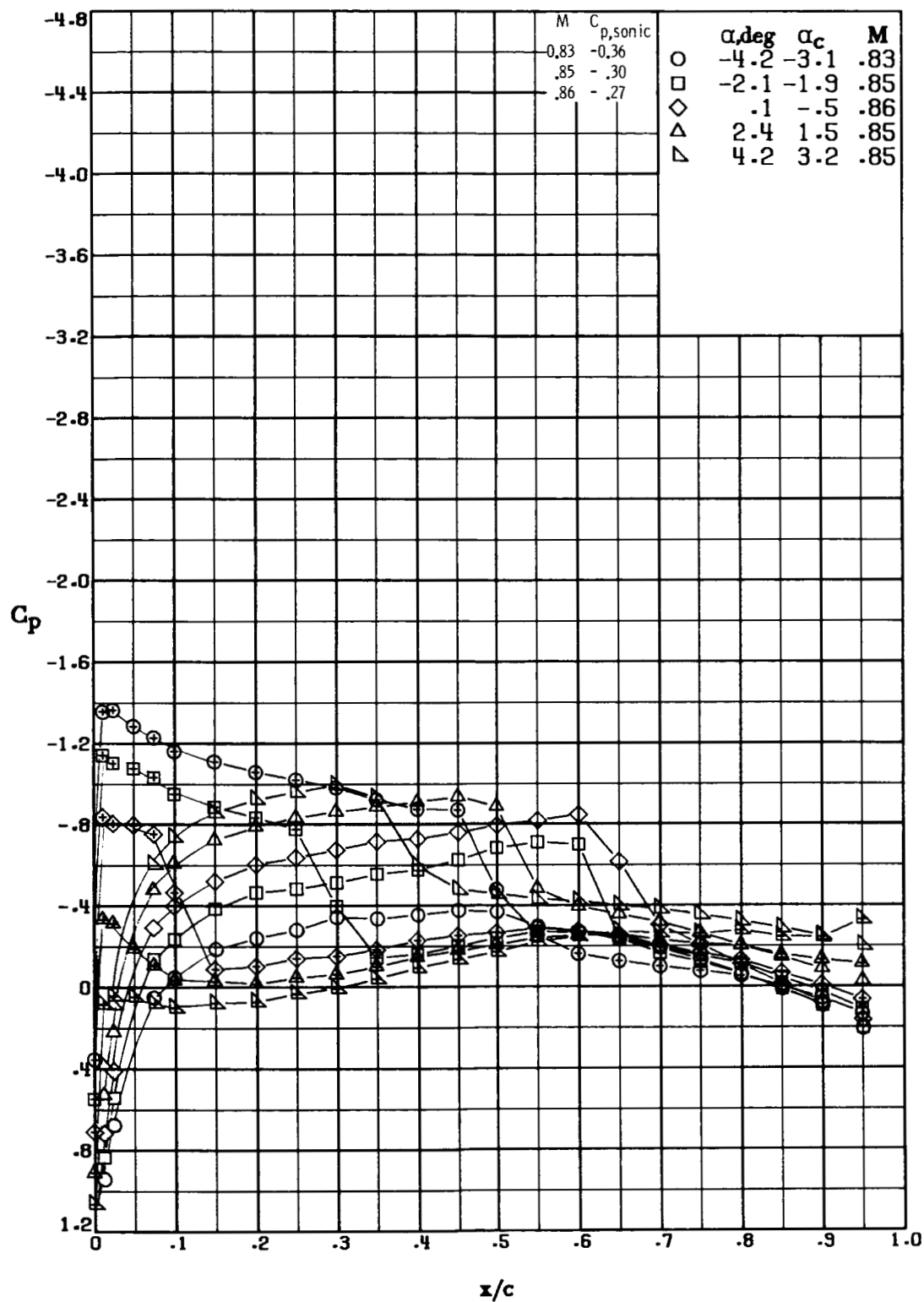
(i)  $M \approx 0.74$ ;  $R \approx 11.0 \times 10^6$ .

Figure 19.- Continued.



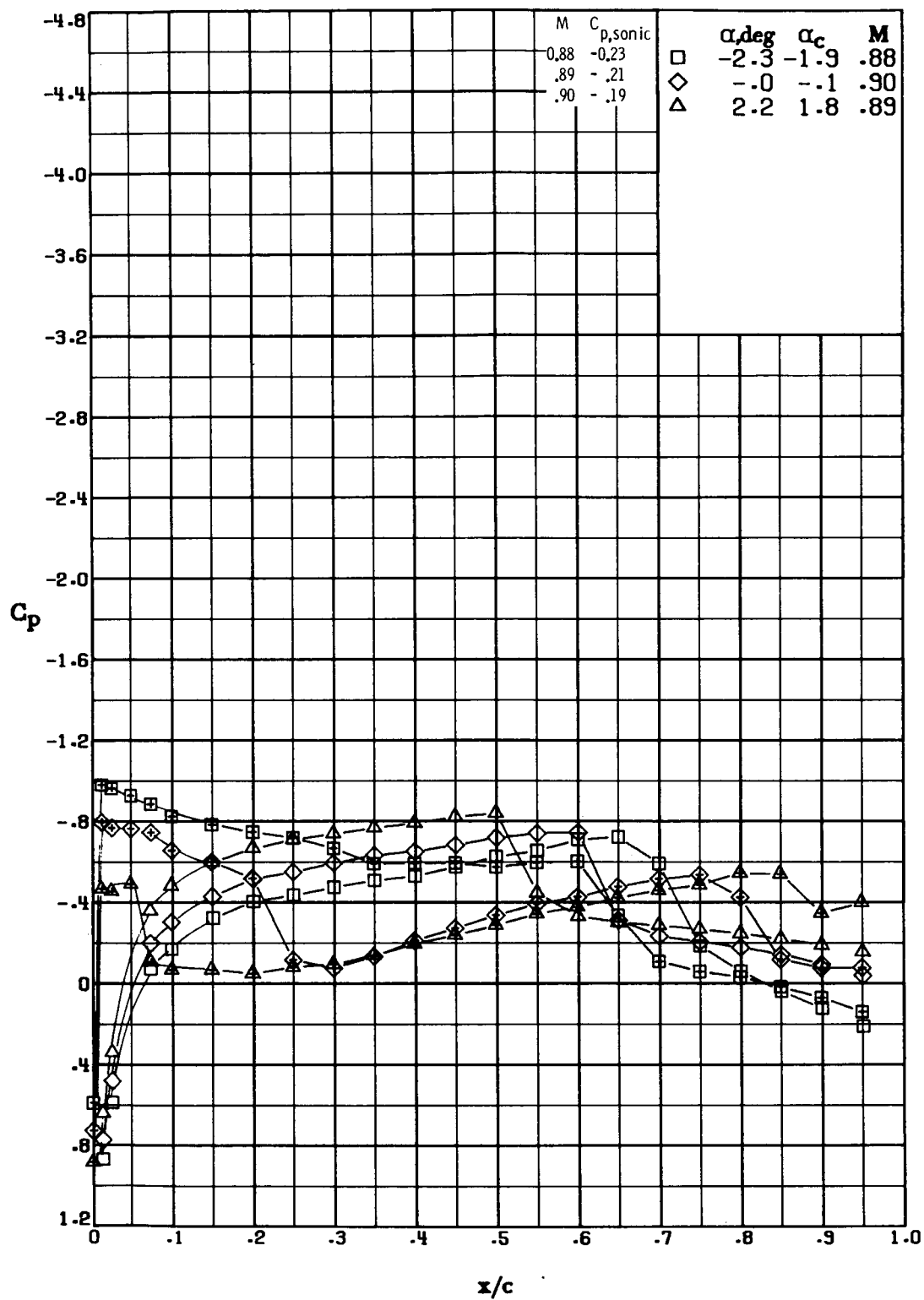
(j)  $M \approx 0.79$ ;  $R \approx 11.8 \times 10^6$ .

Figure 19.- Continued.





(k)  $M \approx 0.85$ ;  $R \approx 12.6 \times 10^6$ .

Figure 19.- Continued.



(1)  $M \approx 0.89$ ;  $R \approx 13.2 \times 10^6$ .

Figure 19.- Concluded.

1. Report No. NASA TP-1965 AVRADCOM TR 81-B-6		2. Government Accession No.		3. Recipient's Catalog No.	
4. Title and Subtitle TWO-DIMENSIONAL AERODYNAMIC CHARACTERISTICS OF AN AIRFOIL DESIGNED FOR ROTORCRAFT APPLICATION				5. Report Date December 1981	
				6. Performing Organization Code 023-10-01-01	
7. Author(s) Gene J. Bingham, Kevin W. Noonan, and William G. Sewall				8. Performing Organization Report No. L-14825	
9. Performing Organization Name and Address NASA Langley Research Center and Structures Laboratory AVRADCOM Research and Technology Laboratories Hampton, VA 23665				10. Work Unit No.	
				11. Contract or Grant No.	
12. Sponsoring Agency Name and Address National Aeronautics and Space Administration Washington, DC 20546 and U.S. Army Aviation Research and Development Command St. Louis, MO 63166				13. Type of Report and Period Covered Technical Paper	
				14. Army Project No. 1L161102AH45	
15. Supplementary Notes Gene J. Bingham and Kevin W. Noonan: Structures Laboratory, AVRADCOM Research and Technology Laboratories. William G. Sewall: Langley Research Center.					
16. Abstract An airfoil designed for helicopter rotor application was investigated at Mach numbers from about 0.35 to 0.90 at Reynolds numbers from $5.1 \times 10^6$ to $9.6 \times 10^6$ . The airfoil (NASA RC(1)-10) was designed to increase maximum normal-force coefficient while maintaining favorable drag-divergence and pitching-moment characteristics observed earlier for the 10-64C airfoil. The RC(1)-10 airfoil has a thickness-to-chord ratio of 0.10 with maximum thickness at 40 percent chord and maximum camber at 27 percent chord. Two modifications were also tested at these Mach numbers and at Reynolds numbers from about $5.0 \times 10^6$ to $13.9 \times 10^6$ . Maximum normal-force coefficient of the RC(1)-10 airfoil varies from 1.14 to 0.90 at Mach numbers from about 0.35 to 0.65, an increase of 0.06 to 0.16 over that of the 10-64C airfoils. Drag-divergence Mach number of the RC(1)-10 is about equal to that of the 10-64C at normal-force coefficients of 0 to 0.40, and less than the 10-64C at normal-force coefficients of about -0.2 and above 0.40. Both modifications to the RC(1)-10 airfoil decreased drag coefficient at zero normal-force coefficient for Mach numbers near drag divergence, but were less beneficial at a normal-force coefficient of -0.2.					
17. Key Words (Suggested by Author(s)) Airfoils Airfoil design Helicopter airfoils			18. Distribution Statement  		
19. Security Classif. (of this report) Unclassified		20. Security Classif. (of this page) Unclassified		21. No. of Pages 77	
				22. Price	